Flow-Induced Vibration of Long Structures

Thesis by

Nicholas Patrick Jones

In Partial Fulfillment of the Requirements

for the Degree of

Doctor of Philosophy

California Institute of Technology

Pasadena, California

1986

(Submitted May 9th, 1986)

Acknowledgements

I wish to thank my advisor, Dr. W. D. Iwan, for his guidance and valuable suggestions during the course of this investigation. Without his assistance I would surely have abandoned the project a number of times.

The financial support of the California Institute of Technology through my involvement with the CADRE (Computer Aided Design, Research and Education) system is gratefully acknowledged.

In the tradition of a retiring member of SOPS (Society of Professional Students), I also extend my thanks and best wishes to all my fellow students and friends in Thomas Building, in particular, Harri, Janet, Mike, Garrett, and George. With their presence and companionship, both on and off campus, the last five years have been made most enjoyable.

I would also like to thank the staff and clients of the Lawrence L. Frank Center of the Crippled Children's Society in Pasadena with whom I have had the pleasure to work. For the past three years, my involvement with the members of the physical conditioning class and instructor, April, have certainly added a great deal to my life, and helped lift my spirits when work was not progressing well.

Finally, I thank my family in New Zealand for their unending support and encouragement over the course of my graduate study. Their continuous presence in mind, if not body, was always a great help. In particular, thanks are due to my mother for the many years she gave to me. This thesis is dedicated to her, with all my love, as a small token of my gratitude.

Abstract

When a body is exposed to a flowing fluid, oscillations can occur due to one or more of several different mechanisms. The resulting large amplitudes of motion and fatigue are potential sources of structural failure. Furthermore, the drag force on a structure can be increased due to the effectively larger cross-sectional area presented to the flow from the oscillation. A complete understanding of the nature of such vibration is essential in the design of many civil and mechanical engineering systems.

Previous solutions to the vortex-induced vibration problem were primarily based on modal analysis, using a one- or two-mode approximation. Use of modal analysis implies a "locked-in" condition: the vortex shedding frequency and a natural frequency of the system are coincident. Observations made on long cable systems indicate that the amplitude of response is smaller than is predicted by a conventional modal analysis. The drag forces on such structures are therefore overestimated by current design approaches.

In very long structures, typical of those found in ocean applications, modes are closely spaced, and it is not reasonable to assume total spanwise correlation in the fluid forces or response. The approach used herein attempts to avoid the limitations associated with the modal solution of such problems by implementing a solution based on traveling waves. The technique draws on earlier theoretical and empirical models for the complex vortex-shedding phenomenon, and incorporates these into a new method for analyzing the structural response problem.

The traveling wave approach can be used to model effectively spanwise variable flow environments by summing the calculated responses of adjacent active sections of

cable. Until this method was developed, there was no suitable method available for modeling flow characteristics of this type. Modal analysis is effectively limited to systems with uniform flow over all or part of the system.

TABLE OF CONTENTS

NOTATION

A	Cylinder or cable amplitude (1/2 peak-to-peak displacement)
$\bar{A}$	Total cable amplitude (1/2 peak-to-peak displacement)
$\bar{A}_i$	Total cable amplitude at i-th segment
$\bar{A}_0$	Total cable amplitude for constant force solution at end of active region
B	Normalized cylinder or cable displacement ($=A/D$)
c	Wavespeed in cable ($=\sqrt{T/\mu}$)
$\hat{c}$	Wavespeed for viscously damped cable
$\bar{c}$	Viscous damping coefficient per unit length
C_a	Added mass coefficient of vibrating cylinder, in direction of flow
C_d	Drag coefficient of vibrating cylinder, in direction of flow
C_{d0}	Drag coefficient of stationary cylinder, in direction of flow
C_{dh}	Drag coefficient, component of force in-phase with cylinder velocity
$C_{dh(max)}$	Maximum drag coefficient (above), as function of B
C_L	Lift coefficient of vibrating cylinder, in direction of flow
C_m	Inertia coefficient of vibrating cylinder, in direction of flow
C_{mh}	Inertia coefficient, component of force in-phase with cylinder displacement
d	Viscous damping coefficient per unit length
D	Cable or cylinder diameter
$f(x,t)$	Applied force per unit length on cable
F	Force per unit length acting on cable or cylinder

F_0	Spanwise constant force magnitude
$G(x,\xi,t)$	Green's function for taut cable
$G^*(x,\xi,t)$	Green's function for taut cable (discrete formulation)
$I_1(x)$	Integral term appearing in traveling wave solution
$I_2(x)$	Integral term appearing in traveling wave solution
k	Stiffness coefficient per unit length (note context)
k	Viscous damping coefficient per unit length (note context)
k/D	Surface roughness parameter
K	Keuligan-Carpenter Number
l	Active length of cable (where vortices are assumed to be shedding)
L	Length of cylinder or cable
m	Mass of cylinder per unit length
m'	Mass of fluid displaced by cylinder per unit length
Re	Reynolds Number
Re_ω	Oscillatory Reynolds Number ($=\omega D^2/\nu$)
S	Strouhal Number
St_m	Strouhal number based on midspan incident flow velocity, U_m, in shear flow
T	Period of oscillation
T	Cable tension
U	Uniform free-stream flow velocity
U_m	Midspan incident flow velocity for sheared flow
U_m	Magnitude of oscillating flow velocity
V_r	Reduced flow velocity ($=\omega_s/S\omega$)

V_{r0}	Parameter appearing in analytical expression for C_{mh}
V_{ref}	"Reference velocity" for sheared flow, usually midspan velocity
$W_n(x)$	n-th eigenfunction for taut cable, length L
y	Displacement of cylinder or cable
Y	Displacement of cylinder or cable
α	Decay rate for amplitude in traveling wave solution
α_i	Value of α corresponding to internal damping for taut cable
β	Rate of phase variation in traveling wave solution
β	Ratio of Reynolds number to Keuligan-Carpenter number
$\bar{\beta}$	Steepness parameter for linear sheared-flow profile
ς_r	Damping ratio in r-th mode
η	Mass parameter ($=\rho D^2/\mu$)
θ	Arbitrary phase term in applied force
θ_0	Arbitrary phase term in constant spanwise applied force
κ	Parameter in traveling wave solution (a function of α and β
λ	Wavelength of traveling wave
λ_n	n-th eigenvalue for taut cable, length L
μ	Mass of cable per unit length
ν	Kinematic viscosity of a fluid
ξ_i	i-th modal solution, as a function of time
ρ	Mass density of fluid
ρ_c	Mass density of cable
ρ_s	Mass density of cylinder

ϕ	Phase angle by which applied force lags velocity in traveling wave solution
$\bar{\phi}$	Phase angle of total displacement in traveling wave solution
$\bar{\phi}_i$	Phase of total displacement of i-th segment in traveling wave solution
$\bar{\phi}_0$	Phase of total displacement at end of active region for constant applied force
ϕ_r	Phase angle for r-th modal solution
Ψ	Phase angle
ψ	Phase angle
ω	Angular oscillation frequency (rad/sec)
ω_n	Angular natural frequency of system (rad/sec)
ω_r	r-th angular natural frequency (rad/sec)
ω_s	Angular Strouhal frequency (rad/sec)
ω_v	Angular vortex-shedding frequency (rad/sec)

CHAPTER 1

Introduction

When exposed to a flowing fluid, a structure may oscillate due to interaction between the body and fluid. Large amplitudes of motion and fatigue are potential sources of structural failure. A complete understanding of the nature of these vibrations is essential in the design of many civil and mechanical engineering components.

The nature of the motion of a structure in a flow depends on many factors, including the geometry of the body, the characteristics of the flow and fluid, and so on. Several quite distinct behaviors can be observed, and the methods of analysis for each vary accordingly. A brief introduction is given below.

1.1 Flow-Induced Vibration

Flow-induced vibrations can occur with both bluff and streamlined bodies in any fluid. Broadly speaking, the different types of behavior may be classified into the following groups.

- *Vortex Shedding:*

As fluid passes a bluff body, the flow separates from the body and rolls up into distinct vortices, which detach from the body and produce both in-line and transverse forces on the body at the frequency of the vortex shedding. This dissertation uses a vortex-shedding model, and a more detailed description of the phenomenon will be given later.

• *Galloping:*

Galloping is observed in some structures with certain cross-sectional shapes, such as "D" or rectangular sections. A commonly observed example is ice-coated power lines, where the modified cross section due to ice buildup is well shaped for this type of aeroelastic instability (see, for example, [11], pp.366-373.) The main characteristics of this type of response are large amplitude oscillations transverse to the flow, at frequencies much lower than the vortex-shedding frequencies for the same cross section. Unlike vortex shedding, there is no characteristic frequency associated with the flow. Motion of the structure in a natural mode produces the instability.

The basic driving force of galloping is the variation of the lift coefficient with the angle of attack of the flowing fluid. As the body moves, the relative velocity changes due to the structure velocity component. If, for a given section, the lift force increases as the body moves from its equilibrium position, then that body is potentially unstable.

As mentioned above, the galloping of power lines in cold climates has been commonly observed. There is not much literature on this phenomenon occurring in water, but this is probably due to the use of members which do not have an unstable cross section (for example, circular cylinders). The galloping conductor problem is due to modification of an otherwise stable shape by ice accretion.

• *Flutter:*

The term flutter has been used, with qualification, to describe a number of different types of flow-induced oscillation. References on the subject are extensive. [14], [64], and [66] give good introductions and point to more complete lists of references.

The term "classical flutter" refers to an unstable oscillation produced by the coupling of two degrees of freedom of the structure (torsional rotation and translation). Classical flutter is observed even if the body is streamlined and no flow separation occurs. The phenomenon was, in fact, first observed in airfoils.

Flutter in a single-degree-of-freedom is also observed. "Stall flutter" describes a torsional mode of airfoil vibration produced by the nonlinear characteristics of the lift force near a stall condition. Structures in strongly separated flows may also undergo torsional vibration, but this is usually associated with non-streamlined bodies, such as bridge decks. This latter case is not a stall flutter, per se.

Flow along a structure can also excite a condition called panel flutter. While mainly observed in supersonic flows, phenomena such as flag or tent flapping are related examples.

The above described fluid-induced vibrations can occur for structures in a reasonably undisturbed uniform or oscillating flow. The presence of structures upstream in a flow can cause changes in the incident flow which also may excite a body into motion. Examples of this are buffeting, due to turbulence in the flow, and wake galloping, where the variation of the lateral pressure across the wake of one body can produce large motions in another downstream.

More complete descriptions of the above phenomena may be found in the references listed, and [66] gives useful introductions to the analysis of each.

1.2 Vortex-Induced Vibration

The work outlined in this dissertation concentrates on the structural aspects of the flow-induced vibration problem. While the approach developed could be applied to any of the above types of behavior, vortex shedding was used as the mechanism of

the exciting force.

The motivation for this choice is the susceptibility of many "long" structures in the marine environment to vortex shedding. Mooring cables, towed arrays and drilling risers are all subjected to sometimes large cross-flows which lead to vortex-induced forces.

An introduction to some of the important characteristics of vortex shedding as a basis to the following work is given below.

1.2.1 Vortex Shedding from a Bluff Body

Figure 1.2.1 shows the basic flow regimes around a **stationary** cylinder in a flow. The Reynolds Number, Re, for the flow is defined as

$$\mathrm{Re} = \frac{UD}{\nu} \tag{1.2.1}$$

where U is the free stream fluid velocity, D is the diameter of the cylinder, and ν is the kinematic viscosity of the fluid.

At very low Reynolds Numbers, the streamlines follow the shape of the body, and the flow does not separate. As the Reynolds Number increases, a pair of fixed Foppl vortices is formed in the wake; then for Re greater than about 40, vortices are shed periodically from alternating sides of the body. Vortex shedding occurs throughout the range of Reynolds Numbers from 40 to about $3\text{x}10^5$, being laminar in the lower range, then becoming turbulent in the latter part. Throughout the transcritical range, regular shedding disappears, but re-establishes itself in the supercritical Re range.

When the body is fixed, the vortex-shedding frequency, ω_v equals the Strouhal frequency, ω_s defined by

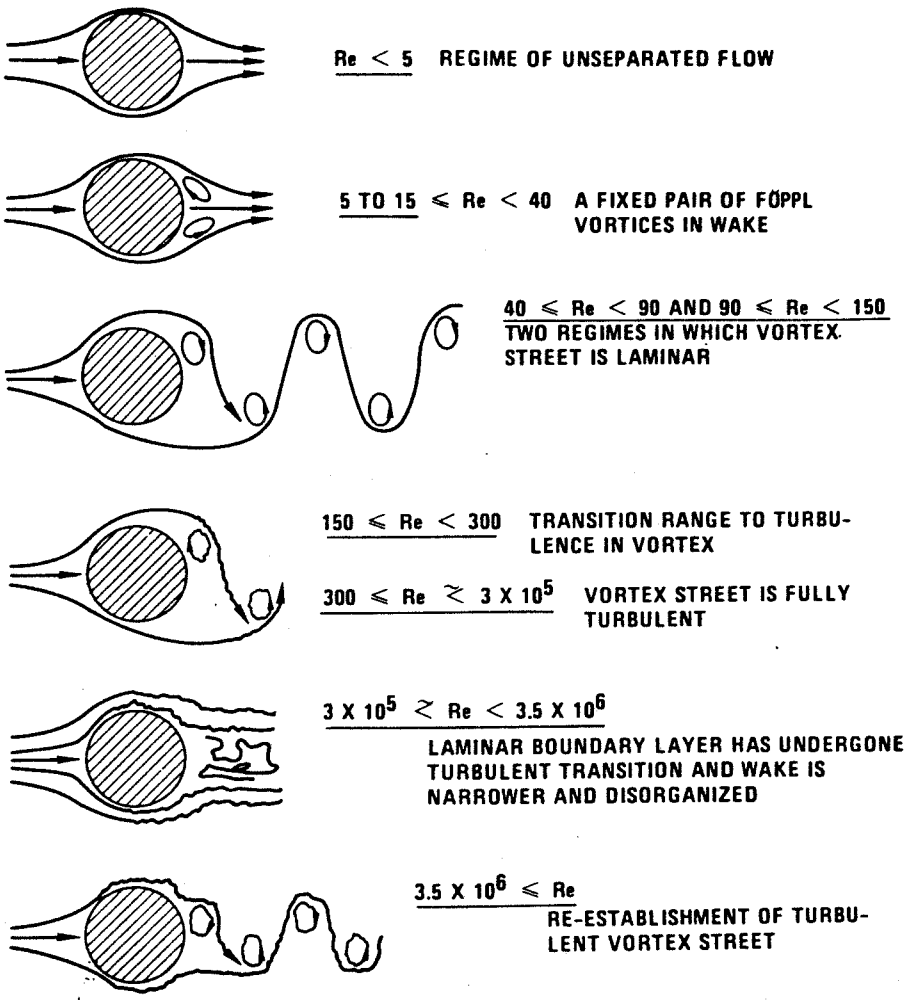

Figure 1.2.1. Regimes of Fluid Flow Around a Circular Cylinder [8]

$$\omega_s = 2\pi S \frac{U}{D}. \tag{1.2.2}$$

S, the Strouhal Number, depends on the Reynolds number and the geometry of the body. The variation of S with Re for a cylinder is shown in Figure 1.2.2. The Strouhal Number is well defined for all but the transcritical range of Reynolds Numbers. For simplicity, unless the exact Reynolds Number is known, the value of S is taken as 0.2 for a cylinder.

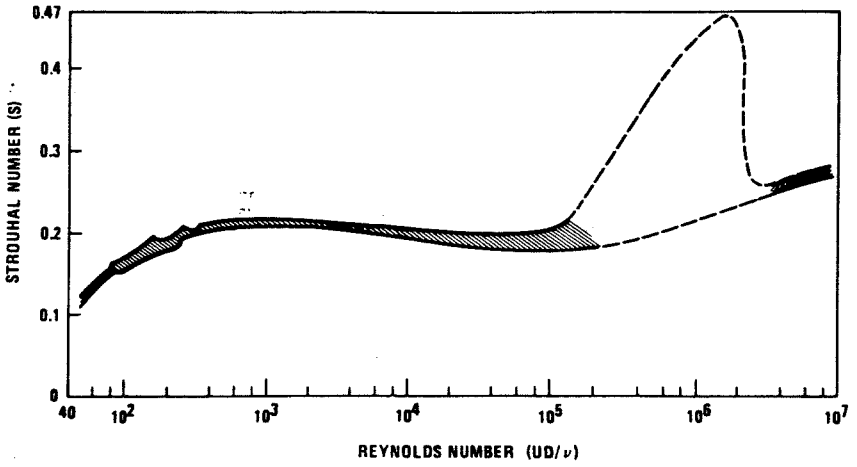

Figure 1.2.2. Strouhal Number versus Reynolds Number for a Circular Cylinder [8]

1.2.2 Effect of Motion of the Body

The shedding of vortices from alternate sides of the body results in a periodic transverse force on the body. If the body is flexible, or flexibly mounted, it will move when subjected to this force. This motion of the body has several effects on the flow:

- The strength of the shed vortices is increased [16].
- The spanwise correlation of the wake is increased [72].
- The frequency of vortex shedding is locked on to the cylinder vibration frequency if the two frequencies are close [5].
- The drag force is increased [5].

The body motion results in a more structured wake than in the stationary case. The moving body is able to feed energy into the fluid, increasing the circulation of the vortices, thereby increasing the force applied to the body. This increase in the "order" of the wake is also manifested in the spanwise direction, as evidenced by the increase in the correlation of the vortex shedding along the span with increasing vibration amplitude.

When a system with a natural frequency ω_n is exposed to a flowing fluid, the frequency of oscillation, ω, is not necessarily equal to the Strouhal frequency, ω_s as defined above. A phenomenon known as frequency entrainment, or lock-in, occurs, whereby the frequency of vortex shedding becomes very close to the natural frequency of the structure. This occurs when the amplitude of vibration becomes large enough to enable the body motion to take control of the shedding process. These large amplitudes occur when a structure is excited at, or near, a natural frequency.

When the body vibrates transversely to the flow, the effective cross-sectional area projected to the flow is increased. The in-line drag force depends on the projected area, and therefore, tranverse vibration can increase the drag force depending on the amplitude of the vibration.

1.2.3 Vortex-Induced Vibration of Long Structures

Field observations [1], confirmed recently by experiment [36,37], have indicated that the lock-in phenomenon, as described in the previous section, does not occur for cable systems where the length-to-diameter ratio is very large (greater than 10^4). There are several reasons for this behavior.

First, as the length of a cable is increased, the difference between consecutive natural frequencies becomes smaller. For large length to diameter ratios, the frequencies are so close that the assumption of lock-in to a single mode is not valid.

Second, the frequency of excitation due to vortex shedding is proportional to the flow velocity. Excitation of the system in one mode requires a reasonably uniform velocity profile. In reality, the flow profile is somewhat nonuniform and the disruption to the shedding process hinders the formation of locked-in response.

The term "lock-in" means that vortices are shed at a frequency corresponding to a particular structural mode of the system. A mode is a standing wave produced by the summation of traveling waves which have been reflected and transmitted by the appropriate boundaries of the system. For example, consider the taut string in Figure 1.2.3.

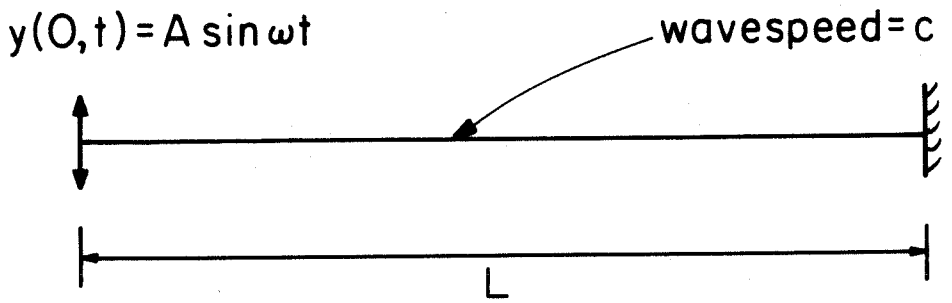

Figure 1.2.3. Example of Long, Damped String

The string is fixed at the right-hand end, and forced at the left-hand end with a sinusoidal excitation equal to one of the undamped natural frequencies. Assume that there is damping present proportional to the string velocity. Initially, a wave is produced which travels from left to right down the string. When this wave reaches the right-hand end, it is reflected from the fixed boundary, and returns along the string in the opposite direction. Upon reaching the left end again, it is reflected once more in such a way as to satisfy the force or displacement boundary condition imposed there. Due to the damping in the system, a steady state will be reached consisting of a left and right traveling wave. The string exhibits a standing wave pattern produced by the interaction of these traveling waves.

If the string is very long and the damping sufficient, waves produced at one end of the string will be of negligible amplitude by the time they reach the other end. It is unlikely that a mode will be produced, as a steady-state condition may never be reached. For the above example, the string is better treated as a semi-infinite string. A traveling wave solution may be sought to the problem, rather than a modal solution.

1.3 The Focus of This Investigation

In the current investigation, a new approach to the vortex-induced vibration problem is presented. In a deviation from the customary modal solution to such problems, a method based on traveling waves is used. This approach is found to be particularly suited to the long cable problem outlined above.

Existing fluid models are adapted to the traveling wave solution for the cable. In particular, the model developed by Iwan and Bothelo [32], based on the experimental results of Sarpkaya [60] is used. The wake oscillator model first proposed by Iwan and Blevins [28], then later modified by Hall and Iwan [26], could also be adapted, although this is considered a topic for future work.

For simplicity, the cable is considered to behave as a taut string. This approximation avoids the inclusion at this stage of additional nonlinear terms in the equation for a slack cable due to the geometry. For many real systems, the curvatures and displacements are sufficiently small that the above assumption is quite accurate. Both linear and nonlinear damping forces on the cable are considered. The fluid model used for the vortex-shedding force is, of course, nonlinear in nature.

The fluid forces acting on the inactive part of the cable (i.e., a region where vortex shedding is not exciting the cable) are modeled using Morison's equation [43]. This

gives a more realistic treatment of the cable damping than a viscous damping approximation.

An approach to the problem of nonuniform flows by the use of the traveling wave method is presented. The response at a point on the string is described in terms of the maximum expected or root-mean-square amplitude of the motion.

1.4 Structure of This Thesis

In Chapter 2, a brief historical review of the subjects pertinent to this research is given. This includes the vortex-induced vibration model developed by Bothelo and the use of the Morison equation for the fluid force on oscillating bodies. Problems associated with existing analysis methods are addressed, and the motivation behind the new approach is outlined.

Chapter 3 presents the basic formulation of the model, including the specialization of Bothelo's work to this approach, the derivation of the basic traveling wave solutions, and the combination of the two into a fluid-structure model for long cables. The techniques for the summation of the traveling wave solutions are outlined. The use of Morison's equation for the inactive regions of the cable is illustrated using the new algorithm.

Based on the analysis in Chapter 3, an approximate technique is developed in Chapter 4 to handle nonuniform flow profiles. In most marine environments, the current profiles are not uniform, so the approach developed in this chapter is necessary for the analysis of such systems.

In Chapter 5, results derived from the analyses of the preceding two chapters are presented and discussed. Comparisons with traditional modal approaches are given

and discussed in the context of the amplitude and frequency response.

A summary, conclusions, and ideas for future work are given in Chapter 6.

CHAPTER 2

Background Material and Previous Work

2.1 Historical Introduction

For many centuries, the effects of flow-induced vibration have been used to generate musical tones, predominantly in wind instruments. The design of these instruments was essentially empirical as there was little understanding of the physics of the generating process.

While da Vinci, in the fifteenth century, had sketched vortices in a flow behind various bluff bodies, it was not until 1858 that the first systematic investigation of vortex-induced vibration was attempted by Strouhal [71]. Through a simple experimental setup (recently reproduced by Hall [25],) Strouhal was able to show that the tones produced by a taut wire in an air stream were proportional to the relative air velocity divided by the diameter of the wire. He also observed that the intensity of the sound produced increased greatly when the vortex-shedding frequency coincided with the natural frequencies of the wire.

Despite Strouhal's discoveries of modal interaction and frequency entrainment, he did not appear to understand the latter phenomenon, and also was under the impression that the wire oscillated parallel to the flow. Rayleigh, in 1879, recognized vortex sheet instability as the source of the vibration and demonstrated experimentally that the wire actually vibrates predominantly perpendicular to the flow [50, Vol. II, pp. 412-413].

The mechanism of vortex shedding and the structure of wakes were investigated by von Karman [73], who was able to show theoretically why the vortices are shed asymmetrically, and to predict the ratio of the longitudinal to lateral spacing of the vortex centers. Von Karman's pioneering analysis has been followed by numerous studies of vortex wakes and the lift and drag forces on bodies in separating flows. The early 1940's brought observations on the response of bodies allowed to vibrate under the influence of the vortex forces. It was not until 1964, however, that the existence of a nonlinear fluid oscillator was hypothesized, first by Bishop and Hassan [5] and later the same year by Marris [40]. Marris' work first outlined the use of the Van der Pol-type equation for the fluid force, based on potential flow considerations for a rotating body in a cross-flow.

Many investigations have followed, experimental [4, 5, 13, 15, 33, 38, 44, 45, 47, 48, 51, 56, 58, 59, 72, 74], theoretical [6, 7, 18-22, 25-31, 34, 41, 54, 60, 62, 65, 67, 68, 69], and theoretical-experimental [9, 17, 32, 39, 49, 53, 70]. The recent increase in the availability of computing resources has led to the development of codes for finite element analysis of the vortex flows and forces associated with fixed bodies. These codes in general are very computation-intensive and have not as yet been applied to moving bodies, precluding their use from the vortex-induced vibration problem. It is anticipated that future work in this area will enable a greater understanding of the problem.

A number of review or "state of the art" publications [3, 8, 23, 40, 61] outline the recent advances in the field at the time of writing and present extensive reference lists.

2.2 Experimental Observations of Vortex-Induced Response

2.2.1 Vortex Shedding from Oscillating Cylinders

Of the investigations referred to above, the work of Sarpkaya [59, 60] was chosen as the basis for this work because of its completeness and use in the modeling approach of Bothelo [9, 32]. Bothelo fitted Sarpkaya's data with interpolation curves which are used to model the vortex-induced forces on the systems considered. The work of Bothelo is discussed more fully later.

Sarpkaya forced a circular cylinder of diameter D to oscillate transversely in a flow channel containing a fluid of density ρ traveling with a fixed velocity, U. The amplitude, A, and frequency, ω, were fixed for a given run, and the force required to impose the displacement on the cylinder was measured as a function of time. Observation of the time histories of the force (Figure 2.2.1) indicates the contribution of components at frequencies other than the exciting frequency when the Strouhal frequency and exciting frequency are not close. A Fourier decomposition was made of the measured in-phase and out-of-phase components of the force in terms of the exciting frequency. It should be recognized that this Fourier analysis will in general not retain the components at the Strouhal frequency, and so the beating phenomenon sometimes observed [59, 70] cannot be modeled.

For a displacement given by

$$Y = A\,Sin\omega t \tag{2.2.1}$$

the force is written by Sarpkaya as

$$F(t) = \tfrac{1}{2}\rho DU^2\left(C_{mh}\,Sin\,\omega t - C_{dh}\,Cos\,\omega t\right). \tag{2.2.2}$$

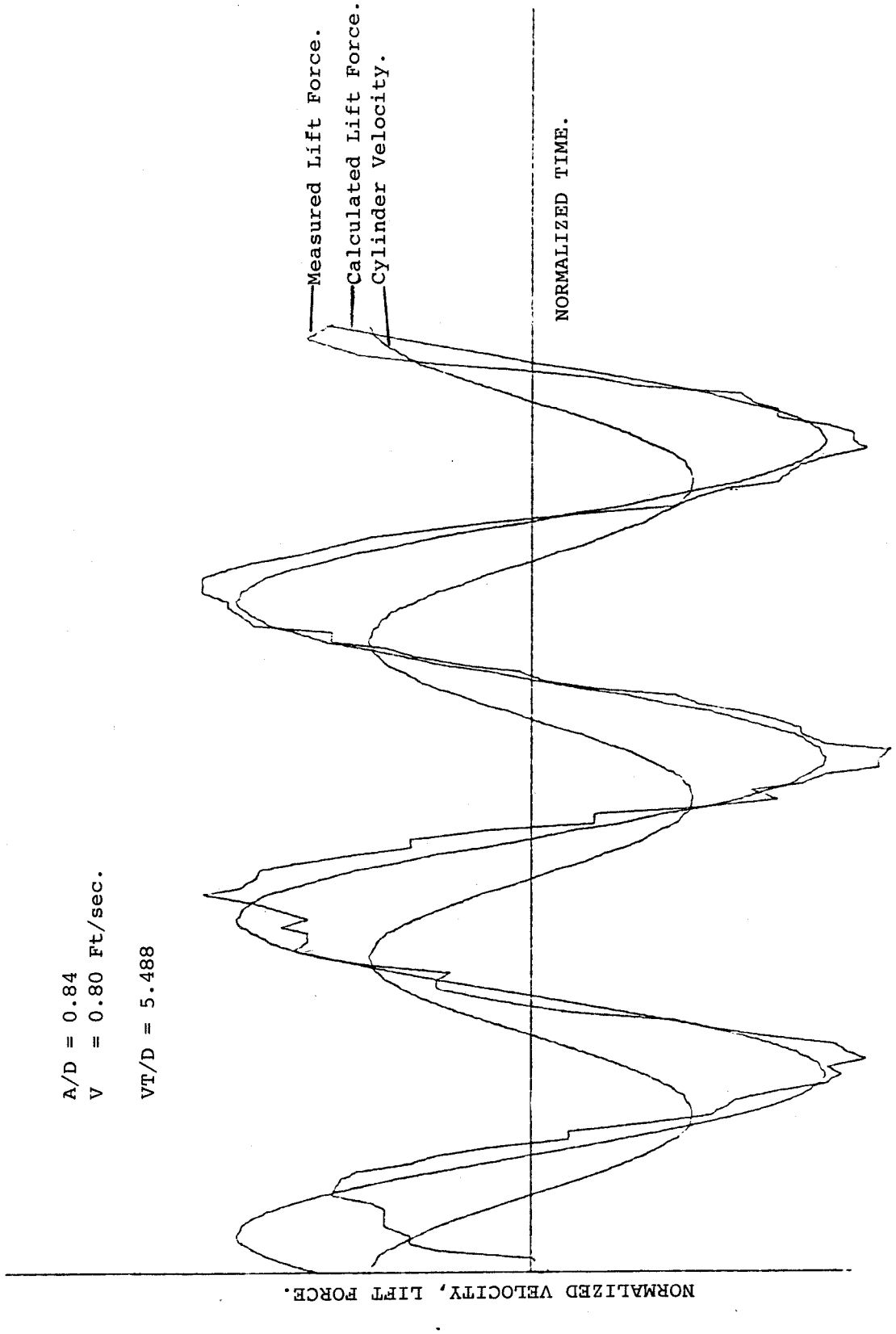

Figure 2.2.1. Measured and Computed Time Histories of Lift Force (from [59])

C_{mh} is the inertia coefficient, and C_{dh} the drag coefficient. Both coefficients are functions of the normalized amplitude, $B(=A/D)$ and the reduced velocity, V_r defined as

$$V_r = \frac{1}{S\frac{\omega}{\omega_s}}. \tag{2.2.3}$$

That is,

$$C_{mh} = C_{mh}(B,V_r) \tag{2.2.4}$$

$$C_{dh} = C_{dh}(B,V_r). \tag{2.2.5}$$

Figures 2.2.2 and 2.2.3 show C_{mh} and C_{dh} versus V_r for various values of the normalized amplitude.

Recent analysis of Sarpkaya's results by Bothelo [9] suggests that there are some inconsistencies in the inertia and drag coefficient data. The data points corresponding to what is presumably one test run do not line up on the reduced velocity axis. Based on the results from an analytical investigation, Bothelo suggests that the C_{mh} are indeed shifted to the right, and uses for his work an assumed zero crossing of $V_{r0} = 5.0$, rather than 5.15 as is indicated by Figure 2.2.3. Consequently, the maximum negative value of C_{dh} occurs when $C_{mh} = 0$. This correction is assumed in the remainder of this dissertation.

2.2.2 Response of Long Cable Systems

Until quite recently, investigations of vortex-induced vibrations of structures were primarily conducted in a laboratory environment. Observations and measurements were made on both rigid and flexible cylinders vibrating transversely in

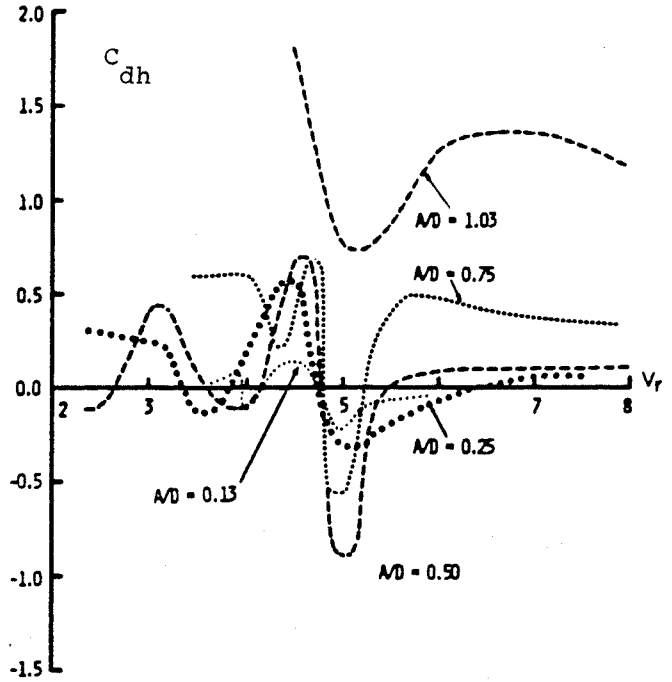

Figure 2.2.2. Experimentally Measured Drag Coefficients C_{dh} versus Reduced Velocity for Various Values of Normalized Amplitude (from [60])

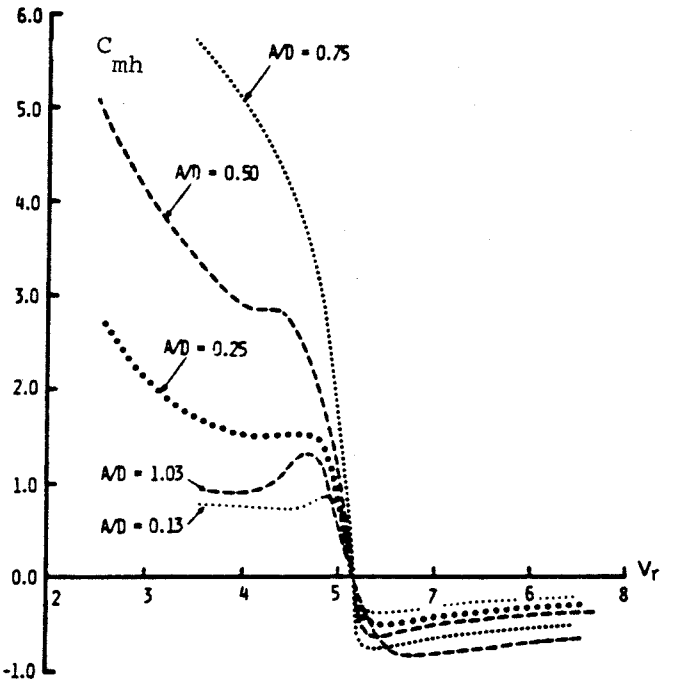

Figure 2.2.3. Experimentally Measured Inertia Coefficients C_{mh} versus Reduced Velocity for Various Values of Normalized Amplitude (from [60])

uniform cross-flows. Emphasis was based on the characteristics of the shedding process, particularly in the region of lock-in. Forced rigid cylinders enabled the study of the drag and inertia forces as the frequency of oscillation was varied near the Strouhal shedding frequency. For flexible models, the relatively short test cylinders or cables used resulted in well-separated modal frequencies, reducing the effects of modal interaction, and enabling single-mode lock-in to be studied in some detail.

In the field, excitation of real structures near a structural natural frequency has also demonstrated the effects of lock-in. Large amplitudes of transverse motion have been observed, as the synchronization of the vortex shedding and the structural vibration results in a large energy input to the structure.

Drag coefficients in the direction of the flow are increased by the transverse oscillation of a structure. For a cylinder vibrating transversely to a uniform incident flow, the drag amplification at lock-in has been approximated by Skop, Griffin and Ramberg [69] as

$$\frac{C_d}{C_{d0}} = 1 + 1.16\left(2\frac{A}{D}\right)^{0.65} \qquad (2.2.6)$$

where A is the amplitude of oscillation, C_d the effective drag coefficient for the vibrating cylinder, and C_{d0} the drag coefficient of the cylinder at rest. Subsequent experimental work [42] confirmed the validity of Equation (2.2.6) as a means of estimating the effective drag coefficients. Average values of C_d greater than 3.0 were recorded for short cables vibrating in a locked-in condition.

The large increase in the drag coefficient results in large forces on the structure parallel to the flow. These large design loads often create problems for the designer in long cable systems.

Based on field observations, Alexander [1] concluded that a locked-in condition and standing wave profile apparently did not occur in a series of tests on long wires towed in the ocean. Amplitudes of vibration generally were substantially lower than what would be predicted by a conventional modal analysis, assuming a locked-in state. It was noted that the shedding appeared to be progressive, producing waves which traveled along the cable and were damped relatively quickly by the fluid.

A significant consequence of this observation is that the drag coefficients generally used for this type of system were probably grossly overestimated. If more reasonable bounds on the expected amplitudes were found, the design loads for long cables could be reduced, and a more efficient structure produced.

More recently, Kim, Vandiver and Holler [37] conducted a series of experiments on long cables subjected to various ocean currents. This work confirmed the traveling wave behavior and absence of lock-in for systems of this type, first observed by Alexander. Frequency spectra recorded at a number of points along the cable indicated the contributions of excitation at many frequencies, not a single-mode lock-in behavior. Consideration of root-mean-square responses over particular frequency intervals also confirmed the importance of hydrodynamic damping in "localizing" the effects of vortex shedding (i.e., vortex shedding at one point on a long cable has little effect on the cable motion at relatively large distances from the excitation).

Kim [36] proposed the use of an infinite string formulation, and presented some analysis based on modeling the vortex-induced forces using a random spanwise lift coefficient. The extension of this approach to a useful design tool was not performed, and the interaction of "active" regions (i.e., parts of the cable where vortex shedding is forcing the cable) and "inactive" regions (where the fluid is passively resisting the

cable motion) was not considered.

2.2.3 Effects of Sheared Flow on Vortex-Shedding Characteristics

Many investigators have studied the effects of uniform flows on cables and other structures. Based on this work, a number of models, both empirical and theoretical, have been proposed for the analysis of the vortex-induced vibration problem. Some of these models are discussed in the next section. Virtually all of these models are two-dimensional in nature, assuming a completely in-phase, monofrequency shedding of vortices along the span.

The case of nonuniform, or, more specifically, sheared flows has not been investigated to the same extent as the uniform flow case. In the last 15 years, a number of studies have looked at the characteristics of the vortex shedding, and the response of cylinders and cables in sheared flows. A comprehensive review is given in [24].

Sheared flows are often approximated as linearly varying velocity profiles. A "steepness parameter," β, is defined for the incident velocity gradient as

$$\beta = \frac{D}{V_{ref}} \frac{dV}{dx} \tag{2.2.7}$$

where $\frac{dV}{dx}$ is the velocity gradient and D is the cylinder diameter. The reference velocity, V_{ref}, is usually taken as the mean (midspan) or, sometimes, the maximum velocity of the incident flow. In practice, for ocean or atmospheric environments, β is small, say less than 0.03 [24].

A number of quite detailed studies of the effects of sheared flows on flexible cables have been performed (for example, [46, 75]). For both fixed and oscillating cables, finite

length "cells" of vortex shedding were observed to occur along the span for low enough values of the shear parameter, $\bar{\beta}$. Figures 2.2.4 and 2.2.5 show examples of the cellular structure of the vortex shedding. In both cases, $\bar{\beta} = 0.0053$ and the Reynolds Number, based on the midspan flow velocity was, $\mathrm{Re}_m = 2.96\mathrm{x}10^3$. Figure 2.2.4 shows the results for a stationary cable, and Figure 2.2.5 the results for the same cable forced to oscillate in its first mode with an amplitude of 0.29 diameters. The parameter St_m is the Strouhal number based on the midspan incident fluid velocity, U_m; i.e.,

$$St_m = \frac{\omega_s}{2\pi}\frac{D}{U_m} \tag{2.2.8}$$

where ω_s is the observed frequency of vortex shedding at a particular location on the cable. Regions of constant St_m indicate cells of shedding at a constant frequency.

The cellular structure in the stationary case is fairly uniformly distributed along the cable span. When vibrated in its first mode, a significant region of lock-in is apparent over the central portion of the span.

Clearly, both the vibration amplitude and the steepness of the incident velocity profile affect the coherence of the vortex shedding along the span. This is illustrated in Figure 2.2.6. The frequency difference which can be sustained in a shear flow clearly increases to a maximum as the amplitude of vibration increases. Therefore, increasing the amplitude tends to increase the coherence length.

As discussed in the preceding section, the amplitudes of vibration of long cables have generally been observed to be lower than the single frequency, locked-in response of shorter systems. Figure 2.2.6 suggests that, for low amplitudes, a coherence length corresponding to a frequency difference of about 0.2 is probably a reasonable approximation. This is discussed further in Chapter 4.

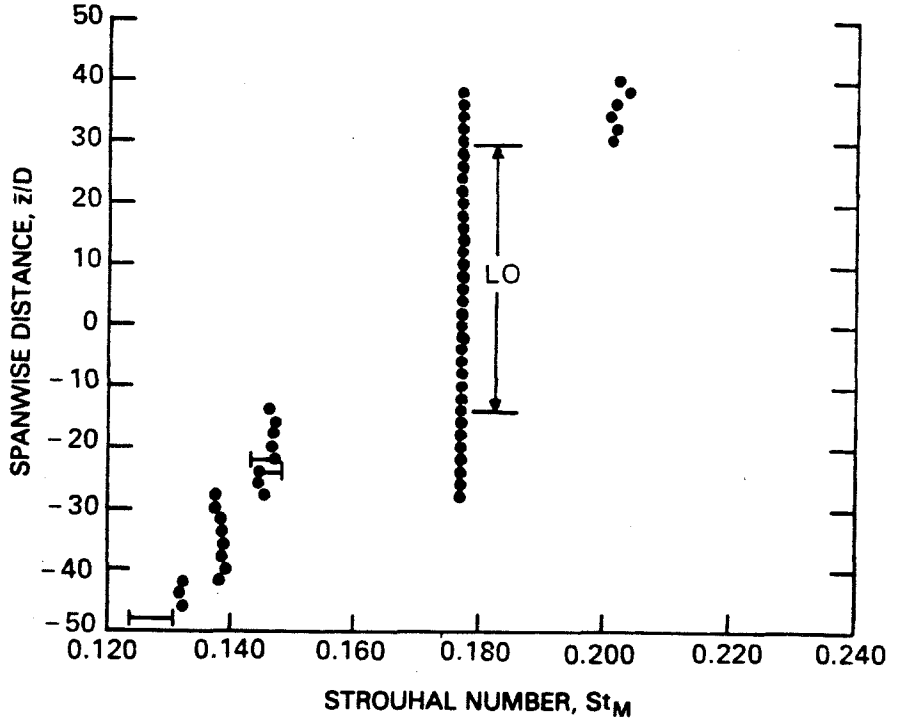

Figure 2.2.4. Local Strouhal Number, St_m versus Spanwise Distance - Stationary Cable (from [46])

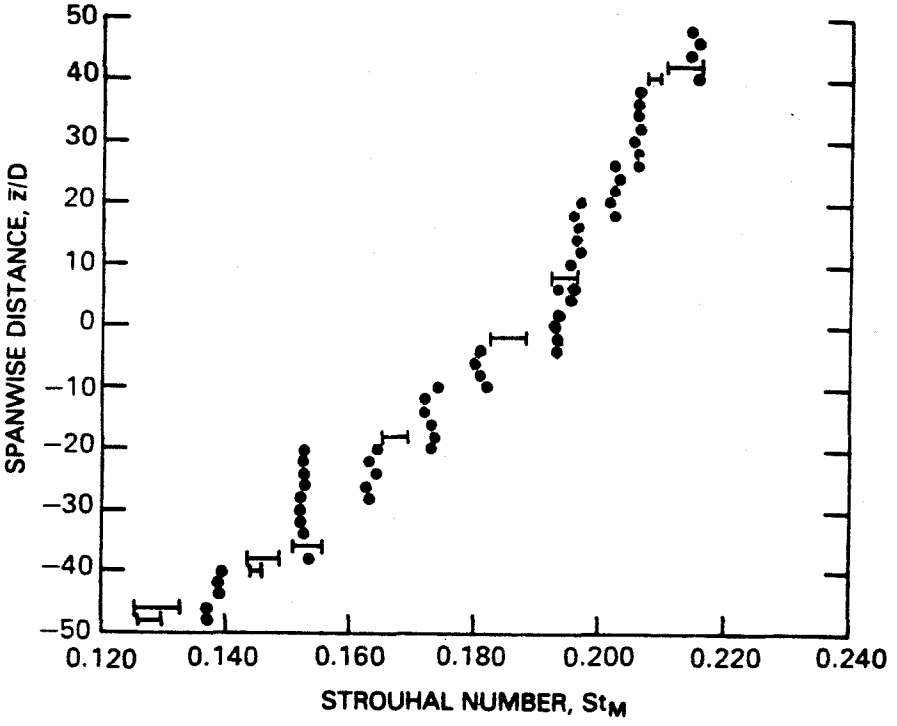

Figure 2.2.5. Local Strouhal Number, St_m versus Spanwise Distance - Vibrating Cable (from [46])

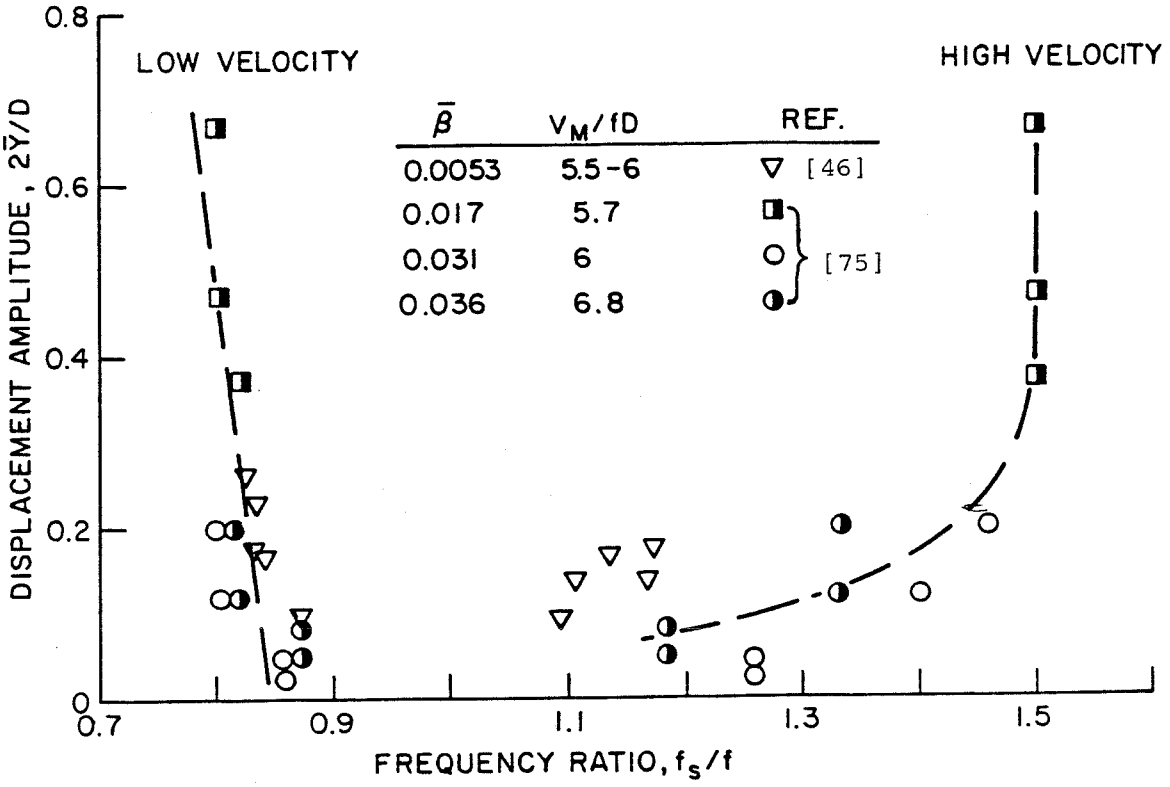

Figure 2.2.6. Local Amplitude and Frequency Boundaries for Lock-In in a Shear Flow (from [46, 75])

Unfortunately, virtually all of the studies of sheared flow have been performed in laboratories, where space limitations restrict the size of the models which can be used. Reference to "long" cables in the context of laboratory experimentation generally means that the models are long enough to minimize "end effects" in the experiments. "Long," as discussed Section 2.2.2, refers to systems with length-to-diameter ratios of order 10^4 or more. While more work is clearly needed to understand the effects of sheared flows on cable systems with these high length-to-diameter ratios, the observations briefly outlined above give some guidance in the modeling techniques

employed in Chapter 4.

2.3 Modeling Vortex-Induced Vibration

2.3.1 Analytical Models

Based on a series of experiments in which a cylinder was oscillated transversely in a flow, Bishop and Hassan [4] observed that the response could be qualitatively described by means of a nonlinear, self-excited fluid oscillator. This idea was later developed by Hartlen and Currie [27], who proposed the lift-oscillator model. This model assumed that the lift coefficient, describing the force transverse to the flow, could be represented by the Van der Pol equation. By performing a curve fit of observed data with response diagrams for the Van der Pol oscillator, they were able to confirm that Bishop and Hassan's idea was indeed a valid way to approach the problem. The lift-oscillator model has been more recently extended by Skop and Griffin [67, 68], who refined the method of parameter selection.

A major drawback of the above described approaches is that the fluid model is somewhat arbitrarily derived, based on qualitative observations, then made to produce a "best fit" of the available data. Marris [40] made the first attempt to motivate the use of the Van der Pol equation based on a potential flow analysis of an analogous case: a rotating cylinder in a constant flow. In 1974, Iwan and Blevins [28] developed the wake-oscillator model, which derived a fluid oscillator representation based on first principles. From consideration of the average transverse momentum in a control volume around a cylinder in a constant flow, it was shown that the fluid could be approximately represented by a hidden flow variable, z, which satisfied the Van der Pol equation. Parameters for the model were extracted from experimental data by considering special cases of the solution (for example, fixed or forced cylinders

in a flow).

Later applications of the wake-oscillator model included spanwise flexible structures [29], and nonuniform systems (attached masses) [30]. In 1981, Hall and Iwan [26] corrected the omission of a buoyancy term from Blevins' derivation, corresponding to a uniform acceleration of the body and the fluid. In addition, Hall studied the effects of modal interference (two modes) by considering four coupled nonlinear differential equations instead of the normal two, and was able to predict lock-in behavior successfully.

The inertia and drag coefficients, C_{mh} and C_{dh}, as defined in Section 2.2.1, can be derived from the models described above. Figure 2.3.1 shows these coefficients for the model and parameters in [28] (based on experiments performed in air and water), while Figure 2.3.2 shows the corresponding curves from [26] (model parameters based on experiments in air only). While the details of the two sets of coefficients are different, the general trends are the same. They may be compared with the corresponding curves in Section 2.2.1 and the interpolation curves discussed in the next section.

2.3.2 Empirical Models

In a new approach to the analysis of the vortex-induced vibration problem, Iwan and Bothelo [32] proposed an analytical-empirical model using the data of Sarpkaya as described in Section 2.2.1. Rather than formulating the problem in terms of two coupled differential equations of motion, one linear representing the structure, and one a nonlinear self-excited oscillator modeling the fluid, Bothelo assumed the force to be given as in Equation 2.2.2 and the displacement to be sinusoidal at the Strouhal frequency or the exciting frequency, depending on the model. This results in a

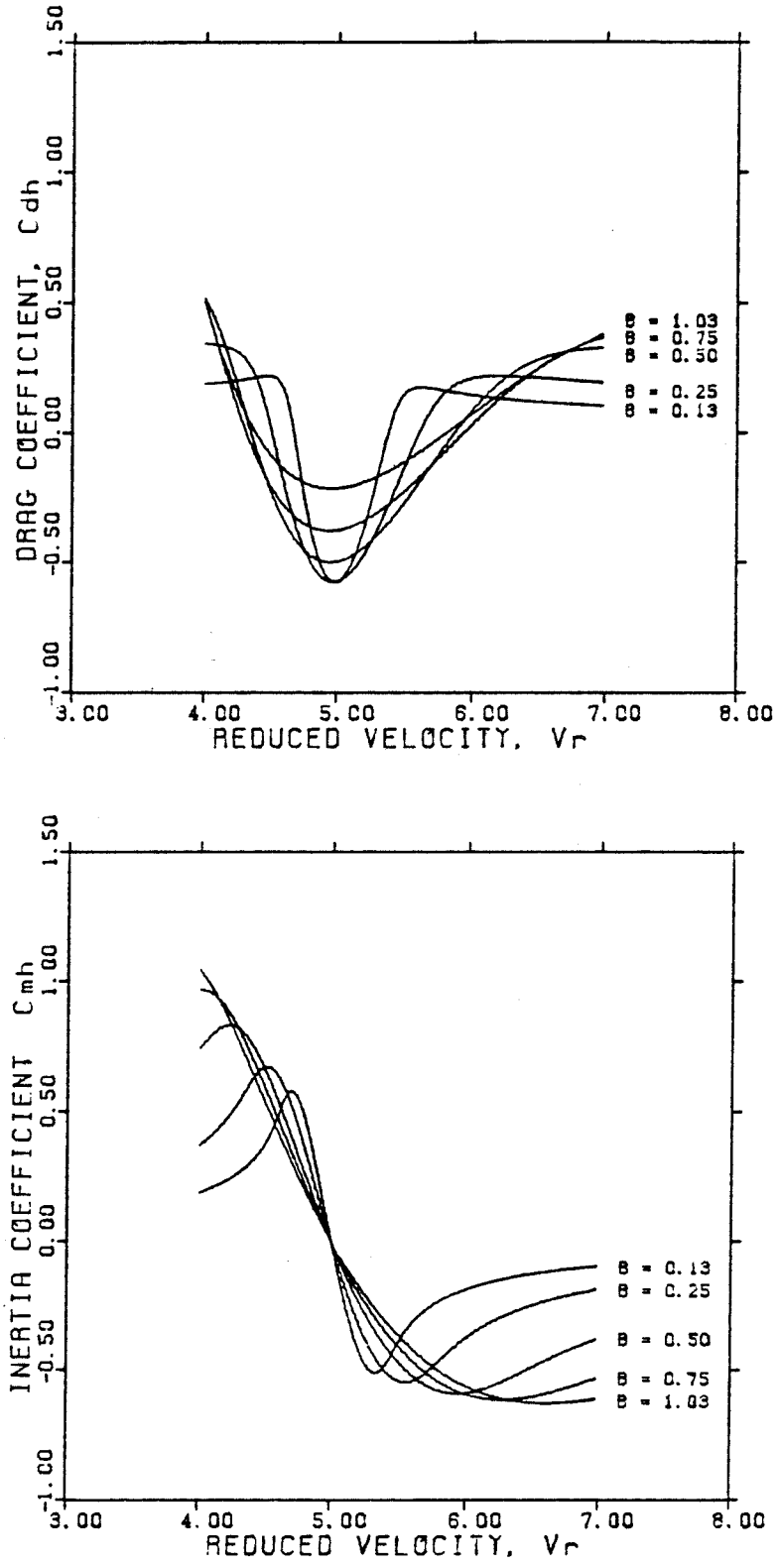

Figure 2.3.1. Predicted C_{dh} and C_{mh} versus Reduced Velocity from Blevins' Model

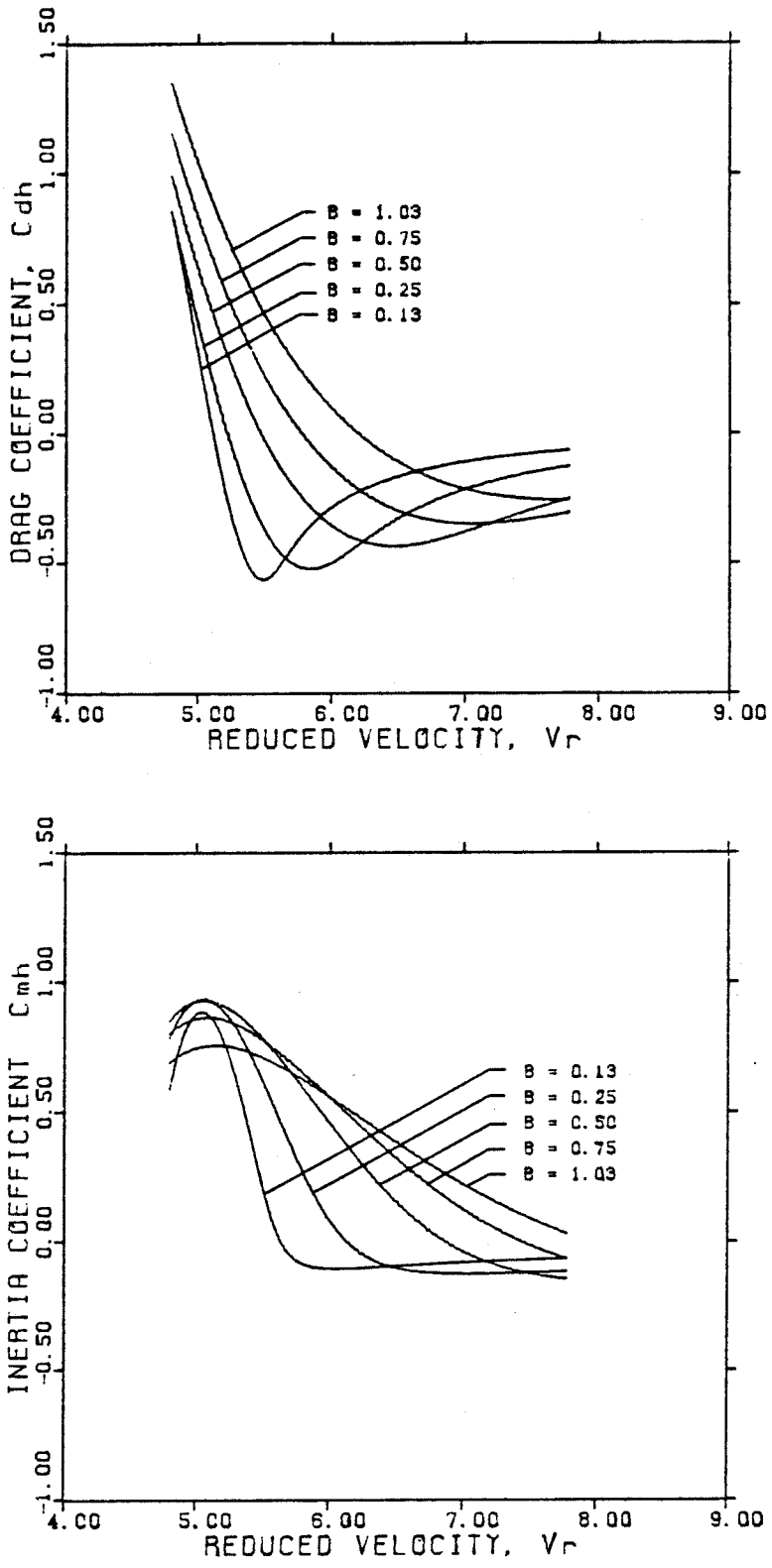

Figure 2.3.2. Predicted C_{dh} and C_{mh} versus Reduced Velocity from Hall's Model

pair of nonlinear algebraic equations, rather than differential equations.

Bothelo proposed two distinct models: a lock-in model and a non-lock-in model. A synopsis of each is given below.

2.3.2.1 The Lock-in Model

Consider the spring-mounted cylinder shown in Figure 2.3.3.

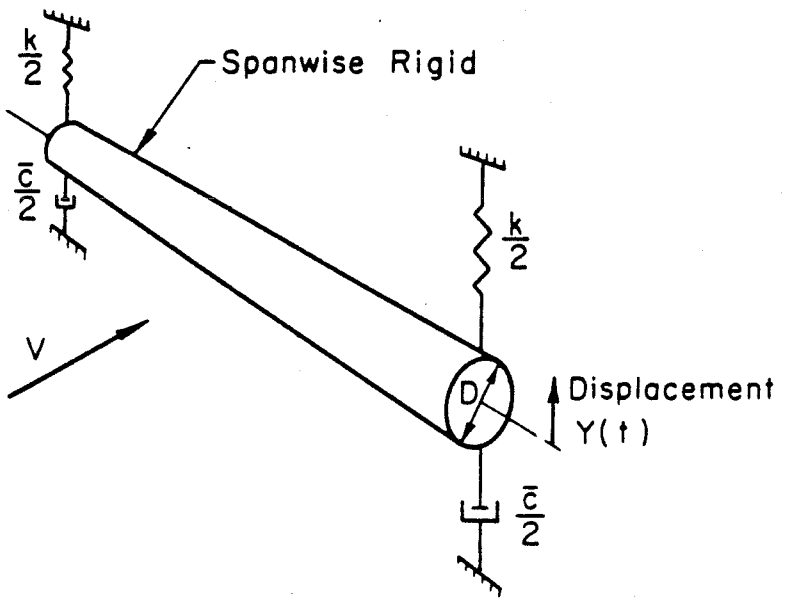

Figure 2.3.3. Spring-Mounted Rigid Cylinder (from [9])

Assume a displacement of

$$Y = A\ Sin\omega t; \tag{2.3.1}$$

then, the differential equation of motion may be written in terms of structural parameters per unit length as

$$m\frac{d^2Y}{dt^2} + \bar{c}\frac{dY}{dt} + kY = F(t) \qquad (2.3.2)$$

where m is the mass per unit length, $\bar{c}$ a viscous damping coefficient per unit length, and k a stiffness per unit length. The applied force may be written

$$F(t) = \tfrac{1}{2}\rho DU^2\left(C_{mh}Sin\omega t - C_{dh}Cos\omega t\right). \qquad (2.3.3)$$

Solution of (2.3.2) and (2.3.3), assuming (2.3.1), yields a pair of nonlinear algebraic equations which must be solved for the amplitude and frequency of response. Note that the drag and inertia coefficients are functions of both amplitude and frequency.

To implement a solution, the drag and inertia coefficients presented by Sarpkaya (Figures 2.2.2 and 2.2.3) were fitted with a series of interpolation curves which were functions of both the normalized amplitude, and the reduced velocity. These curves are shown in Figure 2.3.4.

2.3.2.2 Non-Lock-In Model

In the previous model, the frequency of oscillation was an unknown, found from the solution of a pair of nonlinear algebraic equations. In cases where the Strouhal frequency is far removed from a natural frequency of the system, a different formulation is necessary. In the absence of lock-in, the frequency of oscillation may be taken as equal to the Strouhal frequency, ω_s. However, the phase of the vibration is an unknown in this case. In the lock-in model, the relative phasing of the force and the displacement are given by the variation of the magnitudes of the drag and inertia coefficients with frequency. In the non-lock-in formulation, the frequency is known, so to enable a force balance, the displacement must shift by a constant phase relative to the force. The phase depends on the inertia and drag coefficients corresponding to $\omega = \omega_s$, and the natural frequency and damping of the system. Note that C_{dh} and

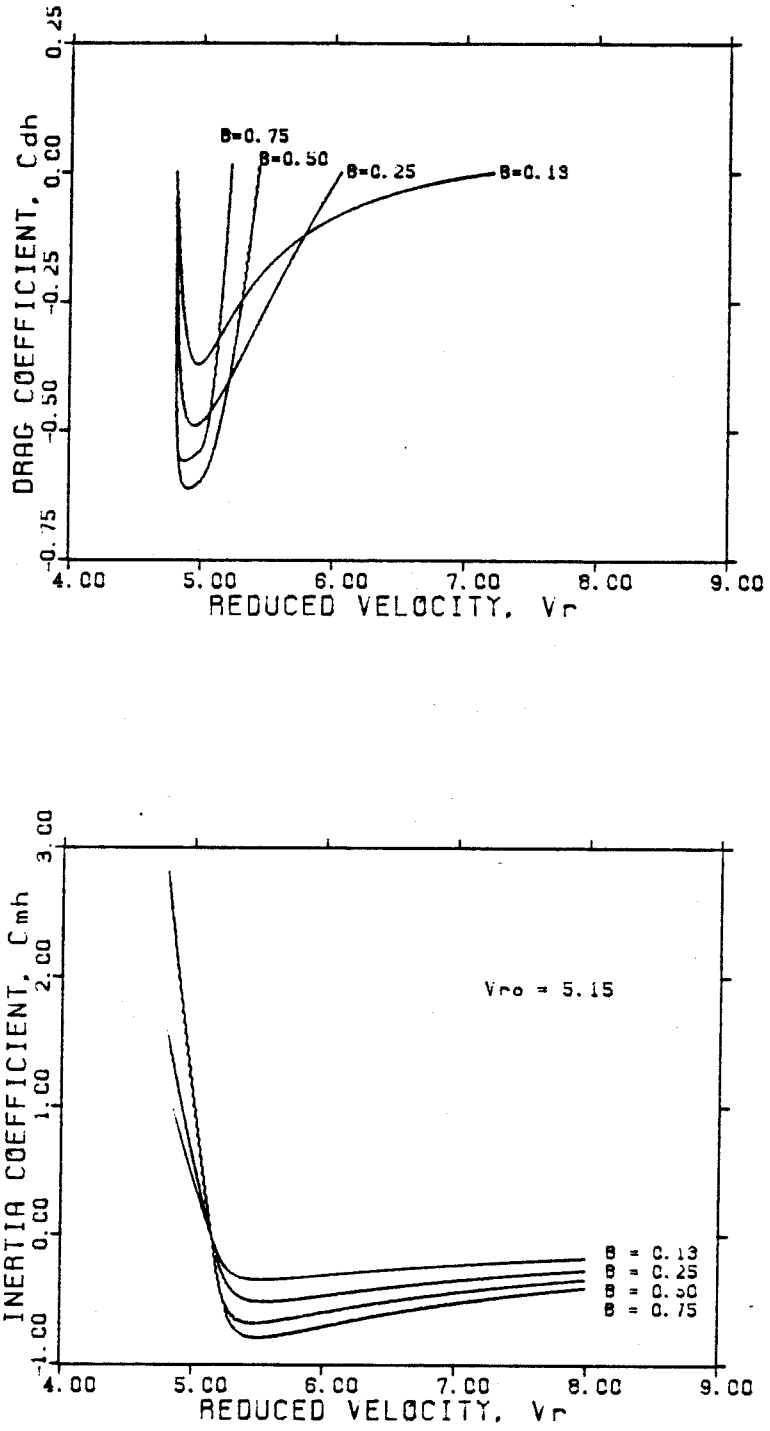

Figure 2.3.4. Interpolation Curves for C_{dh} and C_{mh} versus V_r [32]

C_{mh} are still functions of the amplitude of oscillation, which is an unknown.

Proceeding in a similar way to the lock-in model, the differential equation of motion is written as

$$m\frac{d^2Y}{dt^2} + \overline{c}\frac{dY}{dt} + kY = F(t) \tag{2.3.4}$$

where

$$F(t) = \tfrac{1}{2}\rho DU^2\left(C_{mh}Sin\omega_s t - C_{dh}Cos\omega_s t\right) \tag{2.3.5}$$

with

$$Y = A\ Sin(\omega_s t - \phi). \tag{2.3.6}$$

The non-lock-in problem is much simpler to solve than the lock-in problem, as the amplitude can be solved for independent of the phase, and the phase calculated subsequently [9].

2.3.3 The Discrete-Vortex Model

The discrete-vortex model, first presented by Rosenhead in 1931 [52], is a potential flow representation of the shear layers produced by flow separation from a bluff body in a flow. Sarpkaya and Schoaff [62], presented a comprehensive study based on the discrete-vortex model for the prediction of the flow characteristics, fluid forces and response of a circular cylinder subjected to a uniform flow.

At sufficiently high Reynolds Number, the shear layers present in the wake of a bluff body are quite thin, and the vorticity is confined to spiraled vortex sheets. The discrete-vortex model subdivides the shear layer into a number of small segments, and concentrates the vorticity into line vortices, located at the center of each segment.

Complex function theory may then be used to analyze the flow.

Complex function analysis of potential flow enables the calculation of the vortex velocity due to the influence of all the other vortices and the mean flow. The vortices are convected for a finite time interval using an appropriate convection scheme, and the next set of velocities calculated. New vorticity is introduced to the flow at the separation points in a manner consistent with the boundary layer hydrodynamics. The decay of vortices and interaction of opposite signed vorticity must be considered.

Sarpkaya performed two sets of numerical studies in the investigation. The first considered the modeling of flow past a stationary cylinder in a uniform incident flow. Excellent conformity with experimental results were obtained, provided a reduction of circulation was included in the model.

The second half of the study investigated the response of a cylinder free to move under the applied fluid forces. Comparison of the discrete-vortex model with experimental results indicates that the approach does give a good representation of the cylinder response.

The discrete-vortex model gives good insight into the behavior of a cylinder subject to flow-induced vibration. While there are some unexplained discrepancies between these numerical results and observed experimental data, the model clearly demonstrates the overall nature of the fluid-structure interaction and should be an important tool in the future.

2.3.4 Finite Element Models

While finite element methods have been used successfully for structural mechanics for many years, their application to unsteady fluid mechanical problems is relatively new. To the author's knowledge, a finite element formulation for the

vortex-induced vibration problem has not yet been implemented. A major reason for this is the massive computational effort required to model even the case of a fixed cylinder in a steady flow. However, as new fluid-structure elements and techniques are developed, and as computing power becomes more readily accessible, a more complete understanding of the problem may become possible using this approach.

A recent work by Brooks and Hughes [10] illustrates the power of the finite element method for accurately predicting flow patterns and pressure distributions around a fixed body in an incompressible flow. The growth and detachment of vortices is accurately modeled, and the pressure distribution and net fluid force on the cylinder can be easily obtained. While the moving body problem is significantly more complex and computationally intensive, this is certainly a step in the right direction and presents possibilities for future work.

2.4 Modeling Fluid Resistance Forces

2.4.1 Forces on Oscillating Bodies

The fluid forces on a body in a flow may be decomposed into components parallel and perpendicular to the flow. The component parallel to the flow is generally referred to as an "in-line" force, and the perpendicular component as a "transverse" force. For a fixed body, the in-line force is called the drag force.

The above sections address the problem of transverse forces on oscillating and fixed bodies subject to uniform fluid flows. As in the case of transverse force, the in-line force has components proportional to both the velocity (drag) and acceleration (inertia or added mass effect). This force will now be discussed as a resistance force acting on parts of a cable which are not shedding vortices. In the active region, the cross-flow produces quasi-static drag in the direction of the flow, which is a function of

the amplitude of vibration. While this is an important design consideration, it is not addressed here. Many theoretical and experimental studies have investigated the nature of these fluid forces.

The exact solution for the flow around a cylinder is not possible by using existing analytical techniques, except for a few special cases. Batchelor [2] presents a solution for the force on a cylinder undergoing harmonic oscillation of very small amplitude ($A/D<0.05$). The force is approximately viscous, i.e., proportional to the cylinder velocity, and is given by

$$F = k\frac{dy}{dt} \tag{2.4.1}$$

where y is the harmonic cylinder displacement, and k, the viscous damping coefficient, is given by

$$k = \mu\omega\frac{\rho}{\rho_s}\frac{8\sqrt{2}}{\sqrt{\mathrm{Re}_\omega}}. \tag{2.4.2}$$

ρ is the fluid density, ρ_s the density of the cylinder, and ω the frequency of vibration. Re_ω is called the oscillatory Reynolds Number, given by

$$\mathrm{Re}_\omega = \frac{\omega D^2}{\nu}. \tag{2.4.3}$$

ν is the kinematic viscosity of the fluid. This viscous fluid damping is important for the type of problem considered in this thesis.

While an approximate solution for low amplitudes of vibration exists, no equivalent solution for larger displacements has been found, due to the complexity of the Navier-Stokes equations for higher Reynolds Number flows. The nature of the fluid forces is determined experimentally [55, 58], and the results combined with Equations (2.4.1)-

(2.4.3) to yield an approximate solution for the ranges of amplitude and Reynolds Number encountered in practice.

An early work by Morison and his co-workers [43] has been the basis for many subsequent experimental studies of fluid forces on fixed and oscillating bodies. While originally motivated for the problem of forces on piles due to ocean waves, it has been widely used for oscillating flows in general.

Morison divided the force acting on a stationary body in a moving fluid into two components: one due to the drag, as in the case of constant velocity, and the other due to the acceleration of the fluid. The force per unit length on a cylinder is written in the form:

$$F(t) = \tfrac{1}{2} C_d \rho D U|U| + C_m \rho \frac{\pi D^2}{4} \frac{dU}{dt} \tag{2.4.4}$$

where U and $\frac{dU}{dt}$ are the instantaneous fluid velocity and acceleration, respectively, D is the diameter of the cylinder, and ρ is the density of the fluid. Equation (2.4.4) is generally referred to as the Morison Equation.

C_d and C_m are called the drag and inertia coefficients, respectively. Later investigations [35, 56, 60] showed C_d and C_m to be functions of the amplitude of the motion, the Reynolds Number of the oscillating flow and the surface roughness. That is,

$$C_d = C_d(K, Re, k/D) \tag{2.4.5}$$

$$C_m = C_m(K, Re, k/D) \tag{2.4.6}$$

where

$$K = \frac{U_m T}{D} \tag{2.4.7}$$

$$\mathrm{Re} = \frac{U_m D}{\nu}. \tag{2.4.8}$$

U_m is the magnitude of the velocity, T the period of the oscillation, and k/D is a measure of the relative surface roughness. The parameter K is called the Keuligan-Carpenter Number. For sinusoidal velocities, K may be written as

$$K = 2\pi \frac{A}{D} \tag{2.4.9}$$

where A is the amplitude of the oscillation.

C_d and C_m will generally vary with time also, as their values depend on the instantaneous pressure distribution around the body. Due to the difficulty of measuring the values of these coefficients continuously throughout the cycle, the average values over one period of the oscillation are usually employed.

To specify C_d and C_m, it has been found useful to introduce a new dimensionless group, β, defined by

$$\beta = \frac{\mathrm{Re}}{K} = \frac{D^2}{\nu T}. \tag{2.4.10}$$

Notice that β is related to the oscillatory Reynolds Number defined in Equation (2.4.3). Both β and Re_ω are used in the literature, so it is important that their equivalence be understood. The two are related by

$$\beta = \frac{1}{2\pi}\mathrm{Re}_\omega. \tag{2.4.11}$$

Both Keuligan and Carpenter, and Sarpkaya performed a series of experiments to measure C_d and C_m as functions of K and β for cylinders in oscillatory flows. Keuligan and Carpenter [35] measured the force on plates and cylinders placed in the node of a standing wave. At this location, the vertical water particle velocity is zero, and the horizontal water particle velocity is uniform over the depth. Sarpkaya [58] used a fixed cylinder in a large U-tube, in which the fluid was oscillated very nearly uniformly across the cross-section.

It is apparent now that the dependence on Re or β was overlooked by the initial investigators [35, 55] as they considered only a small range of K values. It was thought that apparent scatter of the points was due to experimental error, rather than to the overlooking of a fundamental parameter (Re or β.) This omission was investigated by Sarpkaya in a more recent work [57, 58, 60]. Summaries of the data obtained are shown in Figure 2.4.1.

The data collected in the initial investigations are, however, still of use for the types of systems considered herein. For values of Re_ω less than 10^4 ($\beta < 1600$), and $K < 10$ ($A/D < 1.6$), the data for C_d and C_m shown in Figure 2.4.1 tend to become independent of β and are functions purely of K. These ranges of parameters encompass those found in vortex-induced vibration problems of long structures. Assuming this independence of β, data for the drag and inertia coefficients are shown in Figure 2.4.2 (from [55]). For the ranges of parameters considered, the drag and inertia coefficients are approximated as:

$$C_d \approx 1.25\frac{A}{D} \tag{2.4.12}$$

$$C_m \approx 2.3 - 0.67\frac{A}{D}. \tag{2.4.13}$$

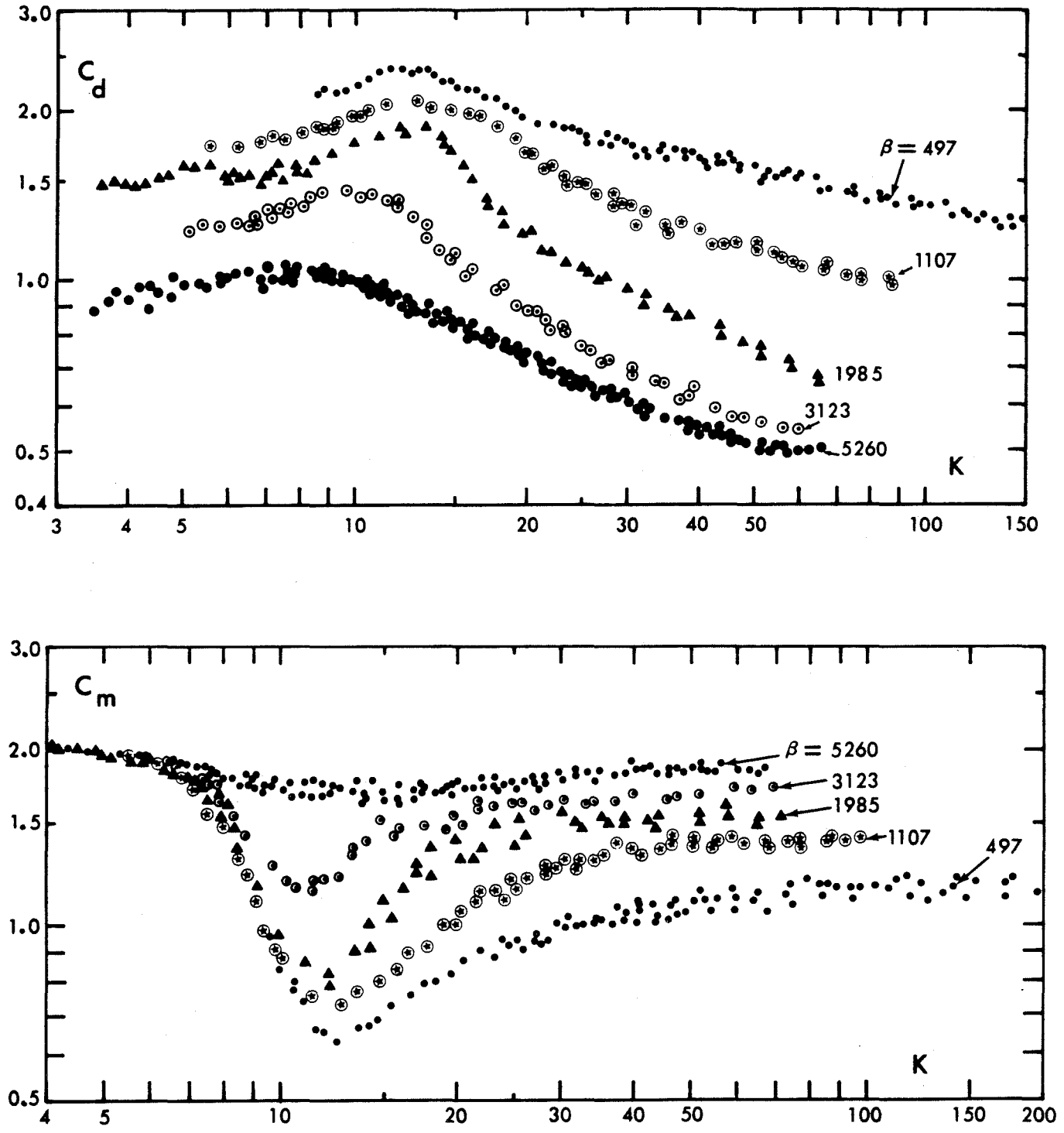

Figure 2.4.1. Drag and Inertia Coefficients versus Keuligan Carpenter Number for Various β (from [58])

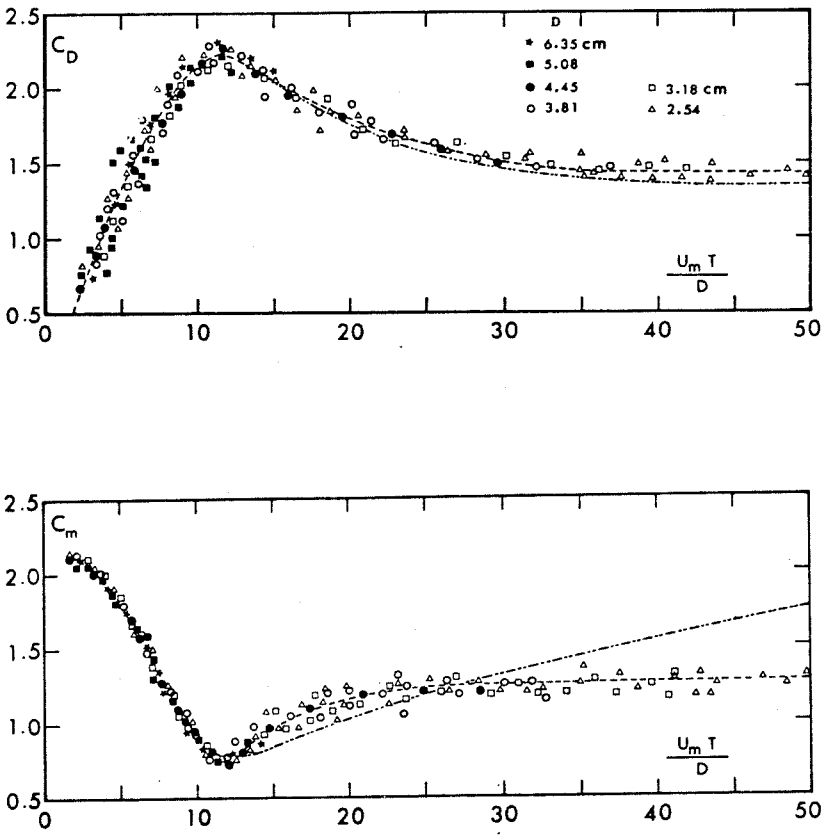

Figure 2.4.2. Drag and Inertia Coefficients versus Keuligan Carpenter Number for Various β (from [55])

Equations (2.4.12) and (2.4.13), in the linearized form of (2.4.4), may be combined with the low amplitude solution (Equation (2.4.1)) to yield an expression for the total fluid force on a cylinder under the full range of amplitudes and Reynolds Numbers encountered.

2.4.2 Forces on Accelerating Bodies in an Accelerating Flow (General Case)

The representation of forces acting on a body in a fluid has often been a source of confusion. The derivation given below presents the dynamics of the problem and the solution to the most general case. The solutions for still fluid or a fixed body are special cases of this general case.

Consider the system shown in Figure 2.4.3.

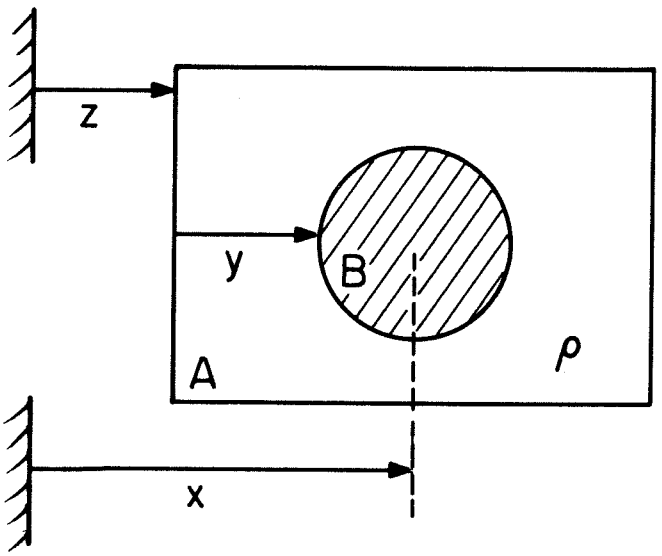

Figure 2.4.3. Accelerating Body in an Accelerating Fluid

The container, A, is filled with fluid of density ρ and a body, B, is immersed in the fluid. The motion of the container is described by z, and the motion of the body

relative to the container, by y.

The container and body are given arbitrary motions in y and z. The fluid force on the body due to the acceleration of the body and the fluid will be

$$f(\ddot{y},\ddot{z}) = m' \ddot{z} - C_a m' \ddot{y}. \tag{2.4.14}$$

m' is the mass of fluid displaced by the body, and C_a is the coefficient of added mass. Now, let

$$x = y + z. \tag{2.4.15}$$

The force may be therefore expressed as

$$f(\ddot{x},\ddot{z}) = m' \ddot{z} - C_a m'(\ddot{x} - \ddot{z}). \tag{2.4.16}$$

The first term on the right-hand side represents the buoyancy force due to the acceleration of the fluid alone. For an accelerating fluid C_a may be generally taken to be 1 for a cylinder, and 0.5 for a sphere. C_a is related to C_m by

$$C_a = C_m - 1 \tag{2.4.17}$$

These values may be derived theoretically from potential flow, and have been experimentally verified.

For nonuniform flows (for example, oscillating flows) and bodies which generate strongly separated flows, the parameter C_a is not constant, but a function of the acceleration, the instantaneous flow velocity, and the surface roughness.

For a fixed fluid, and a harmonically oscillating cylinder, C_a is again taken to be 1 for a cylinder and 0.5 for a sphere, as in the uniformly accelerating fluid case. The value for a cylinder clearly follows from the asymptotes of Figure 2.4.1 as K becomes near zero.

CHAPTER 3

The Traveling Wave Model

3.1 Introduction

One of the more interesting features of vortex shedding is the phenomenon of lock-in. As this refers to locking on to a particular structural frequency, it is not surprising that modal analysis was a natural way to approach the problem of vortex-induced oscillation. Engineers are accustomed to the use of modal analysis for short cables and other structures, where a good representation of the motion can be obtained using the first few modes. Many flow-induced vibration problems have been successfully solved using modal analysis, but there are some cases where it is not appropriate. The response of long cables to vortex shedding is not well suited to a modal analysis approach.

For long structures, such as those found in many ocean engineering applications, modal analysis ceases to be a satisfactory approach due to the existence of very closely spaced modes. Lock-in is generally not observed for these types of structures. Nonuniform flow profiles may also not be amenable to solution by modal analysis, although some approximate techniques have been developed.

In this chapter, a new approach to the problem of vortex-induced vibration of long structures based on traveling waves is presented. The approach avoids difficulties with the close spacing of structural modes, as modal frequencies are not used in the solution. Lock-in is therefore not considered. In a later chapter, lock-in is discussed in

the context of nonuniform flow, but this refers to "cells" of finite length which are excited at a constant frequency.

3.2 Comparison of Modal and Traveling Wave Solutions

There are a number of methods available for solving boundary value problems. Probably the most common is the eigenfunction expansion or modal analysis method, whereby the solution is obtained as the sum of responses in the structure modes. Another approach, which can be used to find the steady-state response to a periodic force, is to assume a motion which is periodic at the frequency of excitation. The solution in the spatial domain can then be found by solving an ordinary differential equation subject to the prescribed boundary conditions. A third method is to use a characteristics approach or traveling wave solution. While usually best suited to problems involving infinite or semi-infinite spatial domains, it is also possible to solve boundary value problems by this method.

The use of both modal analysis and traveling wave analysis is illustrated in the following section. It is shown that modal solutions are not particularly well suited to long structures. A method for summing the traveling wave response of a number of segments is presented, which forms the basis of the approach developed in this thesis.

3.2.1 Modal Solution

Consider the system illustrated in Figure 3.2.1. The string is fixed at $x = L$ and is excited by the displacement boundary condition at $x = 0$

$$y(0,t) = A\sin\omega t \tag{3.2.1}$$

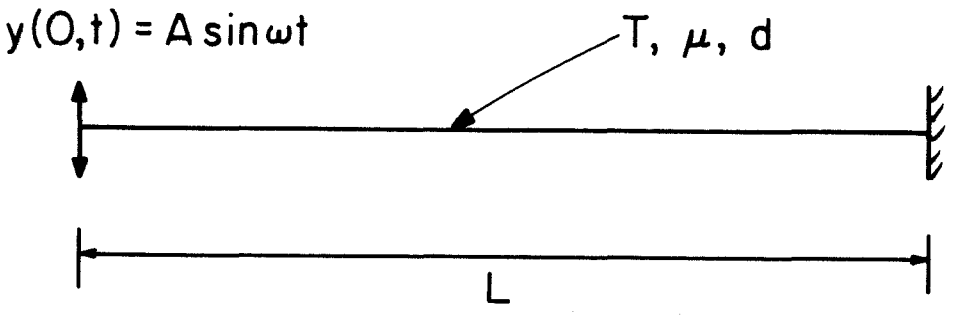

Figure 3.2.1. String with Displacement Boundary Condition

The equation of motion for transverse oscillation of the string is given by

$$\mu \frac{\partial^2 y}{\partial t^2} + d \frac{\partial y}{\partial t} = T \frac{\partial^2 y}{\partial x^2} \tag{3.2.2}$$

where T is the tension in the string, μ is the mass per unit length, and d an assumed viscous damping per unit length. T, μ, and d are assumed constant along the span, and the transverse displacement is assumed to be small.

To solve the problem by modal analysis, a change of variables is performed to produce homogeneous boundary conditions. Let

$$y(x,t) = w(x,t) + (1 - \frac{x}{L}) \sin\omega t \,. \tag{3.2.3}$$

The equation of motion and boundary conditions are then transformed to

$$\frac{\partial^2 w}{\partial x^2} - \frac{1}{c^2} \frac{\partial^2 w}{\partial t^2} - \frac{d}{T} \frac{\partial w}{\partial t} = -\frac{\omega^2}{c^2}(1 - \frac{x}{L}) \left[1 + \left(\frac{d}{\mu\omega}\right)^2\right]^{1/2} \sin(\omega t - \psi) \tag{3.2.4}$$

$$c^2 = \frac{T}{\mu} \tag{3.2.5}$$

$$\psi = \tan^{-1}\left(\frac{d}{\mu\omega}\right) \tag{3.2.6}$$

$$w(0,t) = 0, \; w(L,t) = 0. \tag{3.2.7}$$

The change of variables has the effect of transforming the applied end displacement to a linearly varying spanwise force, but with zero displacement boundary conditions.

The homogeneous problem associated with (3.2.4) is

$$\frac{\partial^2 w}{\partial x^2} - \frac{1}{c^2}\frac{\partial^2 w}{\partial t^2} - \frac{d}{T}\frac{\partial w}{\partial t} = 0 \tag{3.2.8}$$

subject to the boundary conditions (3.2.7). By the use of standard techniques, the eigenvalues and eigenfunctions for the above system can be easily shown to be

$$W_n(x) = A_n \sin\lambda_n x, \; \lambda_n = \frac{n\pi}{L}, \; n = 1,2,3\ldots . \tag{3.2.9}$$

The forced problem, (3.2.4), can be solved by expanding the solution in terms of the eigenfunctions given in (3.2.9). Assume

$$w(x,t) = \sum_{i=1}^{n} \xi_i(t) \sin\frac{i\pi x}{L}. \tag{3.2.10}$$

Substitution of (3.2.10) into (3.2.4) yields

$$\sum_{i=1}^{\infty}\left(-\frac{i^2\pi^2}{L^2}\xi_i(t) - \frac{1}{c^2}\ddot{\xi}_i(t) - \frac{d}{T}\dot{\xi}_i(t)\right)\sin\frac{i\pi x}{L}$$

$$= -\frac{\omega^2}{c^2}(1 - \frac{x}{L})\left(1 + \left(\frac{d}{\mu\omega}\right)^2\right)^{1/2}\sin(\omega t - \psi). \tag{3.2.11}$$

Making use of the orthogonality of the eigenfunctions, the "r-th" modal equation may be written as

$$\ddot{\xi}_r(t) + \frac{d}{\mu}\dot{\xi}_r(t) + \frac{r^2\pi^2c^2}{L^2}\xi_r(t) = \frac{2}{r\pi}\omega^2\left(1 + \left(\frac{d}{\mu\omega}\right)^2\right)^{1/2}\sin(\omega t - \psi). \tag{3.2.12}$$

Solving this equation for $\xi_r(t)$ yields

$$\xi_r(t) = \frac{2}{r\pi}\left[1+\left(\frac{d}{\mu\omega}\right)^2\right]^{1/2} \frac{\omega^2}{((\omega_r^2-\omega^2)^2+(2\varsigma_r\omega\omega_r)^2)^{1/2}} \sin(\omega t-\psi-\phi_r) \quad (3.2.13)$$

$$\omega_r = \frac{r\pi c}{L,} \quad \varsigma_r = \tfrac{1}{2}\frac{d}{\mu\omega_r} \quad (3.2.14)$$

$$\phi_r = \frac{2\varsigma_r\omega\omega_r}{(\omega_r^2-\omega^2)} \quad (3.2.15)$$

and ψ is given by (3.2.6). The complete solution for $w(x,t)$ is given by (3.2.10), and (3.2.3) gives the solution for $y(x,t)$.

A few comments may be made about the nature of the modal solution. As the length, L, becomes large, the difference between consecutive natural frequencies of the system becomes smaller. For systems encountered in some ocean engineering applications, the length is often very large compared to the wavelength corresponding to the vortex-shedding frequency of the cable. The small difference between the frequencies makes classical lock-in to one mode virtually impossible.

Due to the high modal density, the contributions from many modes must be summed to get a meaningful solution from modal analysis. This very rapidly becomes computationally intensive for the type of systems in question.

The nature of the solution is not apparent from the individual terms in the summation. The engineer is interested principally in the amplitude of the cable as a function of x, and this is not easily obtained from the above expression.

3.2.2 Traveling Wave Solution

The system shown in Figure 3.2.1 can also be solved using a traveling wave approach. If the cable is very long and the damping is moderate, the waves produced

by the condition at $x=0$ will be effectively damped out before they reach the right-hand end of the cable. If not, reflections of the waves from the fixed boundary will have to be considered. It is assumed for the remainder of this dissertation that the systems considered are sufficiently long that negligible reflected energy is present, unless specifically stated. The consequence of this assumption is that the string may be treated as semi-infinite. The boundary condition at $x=L$ need not be considered, and an initial value problem consisting of the differential equation (Equation (3.2.2)) and the initial condition (Equation (3.2.1)), need to be solved, rather than the boundary value problem dealt with in the preceding section.

The traveling wave solution to this initial value problem can be shown to be ([50], Vol. 1, pp. 232-233)

$$y(x,t) = Ae^{-\alpha x}\sin(\omega t - \beta x) \tag{3.2.16}$$

where α and β are determined from

$$\alpha^2 - \beta^2 = -\frac{\omega^2}{c^2}, \quad 2\alpha\beta = \frac{d\omega}{T}. \tag{3.2.17}$$

Solving (3.2.17) for α and β gives

$$\alpha = \frac{1}{\sqrt{2}}\frac{\omega}{c}\left[\left(1+\left(\frac{d}{\mu\omega}\right)^2\right)^{1/2} - 1\right]^{1/2} \tag{3.2.18}$$

$$\beta = \frac{1}{\sqrt{2}}\frac{\omega}{c}\frac{d}{\mu\omega}\left[\left(1+\left(\frac{d}{\mu\omega}\right)^2\right)^{1/2} - 1\right]^{-1/2}. \tag{3.2.19}$$

For small values of the dimensionless parameter $\frac{d}{\mu\omega}$ (i.e., low values of viscous damping, or high frequencies of excitation) Equations (3.2.18) and (3.2.19) reduce to

$$\frac{\alpha}{\omega/c} \approx \tfrac{1}{2}\frac{d}{\mu\omega} \tag{3.2.20}$$

$$\frac{\beta}{\omega/c} \approx 1 \ . \tag{3.2.21}$$

Plots of $\frac{\alpha}{\omega/c}$ and $\frac{\beta}{\omega/c}$ are shown in Figure 3.2.2 as functions of $\frac{d}{\mu\omega}$.

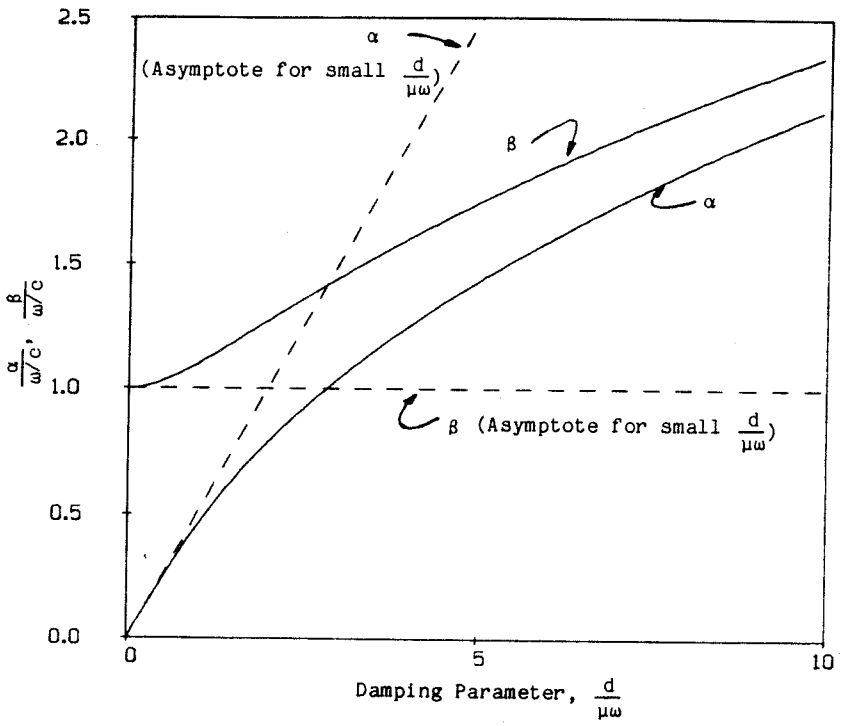

Figure 3.2.2. $\frac{\alpha}{\omega/c}$ and $\frac{\beta}{\omega/c}$ versus $\frac{d}{\mu\omega}$

The force required to produce the displacement at $x = 0$ (Equation (3.2.1)) is given from force balance as

$$f(t) = -T \left.\frac{\partial y}{\partial x}\right|_{x=0} . \tag{3.2.22}$$

Using (3.2.16), this may be written as

$$f(t) = TA(\alpha^2 + \beta^2)^{1/2} \cos(\omega t - \psi) \tag{3.2.23}$$

where the phase angle, ψ, is given by

$$\tan \psi = \frac{\alpha}{\beta}. \tag{3.2.24}$$

Compared with the modal solution presented in the preceding section, the traveling wave solution given by Equation (3.2.15) is clearly more appropriate. Excitation of one mode, particularly a higher one as assumed by the modal approach, is not a realistic assumption. Written in this form, the solution describes a traveling wave, exponentially decaying in amplitude with distance, and with a modified wave velocity of

$$\hat{c} = \frac{\omega}{\beta} \quad (= c \text{ for } \textit{small } \frac{d}{\mu\omega}). \tag{3.2.25}$$

For long cables, this form of solution is significantly more meaningful physically than the corresponding modal solution. There are no natural frequency terms entering the solution directly. Problems of lock-in to particular modes are therefore avoided.

3.3 General Formulation of the Traveling Wave Solution

In the preceding section, the response of a taut string to an applied end displacement was found. The solution obtained may be used to formulate a Green's function, and the response of an arbitrarily loaded cable expressed in terms of an integral equation. In some special cases, the integral equation may be solved exactly, but the general solution to a vortex-excited system must be found numerically.

3.3.1 Green's Function Approach for a Generalized Force

The development in Section 3.2.2 showed that for an applied force given by Equation (3.2.22), the resulting displacement was described by (3.2.16). Generalizing

this argument, consider the case of a harmonic force given by

$$f(x,t) = F(x)\sin(\omega t - \theta(x)) \tag{3.3.1}$$

applied to an *infinite* string, where $\theta(x)$ gives the phase of the force at x. The Green's function for the system may be obtained by letting

$$F(x) = \delta(x-\xi) \tag{3.3.2}$$

where $\delta(x-\xi)$ is a Dirac delta function at $x = \xi$. Then,

$$G(x,\xi,t) = \frac{\kappa}{T} e^{-\alpha|x-\xi|}\cos(\omega t - \beta|x-\xi| + \psi - \theta(\xi)) \tag{3.3.3}$$

where ψ is defined in (3.2.24) and κ is given by

$$\kappa = \frac{-1}{2(\alpha^2+\beta^2)^{1/2}}. \tag{3.3.4}$$

α and β are given by (3.2.18) and (3.2.19), respectively. The factor of 2 in the denominator of (3.3.4) is a consequence of considering an infinite, rather than a semi-infinite, string. Equation (3.3.3) gives the response at x due to the applied force at ξ. The solution for any arbitrary force, $f(\xi,t)$, applied to the string along its span is then given by

$$y(x,t) = \int_{-\infty}^{\infty} G(x,\xi,t)F(\xi)d\xi. \tag{3.3.5}$$

Assume that the total displacement, $y(x,t)$, may be written as

$$y(x,t) = \bar{A}(x)\cos(\omega t - \bar{\phi}(x)) \tag{3.3.6}$$

where $\bar{A}(x)$ and $\bar{\phi}(x)$ are the amplitude and phase of the *total* displacement along the cable. In many cases, the applied force may be written as a function of these

amplitude and phase variables. In particular, for the types of forces considered in this dissertation, it is assumed that the force can be written

$$f(x,t) = F(\bar{A}(x)) \sin(\omega t - \theta(x)) \tag{3.3.7}$$

where $\theta(x)$ is in general a function of both $\bar{A}(x)$ and $\bar{\phi}(x)$.

As an example, consider the application of an external force proportional to the local total velocity of the cable. In this case,

$$f(x,t) = k \frac{\partial y}{\partial t} \tag{3.3.8}$$

where k is a constant. Clearly, this type of force represents an externally applied viscous damping. By the use of the solution form for displacement given in (3.3.6), the force described by Equation (3.3.8) may be written in the form of (3.3.7) with

$$F(\bar{A}(x)) = -k\omega\bar{A}(x) \tag{3.3.9}$$

and

$$\theta(x) = \bar{\phi}(x). \tag{3.3.10}$$

Substitution of (3.3.3) and (3.3.7) into (3.3.5), and using (3.3.6) yields

$$\bar{A}(x) \cos(\omega t - \bar{\phi}(x)) = \int_{-\infty}^{\infty} \frac{\kappa}{T} F(\bar{A}(\xi))\, e^{-\alpha|x-\xi|} \cos(\omega t - \beta|x-\xi| + \psi - \theta(\xi)) d\xi \tag{3.3.11}$$

Expanding and collecting the terms in $\sin\omega t$ and $\cos\omega t$ result in the pair of equations

$$\bar{A}(x) \sin\bar{\phi}(x) = \frac{\kappa}{T} I_1(x) \tag{3.3.12}$$

$$\bar{A}(x) \cos\bar{\phi}(x) = \frac{\kappa}{T} I_2(x) \tag{3.3.13}$$

where $I_1(x)$ and $I_2(x)$ are given by

$$I_1(x) = \int_{-\infty}^{\infty} F(\bar{A}(\xi))\, e^{-\alpha|x-\xi|} \sin(\beta|x-\xi| - \psi + \theta(\xi))d\xi \tag{3.3.14}$$

$$I_2(x) = \int_{-\infty}^{\infty} F(\bar{A}(\xi))\, e^{-\alpha|x-\xi|} \cos(\beta|x-\xi| - \psi + \theta(\xi))d\xi . \tag{3.3.15}$$

The amplitude and phase may be then found from

$$\bar{A}(x) = \frac{\kappa}{T}(I_1^2(x) + I_2^2(x))^{1/2} \tag{3.3.16}$$

$$\tan\bar{\phi}(x) = \frac{I_1(x)}{I_2(x)} . \tag{3.3.17}$$

The solution presented in (3.3.14)-(3.3.17) clearly requires solution of the integral equations, in general coupled in $\bar{A}(x)$ and $\bar{\phi}(x)$. While an iterative numerical scheme is generally required in the case of nonlinear $F(\bar{A}(x))$, there are some cases where the set of equations may be solved exactly. An example is presented below.

3.3.2 Integration of Integral Equation for Constant Spanwise Force

To illustrate the implementation of the solution presented above, the system shown in Figure 3.3.1 is considered. A spanwise constant harmonic force is applied over an "active" region $-a \leq x \leq a$ to a string with internal damping represented by α. Outside the active region, the applied force is zero.

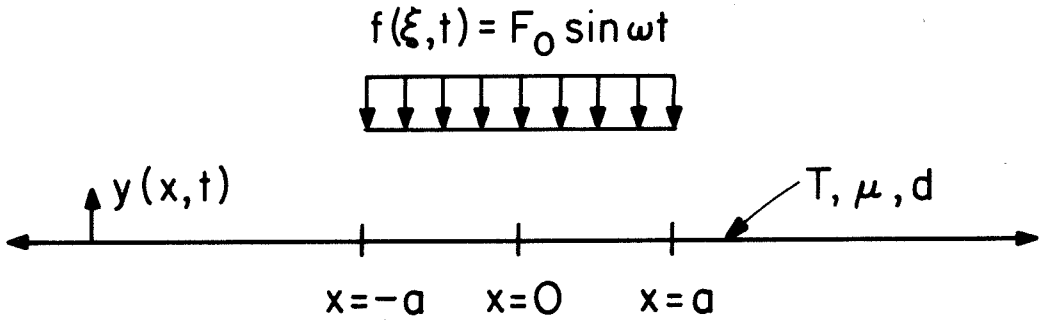

Figure 3.3.1. Spanwise Constant Force over an Active Region

Equation (3.3.7) may be written

$$\begin{aligned} f(x,t) &= F_0 \sin(\omega t - \theta_0), \ -a \le x \le a \\ &= 0 \qquad\qquad\qquad |x| > a\,. \end{aligned} \tag{3.3.18}$$

In this case,

$$F(\bar{A}(x)) = F_0 = \textit{constant} \tag{3.3.19}$$

and

$$\theta(x) = \theta_0 \tag{3.3.20}$$

where θ_0 is an arbitrary constant phase. Equations (3.3.14) and (3.3.15) become

$$I_1(x) = F_0 \int_{-a}^{a} e^{-\alpha|x-\xi|} \sin(\beta|x-\xi| - \psi + \theta_0) d\xi \tag{3.3.21}$$

$$I_2(x) = F_0 \int_{-a}^{a} e^{-\alpha|x-\xi|} \cos(\beta|x-\xi| - \psi + \theta_0) d\xi\,. \tag{3.3.22}$$

These equations may be integrated directly, taking care to preserve the signs under the absolute value signs. For example, for $x > a$, all the arriving waves are all traveling to the right, while in the active region, both left and right traveling waves must be considered.

The solution to the right of the active region, $x > a$, may be shown to be

$$\bar{A}(x) = \bar{A}_0\, e^{-\alpha(x-a)} \tag{3.3.23}$$

$$\bar{A}_0 = \frac{1}{2(\alpha^2+\beta^2)} \frac{F_0}{T} \left(1 + e^{-4\alpha a} - 2e^{-2\alpha a} \cos(2\beta a)\right)^{1/2} \tag{3.3.24}$$

where $\bar{A}_0$ is the amplitude at $x = a$. Similarly, the phase is given by

$$\bar{\phi}(x) = \bar{\phi}_0 + \beta x \tag{3.3.25}$$

$$\bar{\phi}_0 = -\psi + \theta_0 - \frac{\alpha \tan\beta a - \beta \tanh\alpha a}{\beta \tan\beta a - \alpha \tanh\alpha a} \tag{3.3.26}$$

where $\bar{\phi}_0$ is the phase at $x = a$. The solution to the left of the active region is similar, with a replaced by $-a$.

In the active region, the solution becomes more complex, due to the contribution of waves traveling in both directions. The amplitude and phase in this region is given by

$$\bar{A}(x) = \frac{1}{\alpha^2+\beta^2}\frac{F_0}{T}\Big\{1 + e^{-2\alpha a}(\sin^2(\beta a-\Psi) + \sinh^2\alpha x) + 2e^{-\alpha a}(\cos(\beta a-\Psi)\sinh\alpha x\cos(\beta x+\Psi) + \sin(\beta a-\Psi)\cosh\alpha x\sin(\beta x+\Psi))\Big\}^{1/2} \quad .....(3.3.27)$$

$$\tan\bar{\phi}(x) = \frac{\cos\Psi + e^{-\alpha a}(\sinh\alpha x\cos\alpha x\cos(\beta a-\Psi) + \cosh\alpha x\sin\beta x\sin(\beta a-\Psi))}{\sin\Psi + e^{-\alpha a}(\cosh\alpha x\cos\alpha x\sin(\beta a-\Psi) + \sinh\alpha x\sin\beta x\cos(\beta a-\Psi))} \quad .....(3.3.28)$$

where

$$\Psi = 2\psi - \theta_0. \quad (3.3.29)$$

The solution for a load which is antisymmetric about $x = 0$, producing a zero displacement condition at $x = 0$, can be derived in a similar manner. The results are not presented here.

3.4 A Discrete Approach to the Traveling Wave Formulation

The solution for an arbitrarily forced string presented in the previous section (Equation 3.3.5) may be solved in closed form for only a limited number of special cases. The nonlinear nature of the fluid forces in the flow induced vibration problem precludes the exact integration of Equation (3.3.5) as was possible for the example in Section 3.3.2.

To generate a solution to problems with more general applied forces, the results of the preceding section are used to derive an approximate solution for a spanwise

constant force applied to a "small" active length. The whole cable can then be subdivided into many small segments, and the forces on each segment calculated. The contributions of the waves produced by all the segments can then be summed to yield the total amplitude and phase at a particular location. Note that although the applied forces may be nonlinear functions of amplitude, the cable system itself is linear, so superposition of the responses of individual segments is valid.

In general, the force at a point is a function of the total amplitude, which is an unknown quantity. A solution must be therefore be generated in an iterative manner, using the most current value of the amplitude to estimate the applied force. A brief description of the algorithm and programming considerations is presented in Appendix I.

3.4.1 Constant Force over a Small Finite Length Element

Consider the taut, infinite, string as shown in Figure 3.4.1.

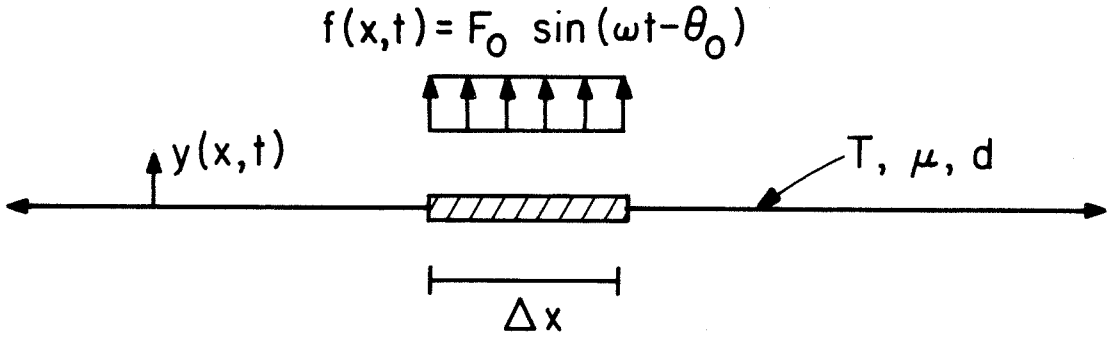

Figure 3.4.1. Force on a Finite Length Segment

The string is excited by a constant force over a finite length, Δx, symmetrically located about $x = 0$. It is assumed that the length, Δx, is small compared to the wavelength associated with the forcing frequency; i.e.,

$$\frac{\Delta x}{\lambda} \ll 1. \tag{3.4.1}$$

λ is the wavelength of the traveling wave produced at a point, defined by

$$\lambda = 2\pi\frac{c}{\omega}. \tag{3.4.2}$$

The string is assumed to be damped with an internal viscous damping force which is proportional to the string velocity. While a better approximation for internal damping is a force proportional to the rate of change of curvature, i.e., $\frac{\partial^3 y}{\partial t \partial x^2}$, it can be shown that the Green's function obtained has the same form. The equations defining α and β differ from Equations 3.2.18 and 3.2.19, however. Since the assumed internal damping is represented by α, rather than by a coefficient in the equation of motion, and as this value is generally much smaller than that due to the viscous fluid effects discussed later, the assumption above is used for simplicity in analysis.

Recall the example presented in Section 3.2.2. For a constant spanwise force over the region $-a \leq x \leq a$ as given by Equation 3.3.18, the solution outside the active region, $x > a$, was given by Equations (3.3.23)-(3.3.26).

Consider the case when the active length ($\Delta x = 2a$) becomes small, such that $\alpha a \ll 1$ and $\beta a \ll 1$. Expansion of (3.3.24) in a power series, and retaining the lowest order terms in a, yields

$$\bar{A}_0 = \frac{1}{2(\alpha^2 + \beta^2)} \frac{F_0}{T} 2a + o(a^2) \tag{3.4.3}$$

or,

$$\bar{A}_0 = \frac{1}{2(\alpha^2 + \beta^2)} \frac{F_0}{T} \Delta x + o(\Delta x^2). \tag{3.4.4}$$

The phase term, $\bar{\phi}_0$ becomes

$$\bar{\phi}_0 = -\psi + \theta_0 + o(\Delta x^2). \tag{3.4.5}$$

Based on the above analysis, and using the results of Section 3.3, a Green's function, $G^*(x,\xi,t)$, corresponding to a force of

$$f(x,t) = F(x)\sin(\omega t - \theta(x)) \tag{3.4.6}$$

with

$$F(x) = \delta(x-\xi)\Delta x \tag{3.4.7}$$

can be defined by

$$G^*(x,\xi,t) = \frac{\kappa}{T} e^{-\alpha|x-\xi|}\cos(\omega t - \beta|x-\xi| + \psi - \theta(\xi)). \tag{3.4.8}$$

Note that this function corresponds to a spanwise constant force applied to an element of length Δx centered at $x = \xi$. As before, $\theta(\xi)$ represents the spatial variation of the phase of the applied force.

Notice that $G^*(x,\xi,t)$, as defined by (3.4.8) and $G(x,\xi,t)$ in Equation (3.3.3), are of exactly the same form, although the definitions (based on a point load or load over a small finite length) differ slightly.

3.4.2 Summation of Infinitesimal Response Functions

Consider the finite length active region shown in Figure 3.4.2. The region is subdivided into n "small" segments such that

$$\frac{\Delta x}{\lambda} \ll 1. \tag{3.4.9}$$

In Section 3.3.1, the total response of the cable, $y(x,t)$, was written in terms of a convolution of the Green's Function and the spanwise force (Equation 3.3.5). In

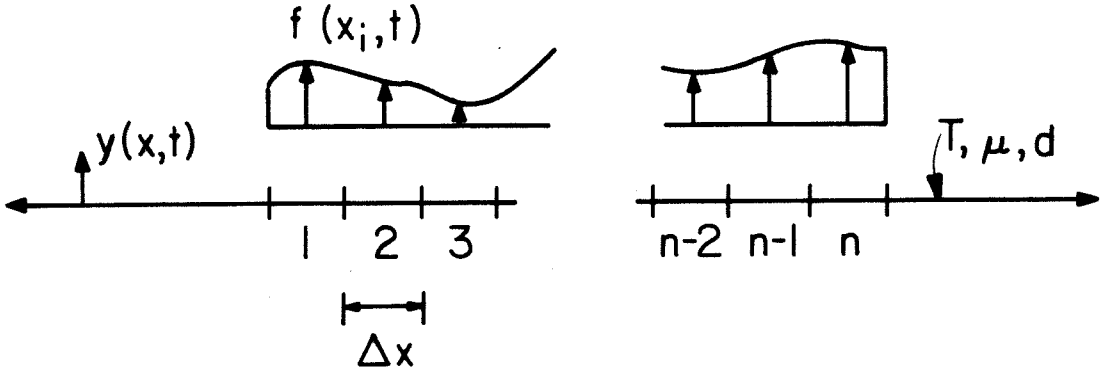

Figure 3.4.2. Discretization of the Active Region

discrete form, Equation 3.3.5 may be written

$$y(x_m,t) = \sum_{i=1}^{\infty} G^*(x_m,x_i,t)\, F(x_i)\, \Delta x \qquad (3.4.10)$$

where the integral has been replaced by a summation over all the discrete cable segments. For practical purposes, the cable is divided into a finite number of segments, say n, so Equation 3.4.10 is written

$$y(x_m,t) = \sum_{i=1}^{n} G^*(x_m,x_i,t)\, F(x_i)\, \Delta x\,. \qquad (3.4.11)$$

Consistent with the development of Section 3.3.1, assume that the externally applied spanwise force may be written as

$$f(x_i,t) = F(\bar{A}_i)\sin(\omega t - \theta_i) \qquad (3.4.12)$$

and that the total displacement of the ith segment is given by

$$y(x_i,t) = \bar{A}_i \cos(\omega t - \bar{\phi}_i)\,. \qquad (3.4.13)$$

Note that as in the continuous case, θ_i is in general a function of both $\bar{A}_i$ and $\bar{\phi}_i$.

The total displacement at station m, assuming no reflections (a cable of infinite extent), is obtained by summing the right traveling waves emanating from segments 1 to m-1, the wave produced at station m itself, and the left traveling waves from stations m+1 to n. Hence,

$$y(x_m,t) = \sum_{i=1}^{m-1} \frac{\kappa}{T} F(\bar{A}_i)\, e^{-\alpha(x_m - x_i)} \cos(\omega t - \beta(x_m - x_i) + \psi - \theta_i)$$

$$+ \frac{\kappa}{T} F(\bar{A}_m) \cos(\omega t + \psi - \theta_m) \qquad (3.4.14)$$

$$+ \sum_{i=m+1}^{n} \frac{\kappa}{T} F(\bar{A}_i)\, e^{\alpha(x_m - x_i)} \cos(\omega t + \beta(x_m - x_i) + \psi - \theta_i).$$

Equation (3.4.14) may be simplified to yield

$$y(x_m,t) = \sum_{i=1}^{n} \frac{\kappa}{T} F(\bar{A}_i)\, e^{-\alpha|x_m - x_i|} \cos(\omega t - \beta|x_m - x_i| + \psi - \theta_i)$$

$$= \sum_{i=1}^{n} \frac{\kappa}{T} F(\bar{A}_i)\, e^{-\alpha|x_m - x_i|} \left[\cos\omega t \cos(\beta|x_m - x_i| - \psi + \theta_i)\right.$$

$$\left. + \sin\omega t \sin(\beta|x_m - x_i| - \psi + \theta_i)\right] \qquad (3.4.15)$$

Equating (3.4.15) to the total displacement of segment m generated by Equation (3.4.13), the amplitudes $\bar{A}_m$ and the phases, $\bar{\phi}_m$ may be expressed as

$$\bar{A}_m = \frac{\kappa}{T}\left(\left[\sum_{i=1}^{n} F(\bar{A}_i)\, e^{-\alpha|x_m - x_i|} \cos(\beta|x_m - x_i| - \psi + \theta_i)\right]^2\right.$$

$$\left. + \left[\sum_{i=1}^{n} F(\bar{A}_i)\, e^{-\alpha|x_m - x_i|} \sin(\beta|x_m - x_i| - \psi + \theta_i)\right]^2\right)^{1/2} \qquad (3.4.16)$$

$$\tan\bar{\phi}_m = \frac{\sum_{i=1}^{n} F(\bar{A}_i)\, e^{-\alpha|x_m - x_i|} \cos(\beta|x_m - x_i| - \psi + \theta_i)}{\sum_{i=1}^{n} F(\bar{A}_i)\, e^{-\alpha|x_m - x_i|} \sin(\beta|x_m - x_i| - \psi + \theta_i)}. \qquad (3.4.17)$$

$\bar{A}_m$ and $\bar{\phi}_m$ can be determined utilizing a simple iterative numerical scheme. Initial values of $\bar{A}_m$ and $\bar{\phi}_m$ may be chosen arbitrarily. The forces on each segment corresponding to these initial values are calculated, and then new values of $\bar{A}_m$ and $\bar{\phi}_m$ are found from (3.4.14) and (3.4.15). The new forces are calculated, and the process repeated until convergence is attained.

3.5 Modeling Active Cable Forces

The fluid forces acting on the cable systems under consideration fall under two basic classifications. In the first are active forces, produced by the shedding of vortices from a segment and by driving the cable at a particular frequency. In the second are passive forces, which comprise resistive forces on the cable due to its motion in the fluid. Both types of forces can be included in the preceding analysis. Whether they are active or passive will be indicated by the sign of the forcing term. In general, a cable will have both active and passive regions, and the combination of the two gives the required solution.

3.5.1 Constant Spanwise Force

The simplest force to be considered applied to the cable is a spanwise constant force. This case has already been considered in Section 3.3, as it is one of the few types of applied loads for which an exact solution can be obtained. By our also solving this problem with the discrete formulation, the effects of discretization errors can be investigated and the results used to assist in choosing appropriate discretization intervals for more complex force types.

Proceeding as in Section 3.3.2, assume an applied force of the form

$$f(x_i,t) = F_0 \sin\omega t\,. \tag{3.5.1}$$

This is equivalent to the generalized force given in (3.4.25), with

$$F(\bar{A}_i) = F_0 = constant \tag{3.5.2}$$

and

$$\theta_i = 0. \tag{3.5.3}$$

3.5.2 Vortex-Induced Forces

The empirical model of Bothelo [32], based on Sarpkaya's measured data [59], will be used to represent the vortex-induced force on the active section of the cable. Sarpkaya measured the force on circular cylinders in a uniform flow with a transverse displacement given by Equation (2.1.1). The force measurements were resolved into components 90^o and 180^o out of phase with the displacement, called inertia and drag coefficients, respectively (see Section 2.2).

For an assumed displacement given by Equation (3.4.8), the force can be represented as

$$f(x_i,t) = \tfrac{1}{2}\rho DU^2\Big(C_{mh}\cos(\omega t-\bar{\phi}_i) + C_{dh}\sin(\omega t-\bar{\phi}_i)\Big). \tag{3.5.4}$$

The coefficients C_{mh} and C_{dh} are the inertia and drag coefficients, respectively. Recall that these coefficients are both functions of the reduced velocity and the normalized amplitude, as discussed in Section 2.2.

The frequency of excitation will be near the shedding frequency, as there are no modes to produce a lock-in effect. In this region, C_{mh} is small, and C_{dh} will be near its maximum negative value. The main assumptions of this development are, therefore:

1. The frequency of vibration is approximately equal to the Strouhal shedding

frequency,

2. The force on the active element is a function of the total amplitude at the element location,

3. The significant force on the element is 90^o out of phase with the displacement at the element location.

The fluid forces on an infinitesimal segment of length Δx excited by vortex shedding may therefore be written in the form of (3.4.25) with

$$F(\bar{A}_i) = \tfrac{1}{2}\rho D U^2 C_{dh(max)} \tag{3.5.5}$$

and

$$\theta_i = \bar{\phi}_i . \tag{3.5.6}$$

From Bothelo's curve-fitting [32], the term $C_{dh(max)}$ is approximated by

$$C_{dh(max)} = -1.375 B_i^2 + 1.483 B_i + 0.2 \tag{3.5.7}$$

where B_i is the amplitude, $\bar{A}_i$, normalized by the diameter D. The above curve was obtained by fitting data of Sarpkaya and Blevins, as shown in Figure 3.5.1.

3.6 Modeling Fluid Resistance Forces

Two commonly used models for the damping of a structure in a fluid are viscous damping, and Morison's equation (see Section 2.4). Both are considered here. Viscous damping is used to test the algorithm presented in the previous sections, and may be used to simplify the solution in the more complex flow cases considered later. Morison's equation is also used, as this gives a more realistic treatment of the fluid resistance. There are some marked differences in the response between viscous and

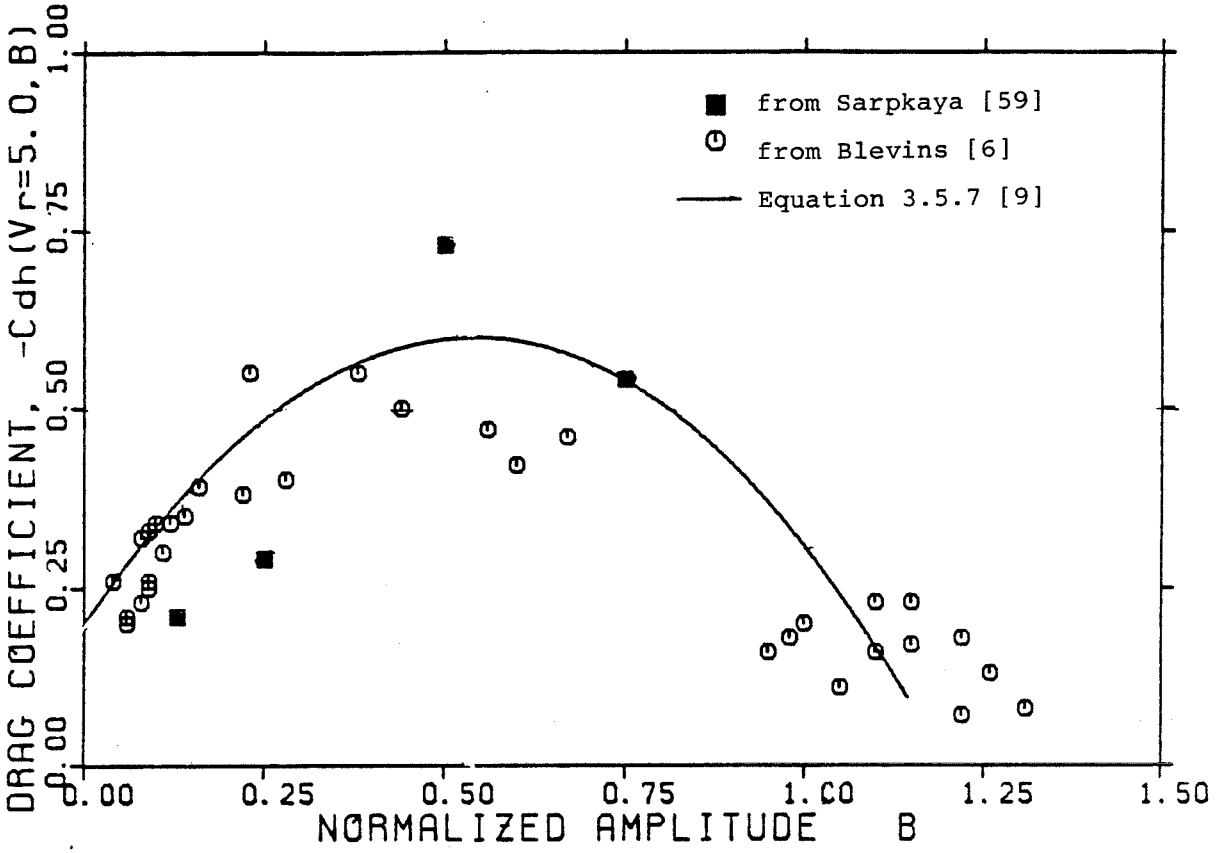

Figure 3.5.1. Drag Coefficient at Peak Amplitude Response (from [32])

Morison damping.

3.6.1 Viscous Damping

Linear viscous damping is considered first due to its simplicity. Suppose the cable is damped with an external force proportional to the cable velocity. Then the force on the cable segment per unit length may be written as

$$f(x_i,t) = -k\frac{\partial y}{\partial t}\bigg|_{x=x_i} \tag{3.6.1}$$

where k is the coefficient of external viscous damping. This force is 90^o out of phase with the displacement and opposes the velocity. Assuming the total displacement of segment i to be given by (3.4.13), the viscous force is written as

$$f(x_i,t) = k\omega\bar{A}_i \sin(\omega t - \bar{\phi}_i). \tag{3.6.2}$$

Again, the force in (3.6.2) may be written in the form of (3.4.12) with

$$F(\bar{A}_i) = k\omega\bar{A}_i \tag{3.6.3}$$

and

$$\theta_i = \bar{\phi}_i. \tag{3.6.4}$$

3.6.2 Morison or Velocity-Squared Damping

The use of Morison's equation (2.4.4) to represent the in-line fluid forces on an oscillating body was discussed in Section 2.4. The incorporation of this resistance force into the traveling wave model will now be discussed.

As before, assume that the total displacement of the ith segment is given by (3.4.13). This represents a segment velocity of

$$\left.\frac{\partial y}{\partial t}\right|_{x=x_i} = -\omega\,\bar{A}_i \sin(\omega t - \bar{\phi}_i). \tag{3.6.5}$$

The lowest harmonic of the total force acting on the segment (from (2.4.4)) is given by

$$F(x_i,t) = \tfrac{1}{2}\rho\omega^2\bar{A}_i^2 D\left[\frac{8}{3\pi}\,C_d \sin(\omega t - \bar{\phi}_i) + \frac{\pi}{2}(C_m - 1)\frac{D}{\bar{A}_i}\cos(\omega t - \bar{\phi}_i)\right]. \tag{3.6.6}$$

Expressing Equation (3.6.6) in the form of (3.4.12)

$$f(\bar{A}_i) = \tfrac{1}{2}\rho\omega^2\bar{A}_i^2 D C_L \tag{3.6.7}$$

where

$$C_L = \left[\left(\frac{8}{3\pi}\right)^2 C_d^2 + \left(\frac{\pi}{2}\right)^2\left(\frac{D}{\bar{A}_i}\right)^2 (C_m - 1)^2\right]^{1/2} \tag{3.6.8}$$

and

$$\theta_i = \bar{\phi}_i - \frac{3\pi^2}{16} \frac{D}{\bar{A}_i} \frac{(C_m - 1)}{C_d}. \tag{3.6.9}$$

The variation of C_d and C_m with amplitude and frequency has been discussed in Chapter 2. To implement solutions when Morison type damping is used, it must be remembered that

$$C_d = C_d(\bar{A}_i, \omega) \tag{3.6.10}$$

and

$$C_m = C_m(\bar{A}_i, \omega). \tag{3.6.11}$$

This dependence becomes most important for low amplitude regions of response, when the drag has a large viscous component, reflected by large increases in the coefficient C_d.

CHAPTER 4

Application to Nonuniform Flow

4.1 Introduction

In the preceding chapter, a method was developed to solve the vortex-induced vibration problem for a long cable system, when the current was uniform over a certain length of the cable (the active length). In practice, ocean currents are highly nonuniform, so the technique is not applicable as it stands. Some modification is necessary to apply the method to the type of currents expected in the real ocean environment.

An approximation made for many nonuniform flow profiles is that of a linearly varying shear flow (see Chapter 2). While this is obviously a rather crude approximation to the real case, it is nonetheless a good starting point for the analysis of general nonuniform flows. A number of assumptions are necessary to adapt the traveling wave approach to the sheared flow situation. While these assumptions may appear to oversimplify a complex situation, there is little other recourse, due to the paucity of both analytical and experimental results in this area.

The assumptions for the modeling are outlined below:

• Vortex shedding occurs in finite length "cells" along the span. The shedding frequency at each of these cells is determined by the local flow velocity and the Strouhal Number, according to the Strouhal relationship, as discussed in Chapter 1.

The length of each cell is a function of the shear parameter, β, for the particular flow situation under consideration. An approximate relationship will be derived shortly for this dependence, based on experimental data on vibrating flexible cables in a shear flow.

• A cell does not "see" the amplitude and frequency of the waves produced by adjacent cells; i.e., the shedding characteristics and forces at one cell are independent of neighboring cells. This implies that the effect of each cell on the total solution for the cable may be calculated as a separate problem, and these are then superposed in an appropriate way to obtain the complete solution. This assumption may be justified physically in that if one cell "saw" the frequency of an adjacent cell, it would lock on to that frequency, and the two cells would coalesce into one. There has been no experimental work done, to the author's knowledge, on this aspect.

• The damping of the fluid in the system has a localizing effect on the solution. That is, the response at a point a few cells away from a given location due to the force at that location is negligible. This assumption is used to simplify the superposition of the individual solutions, and is discussed more fully later.

• The cable itself is a linear system. The applied external forces are nonlinear in nature. However, by the first assumption, these forces have been essentially decoupled from one another, so the force at one cell is affected only by the amplitude and frequency of that cell - the force is unaffected by neighboring cells. This, combined with the linearity of the cable, implies that superposition of the individual solutions is valid. The assumed independence of the response also suggests that a root-mean-square summation of the amplitude is an appropriate superposition scheme, although an upper bound solution may be found by a straight amplitude summation. In view of

the unsteady nature of the real forces, the former method is preferred for design purposes.

Based on the above assumptions, a suggested procedure for the analysis of sheared flow profiles is presented below.

4.2 Cell Length

Before discussing the calculation of appropriate cell lengths, it is necessary to consider the range of values of the shear flow parameter, $\bar{\beta}$. As outlined in Chapter 2, $\bar{\beta}$ is usually less than 0.03. Consider, as an example, the case of a long cable, 1" in diameter, with a linear sheared flow varying from 17 feet per second to zero in 100 ft. This could represent the incident normal velocity on a long towed cable, for example, where the tow speed was 10 knots. If $\bar{\beta}$ is calculated for this system, using the midspan velocity as the reference velocity, a value of $\bar{\beta} = 0.0017$ is obtained. While this is quite an extreme variation in flow profile, the value of $\bar{\beta}$ is quite small, and certainly at the low end of the values used in the laboratory experiments mentioned earlier.

Griffin [24] presents an approximate technique for the prediction of cell length given the shear parameter and making use of the data of Woo, et al [75]. Unfortunately, this development is based on a modal solution, and is not directly applicable to this work. For the solution technique used in this dissertation, an even simpler technique is possible, and is presented below.

The expression for $\bar{\beta}$ (Equation 2.2.7) when the nonuniform flow is linear may be simplified to

$$\bar{\beta} = \frac{D}{V_{ref}} \frac{\Delta V}{\Delta x} \tag{4.2.1}$$

where V_{ref} is generally taken as the midspan velocity, and ΔV, the difference in velocity between the ends of the linear sheared flow region. Rearranging this equation, the cell length, $\frac{\Delta x}{D}$, may be written

$$\frac{\Delta x}{D} = \frac{\Delta V}{V_{ref}} \frac{1}{\beta}. \tag{4.2.2}$$

$\frac{\Delta V}{V_{ref}}$ represents the variation in the flow velocity from the midspan flow velocity in the cell. Making use of the Strouhal relationship, (4.2.2) may be written

$$\frac{\Delta x}{D} \approx \frac{\Delta \omega_s}{\omega_s} \frac{1}{\beta}. \tag{4.2.3}$$

The first term on the right-hand side of (4.2.3) represents what is termed the lock-in bandwidth. Various investigators have studied the range of this parameter. An example has been already presented in Figure 2.2.6. Additional data were generated by Koopmann [38] and are presented in Figure 4.2.1 below.

While these data were obtained in uniform flows, by changing the flow velocity and hence natural shedding frequency while the structure was vibrating at a natural frequency, they are still applicable here. Consider a segment of the cable which is oscillating at a given frequency due to waves traveling down the cable from a nearby active cable region. Suppose a transverse flow velocity is now "turned on" at that point with a natural Strouhal frequency which differs from the vibration frequency. Depending on the frequency difference and the vibration amplitude, the shedding will either lock-in to the existing frequency, or cause an oscillation of its own, at the Strouhal frequency. The required frequency difference can be determined from Figures 2.2.6 and 4.2.1.

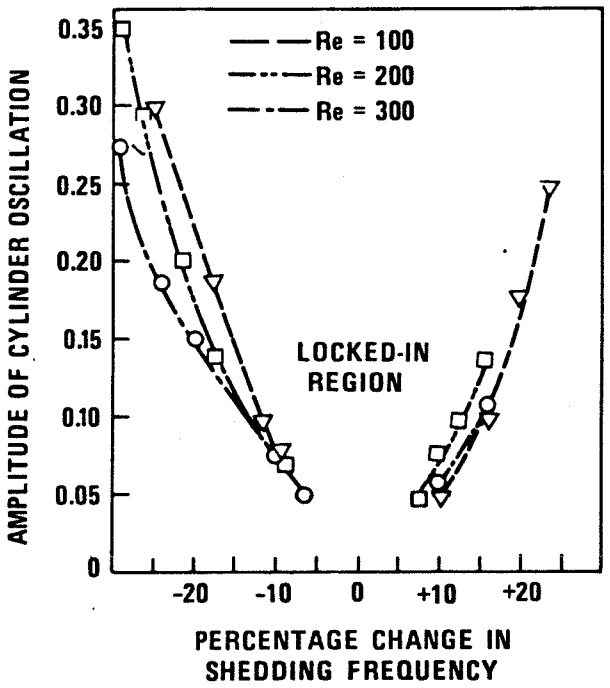

Figure 4.2.1. Regions in which Cylinder Motion Controls Shedding Frequency, from [38]

Clearly, the frequency difference depends on the amplitude of vibration, which is unknown a priori. As a reasonable estimate, it is sufficient to assume that the vibration amplitude *at a given frequency* will be small, even though the total amplitude may be large. Therefore, the lower asymptote of the frequency difference presented in the figures may be assumed, and taken as approximately ± 0.1. While this appears a somewhat crude method of selection, the lack of appropriate experimental data for the cases under consideration precludes a more detailed analysis at this stage.

Returning to Equation 4.2.3, the term $\frac{\Delta\omega_s}{\omega_s}$ may now be taken as 0.2, so the equation simplifies to

$$\frac{\Delta x}{D} \approx 0.2 \frac{1}{\beta}. \tag{4.2.4}$$

Given a value of β, the cell length may now be estimated for a particular case. Note that for a β of order 0.0017, the cell length becomes approximately 120 diameters.

4.3 Combination of Cell Responses

From the development in the preceding section, the length of a cell for a particular flow profile may be determined. The system may be divided into a series of cells of this length; then, based on the analysis in the preceding chapter, the response in amplitude and phase of each cell may be determined, assuming a constant shedding frequency. Each of the cells will vibrate at a slightly different frequency, so the amplitude and phase response will vary slightly from one cell to the next.

The individual cell responses now must be "added" to produce the total response of the system. With the use of the assumptions outlined at the beginning of the chapter, the various responses are taken as independent, and may therefore be combined by a root-sum-square or direct addition. Keeping in mind the observation that the change in frequencies between adjacent cells is small (20%), and that the computed amplitude response difference is also small, the response of a segment can easily be shown to exhibit a beating type behavior, with a low beat frequency due to the small frequency difference. For this reason, it is felt that a direct addition of responses would give a good estimate of the *maximum* response of the system at any point. However, from a design viewpoint, there is a reasonable chance that the phasing of the response in

adjacent cells is such that the amplitude is small for a long time, due again to the low beat frequency. For this reason, it is deemed valuable to also present a root-sum-square combination of the individual responses which represent an "expected value" of the amplitude of response. This approach will be of more significance if a random vibration approach is used in the individual response calculation. This is a subject for future work, and is not discussed further here.

4.4 Simplification of Approach for Observed Response

It has been observed, and reported by Griffin [24 p. 26], that for many real flows, the sheared nature of the flow had virtually no effect on the response of the structure for moderate values of the shear parameter. For these cases, the response predicted by the assumption of uniform flows was quite accurate. This is attributable to the fact that for the relatively short members under consideration, the natural frequencies were widely spaced and that the large amplitudes produced enable lock-in for wide frequency ranges. This range easily encompassed the entire length of the structure.

It is believed, for long systems, that the effects of the sheared nature of the flow can also be further simplified. Several test runs performed indicated that the change in amplitude response is relatively insensitive to the frequency. This was observed when the responses of a number of cells with equal lengths at different frequencies, consistent with a sheared profile, were computed.

As a simplification, therefore, it is suggested that the response is computed for a frequency based on the midspan flow velocity, using the estimated cell length. The total amplitude response of the system for this case may then be found by summing this one response curve, shifted as appropriate to the various cell locations. This reduces significantly the computation involved. Examples of the application of this

approach are presented in the following chapter.

4.5 Application to General Nonuniform Flows

The preceding sections describe application of the traveling wave solution to a sheared flow profile. The procedure was to calculate a cell length based on the shear parameter and a frequency difference, solve the corresponding system for amplitude and phase response, then combine the amplitude functions in an appropriate way to find the total response.

For the general nonuniform flow, where a linear profile is not an accurate representation, the above method may still be applied. Rather than calculate a cell length based on the shear parameter, β, it is necessary to use a more general definition. Consider the arbitrary example flow profile in Figure 4.5.1.

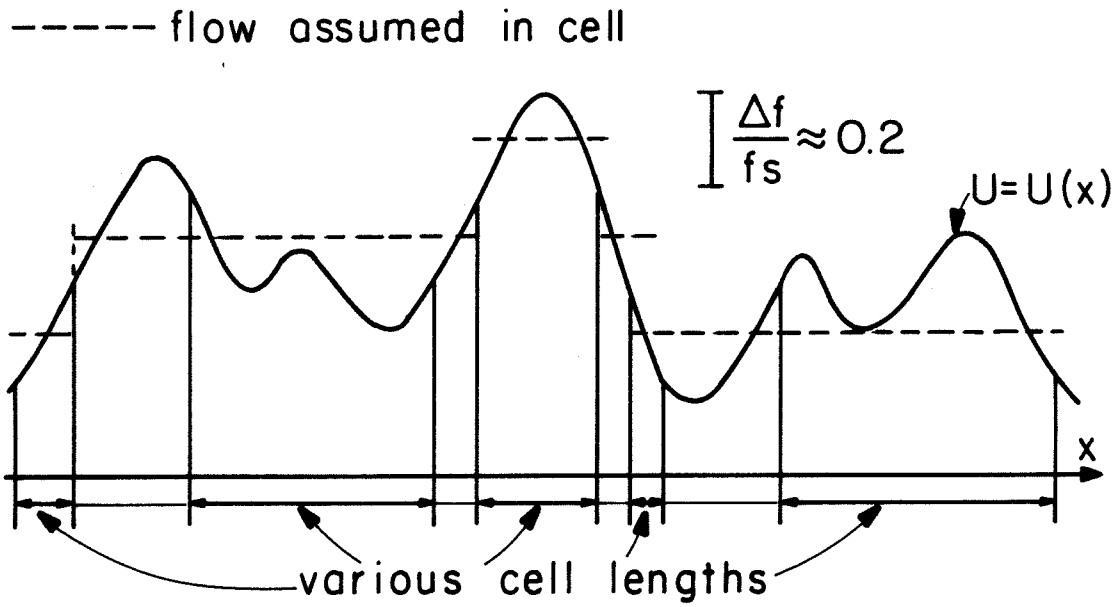

Figure 4.5.1. Example of Arbitrary Nonuniform Flow Profile

Using the frequency difference of 0.2 as before, we find it possible to approximately

divide the system into a number of now *unequal* length cells as shown. The response of each cell may be computed as before, and the results added.

With further work, the approach described may be modified to include the modeling of the effects of nonuniformity in the flow. Clearly, a constant or linearly varying flow velocity are idealizations of real flows. Even in a flow assumed uniform, disturbances due to turbulence will affect the cell length, in general reducing it from what is assumed in this chapter. A thorough understanding of these effects, probably best approached from a random vibration viewpoint, is necessary before a truly accurate representation of nonuniform systems is possible. This is beyond the scope of this work, and will require much experimental work, in addition to the development of new theoretical models.

CHAPTER 5

Results and Discussion

The following Chapter presents the results obtained from the developments in the two preceding chapters. Various combinations of the active and resistance forces are illustrated. The constant active force with viscous damping passive force examples are important as a check on the solution algorithm. Exact analytical solutions are possible for this case, and through comparison with the computed values, some guidelines for discretization interval and "convergence damping" are possible.

Convergence damping, as mentioned above, refers to an artificial increase in internal damping used to improve the convergence of the algorithm. Optimal values may be chosen to obtain the best performance of the iteration scheme. More details on convergence damping may be found under "Programming Considerations" in Appendix I.

The significant results for this thesis appear in Section 5.3.2. These examples illustrate the results for applied vortex-induced forces over the active region (i.e., where the shedding of vortices is feeding energy into the cable), and for Morison-type fluid resistance over the inactive region (i.e., where the fluid is extracting energy from the cable motion). Some very interesting phenomena are observed, and linked to field observations described in Chapter 2.

Section 5.4 presents results and discussion for the application of the above results to nonuniform flow profiles. While there is little experimental data available to

appraise the results critically, it is felt that the solutions presented are physically reasonable, and the approach applicable to problems of this sort.

5.1 Choice of Parameters

Due to the many parameters involved in describing the solutions, it has not been possible, nor deemed particularly valuable at this stage, to perform extensive parameter studies. The results presented use data from what is believed to be physically realistic problems thereby, giving an overall feel for the type of solution which may be expected.

While the analysis outlined is clearly applicable for a wide range of parameters, it is convenient to choose values which exemplify the range likely to be encountered in practice. Typical values of the various parameters chosen are outlined below, with a brief description of the reasons for the choice.

5.1.1 Cable System Parameters

- Mass Parameter, η : The mass parameter is defined as:

$$\eta = \frac{\rho D^2}{\mu} = \frac{4}{\pi}\frac{\rho}{\rho_c} \tag{5.2.1}$$

where μ is the mass of the cable per unit length, ρ_c the mass density of the cable, and ρ the fluid density. As the work in this dissertation concentrates systems where the assumed fluid damping is relatively large (i.e., water as opposed to air), it is assumed that a representative value for ρ is the density of water (i.e., approximately 1000 $\frac{kg}{m^3}$). The cable density is assumed to be at either of two extremes. Light cables of material such as Kevlar have a specific gravity of about

1 (i.e., $\frac{\rho}{\rho_s} \approx 1$). One of the cables used in the experiments of Kim et al. [37] was chosen as representative, and a value of η of 1.144 was chosen. The other extreme is that of a heavy cable in water (such as steel, with a specific gravity of about 6-7). For this case, η was taken to be 0.2.

It should be noted that the added mass of the cable, and therefore total effective mass of the cable (cable plus added mass), can be expressed in terms of η if the cable density (or, alternatively, wavespeed for traveling waves in the cable) is known.

- Frequency of Exciting Force: A convenient way to represent this quantity is as the wavelength of the exciting force, λ. Recalling that the wavelength normalized by the diameter may be written as:

$$\frac{\lambda}{D} = 2\pi\frac{c}{\omega D} \tag{5.2.2}$$

and using the expression for vortex shedding frequency from the Strouhal relationship (Equation 1.2.2), we may write the wavelength corresponding to a vortex-induced force

$$\frac{\lambda}{D} = \frac{1}{S}\frac{c}{U} \tag{5.2.3}$$

where S is the Strouhal Number, U the incident fluid velocity, and c the wavespeed associated with the cable (in air). While U, representing a current velocity, is limited for most practical problems to less than about 10-20 ft/sec, the wavespeed in the cable can vary greatly, depending on the tension and mass per unit length of the cable (Equation 3.2.5). A representative value for $\frac{\lambda}{D}$ is taken as 1000. For the cable mentioned above used in [37], the value was calculated to be

approximately $\frac{\lambda}{D}=720$. Keeping in mind that the cable was light, and the tension low, we estimate that for heavier cables, for example, steel wire, sustaining higher tensions, the ratio may be similar.

- Internal Damping, α_i: The internal damping for a cable of the type considered in this dissertation is in general very low. Kim [36] estimates a modal damping of about 0.16% in the first mode for one of the cables tested. This translates to a value of α of approximately 2 x 10^{-5} in Equation (3.2.18). What is important, however, is that the internal damping is much lower than the externally applied fluid damping. The value chosen, therefore, is not critical to the overall solution because it is overshadowed by the external damping. Thus the value stated above was assumed to be suitable for most of the test cases run herein.

5.1.2 Flow Case Parameters

- Active Length, l/D: This refers to the length of the cable that is being actively excited by the applied force. This varies according to the particular example, and may be anything from a few diameters to several thousand diameters. The active length is one of the parameters that is varied in the presented examples to illustrate features of the various solutions.

  It should be noted that for many real flow situations, active lengths of several hundred or more diameters are not physically realizable. This implies a steadiness in the flow which is not generally found. This problem is addressed in more detail in Section 5.4. It has also been observed that long active lengths result in solutions which are slow to converge. For both these reasons, few long active length cases are included.

5.1.3 External Force Parameters

- Constant Applied Force Magnitude, F_0D/T: This parameter corresponds to the cases involving a constant force (in magnitude and phase) over the active region. As stated above, any value of force could be chosen, and the results would be valid. It was convenient for testing purposes to use values which produced solution amplitudes of the same order of magnitude as would be expected in the vortex-induced oscillation case. The dimensionless values used as input to the program $(\frac{F_0D}{T})$ may appear small, but for low internal dampings, the amplitudes produced can become large.

- Coefficient of Viscous Damping, k: This value represents the value of k in Equation 3.6.1. A typical value chosen was that corresponding to the small amplitude viscous damping coefficient asymptote for the fluid resistance given by Equation 2.4.2.

- Viscosity Parameter, Dc/ν: To calculate the oscillatory Reynolds Number, Re_ω (Equation 2.4.3), it is necessary to consider the kinematic viscosity of the fluid. A convenient dimensionless group is $\frac{Dc}{\nu}$. A representative value of ν for water is 1.5×10^{-6}. The product Dc varies with the problem, but again using the data from [36], we found the dimensionless group to be approximately 1.5×10^5. Again, some variation can be expected, but this was chosen as a good value for example purposes.

5.1.4 Numerical Parameters

These parameters affect the convergence of the program for a given system and loading case. The length of cable beyond the active length, the number of segments per wavelength, or discretization interval, and the convergence damping already

mentioned are the three parameters to be discussed. Selection of these values was made in such a way as to speed the convergence and increase the accuracy, with the constraint of minimizing the computation time. The method for choosing these is outlined in Appendix I.

Table 5.2.1 lists the various values of the parameters used for the examples described in the following sections.

5.2 Results for Constant Force

5.2.1 Constant Force, Viscous Damping

As mentioned in the introduction to the chapter, this set of results is useful for checking the solution algorithm for convergence and accuracy. In addition to the program for implementing the traveling wave solution, the exact solution for this case was calculated using Equations 3.3.23 - 3.3.29.

Figures 5.2.1 - 5.2.3 show the solutions for cases 5.2.1(a) - 5.2.1(c), respectively. Superimposed on these figures are the results from the exact solution as outlined above. The two solutions are indistinguishable. For this problem, 100 segments per wavelength were used as the discretization interval, and iteration continued until the average change in amplitude from one iteration to the next was less than 0.01%.

It will be noted from Table 5.2.1 that all the viscous damping was assumed to be *internal* for these cases. It was found by running many iteration checks that the best convergence for all load combinations was obtained by minimizing the externally applied force in the inactive region of the cable. If it was desired to apply an external viscous damping in the inactive region in addition to the internal damping, the method adopted was to apply this to the system as all internal damping. A

TABLE 5.1.1. Parameters for Example Cases

Case ID	η	λ/D	α_i	l/D	F_0	k	Dc/ν
5.2.1(a)	1.144	1000	.0015	500	.00001	0.0	-
5.2.1(b)	1.144	1000	.0015	2500	.00001	0.0	-
5.2.1(c)	1.144	1000	.0015	10000	.00001	0.0	-
5.2.2(a)	1.144	1000	.00002	500	.00001	-	150000
5.2.2(b)	1.144	1000	.00002	1125	.00001	-	150000
5.2.2(c)	1.144	1000	.00002	2500	.00001	-	150000
5.3.1(a)	1.144	1000	.0015	500	-	0.0	-
5.3.1(b)	1.144	1000	.0015	2500	-	0.0	-
5.3.1(c)	1.144	1000	.0015	10000	-	0.0	-
5.3.2(a)	1.144	1000	.00002	500	-	-	150000
5.3.2(b)	1.144	1000	.00002	1125	-	-	150000
5.3.2(c)	1.144	1000	.00002	2500	-	-	150000
5.3.2(d)	0.2	1000	.00002	500	-	-	500000
5.3.2(e)	0.2	1000	.00002	1125	-	-	500000
5.3.2(f)	0.2	1000	.00002	2500	-	-	500000

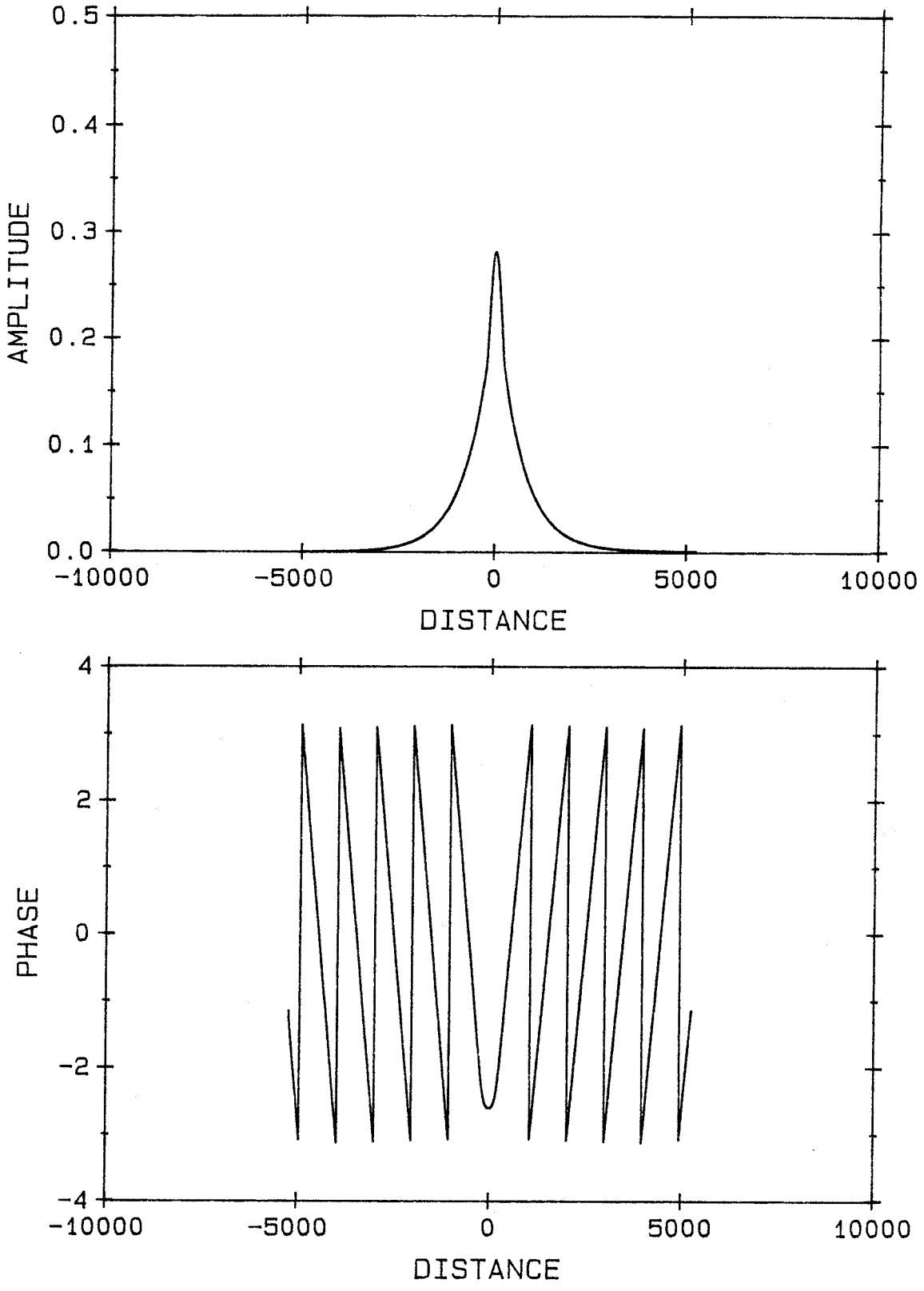

Figure 5.2.1. Amplitude and Phase versus Distance for Case 5.2.1(a)

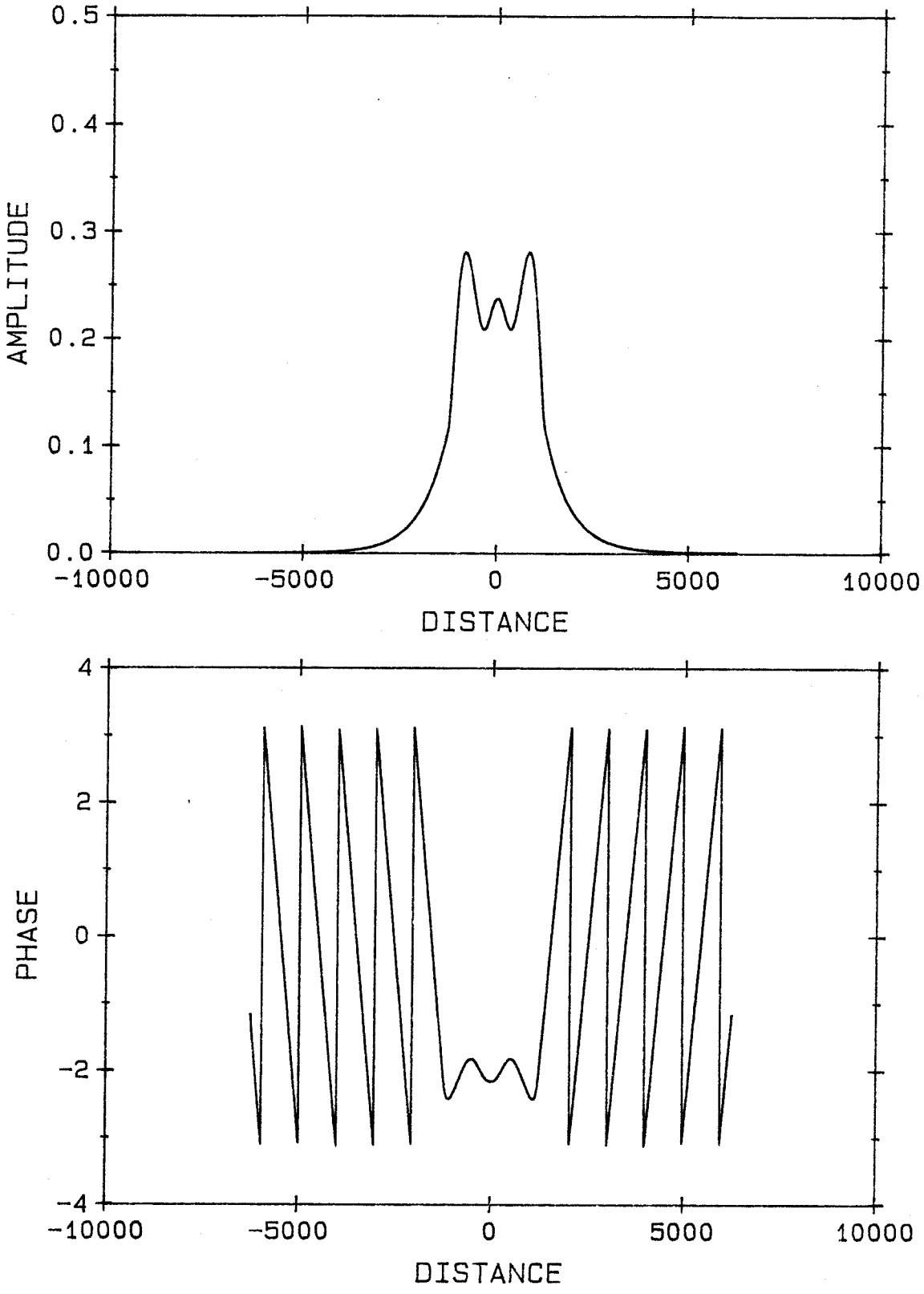

Figure 5.2.2. Amplitude and Phase versus Distance for Case 5.2.1(b)

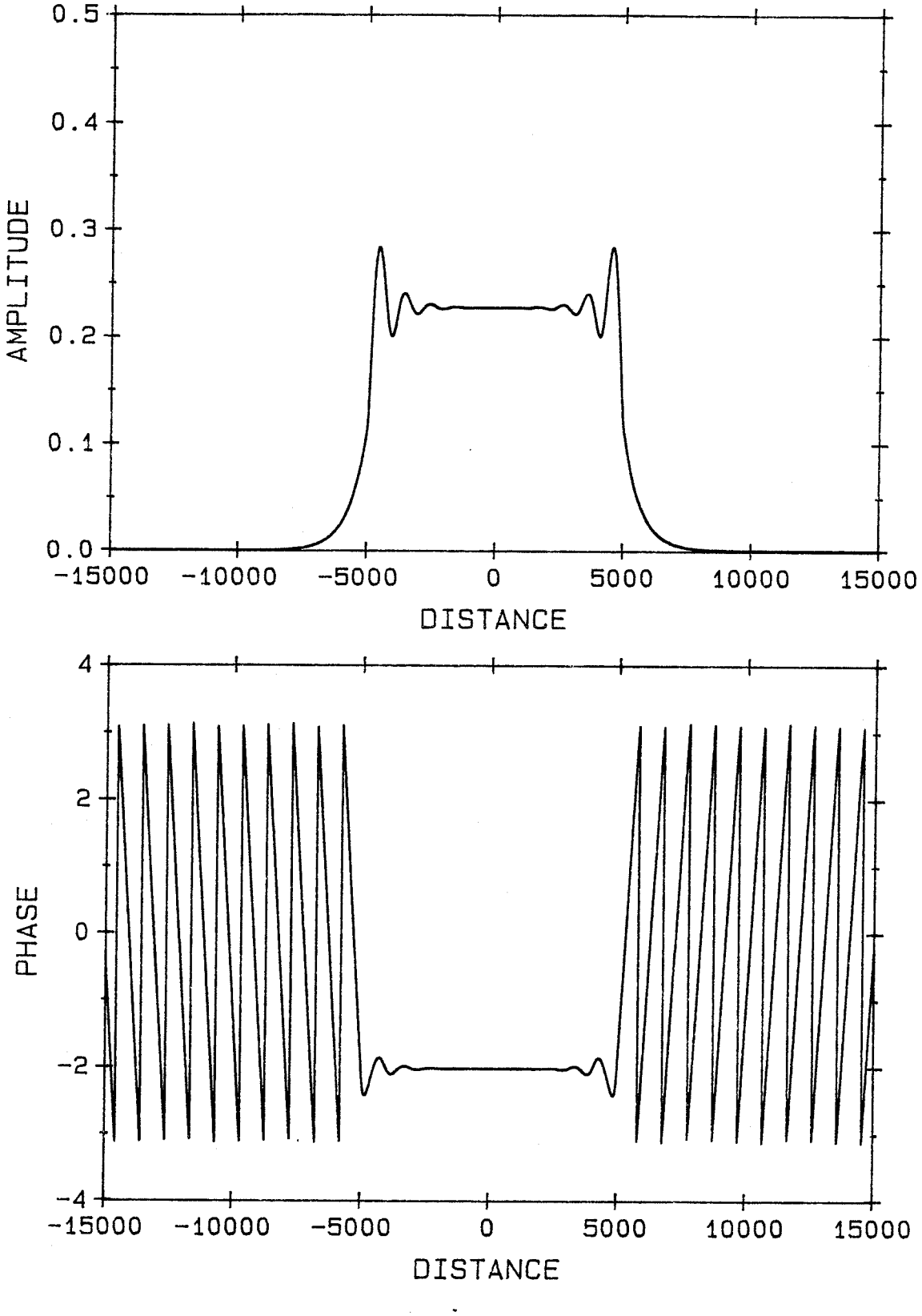

Figure 5.2.3. Amplitude and Phase versus Distance for Case 5.2.1(c)

compensating forcing term, or negative damping in the active region, was then added to the active region with the constant or vortex-induced force already present. This idea is discussed in more detail when Morison damping is considered.

In all the following sections, the abscissa on each plot represents the distance along the cable, normalized by the cable diameter. The amplitudes also are normalized by cable diameter, and the phase given in radians. The sawtooth nature of the phase plots is simply due to the evaluation of the $\tan^{-1}$ function, which is defined between $-\pi$ and π. All the cases considered are symmetric, with the active region located centrally about the "0" position on the abscissa. The length of the active region is given in Table 5.1.1.

A few points may be noted about the nature of the solution. The phase variation is as would be expected. In the inactive region, there is no external force, so the solution is in the form of a traveling wave of exponentially decaying amplitude (see Equations 3.3.23 - 3.3.26). The phase variation is linear with distance, consistent with a traveling wave.

In the active region, the constant spanwise force takes control of the phase, resulting in a distribution which tends to become constant with increasing active length. Some oscillation is apparent at the ends of the active region due to the discontinuity in applied force.

The peak amplitude for this system is approximately constant for the active lengths considered, and always occurs towards the ends of the active region. For longer active regions, the central constant amplitude and phase section increase in size, leaving the ends of the active region unchanged. As the active region is decreased below 500 diameters, the peak amplitude of response clearly becomes

smaller.

It should be noted that this is a well-behaved, linear system. Doubling the force doubles the amplitude. Decreasing the damping, or increasing the frequency of the force also increases the amplitude, although not linearly due to nonlinear dependence on α and β.

The solution algorithm always converges in one iteration for these problems. Since neither the active nor inactive forces depend on the unknown amplitude or phase of the cable, the solution obtained after one pass is the exact solution. The cases that follow do not behave in this way, however.

5.2.2 Constant Force, Morison Damping

The results for applying a constant force with Morison-type fluid damping in the inactive region are shown in Figures 5.2.4 - 5.2.6, corresponding to cases 5.2.2(a) - 5.2.2(c) in Table 5.2.1.

It was noted in the preceding section that the best convergence results were obtained by minimizing the extent of the force that was applied externally. The Morison-type damping includes two terms - one proportional to velocity (drag term) and one proportional to acceleration (inertia term). The above comment was still found to apply, except that in this case both components of the fluid resistance needed to be considered, in addition to the fact that the "drag" term is not purely a viscous damping.

For problems involving Morison-type fluid resistance, the following approach was adopted. While the "drag" term is nonlinear in amplitude, the small amplitude asymptote is viscous in nature. This asymptotic value was added to the internal

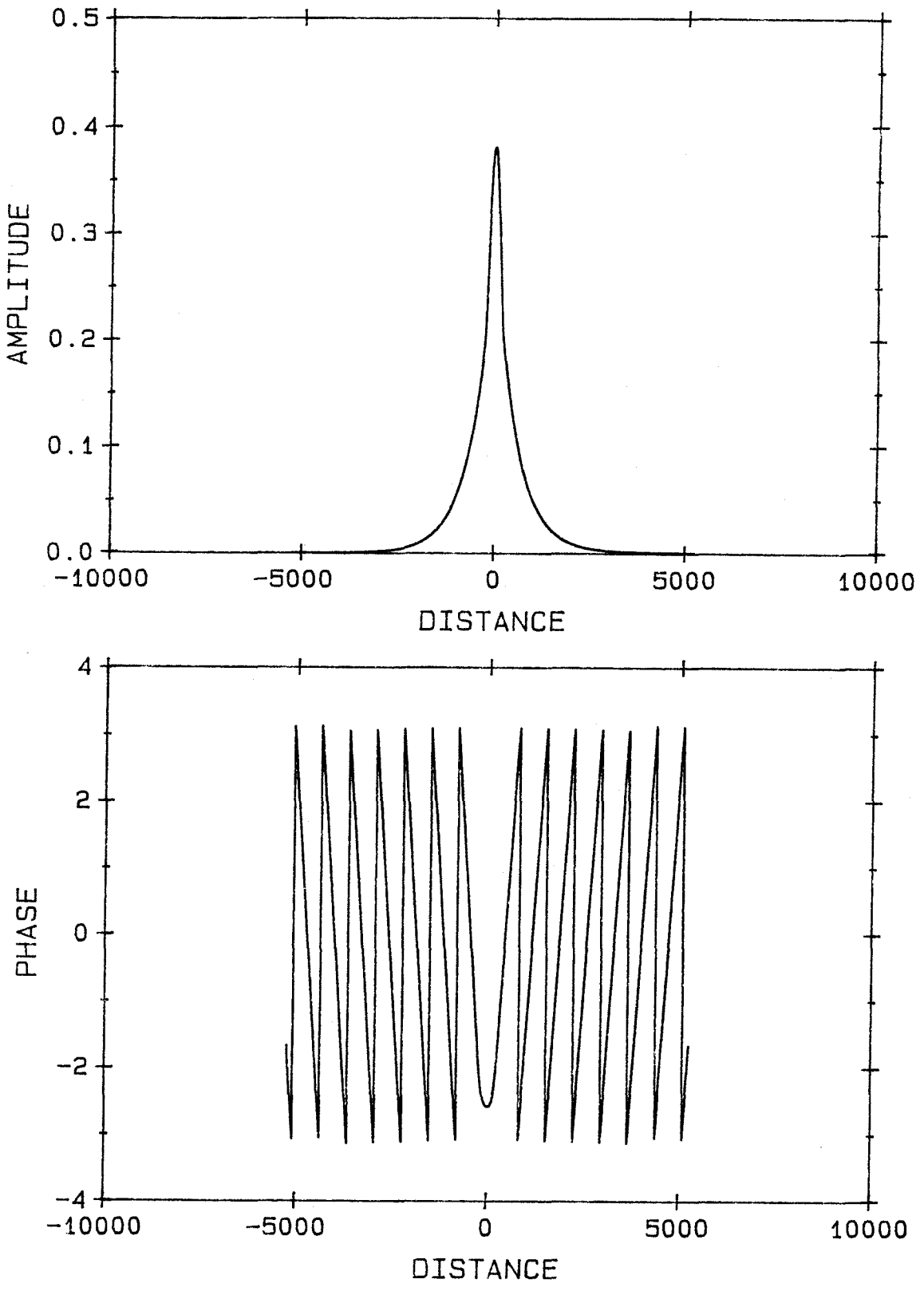

Figure 5.2.4. Amplitude and Phase versus Distance for Case 5.2.2(a)

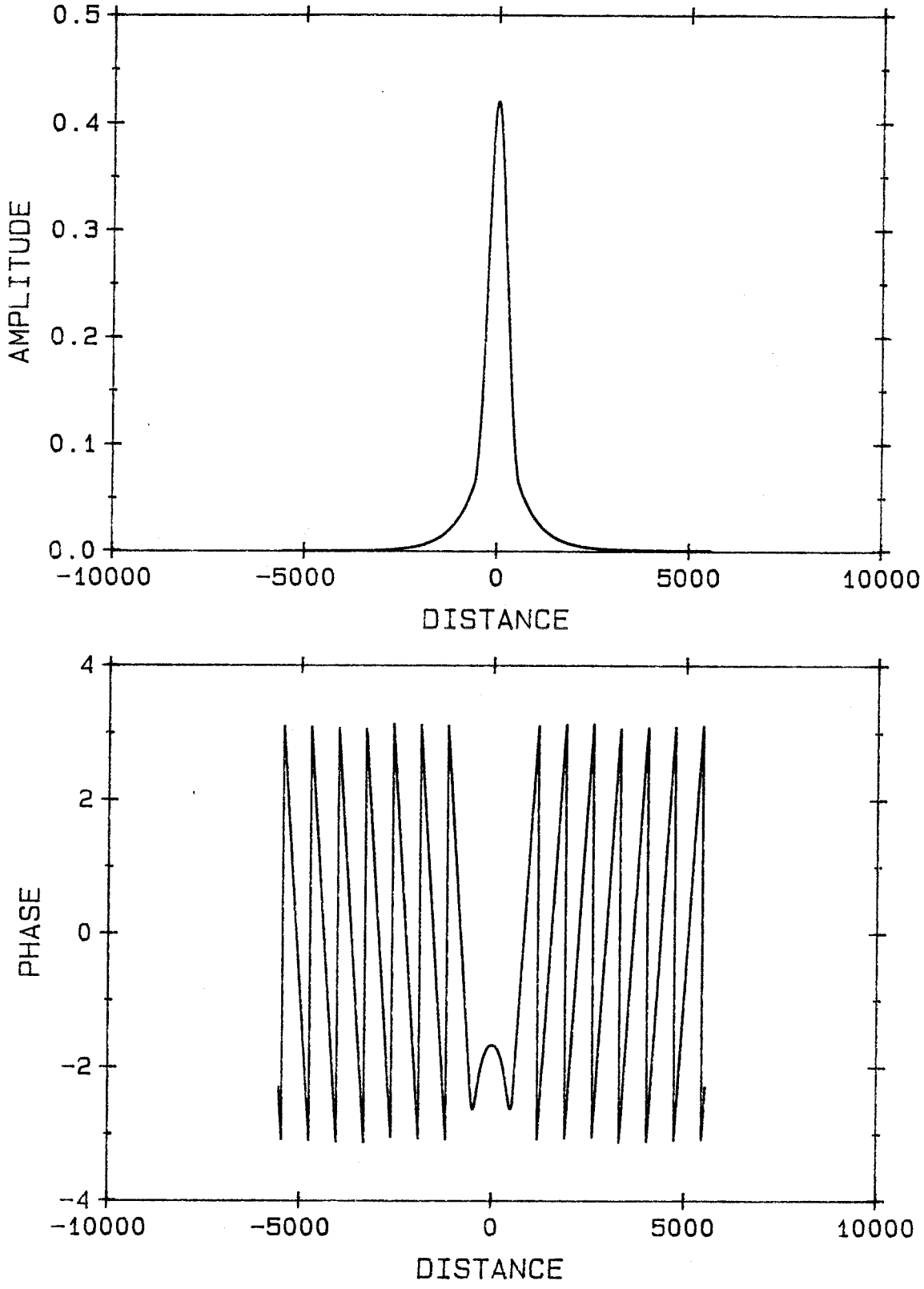

Figure 5.2.5. Amplitude and Phase versus Distance for Case 5.2.2(b)

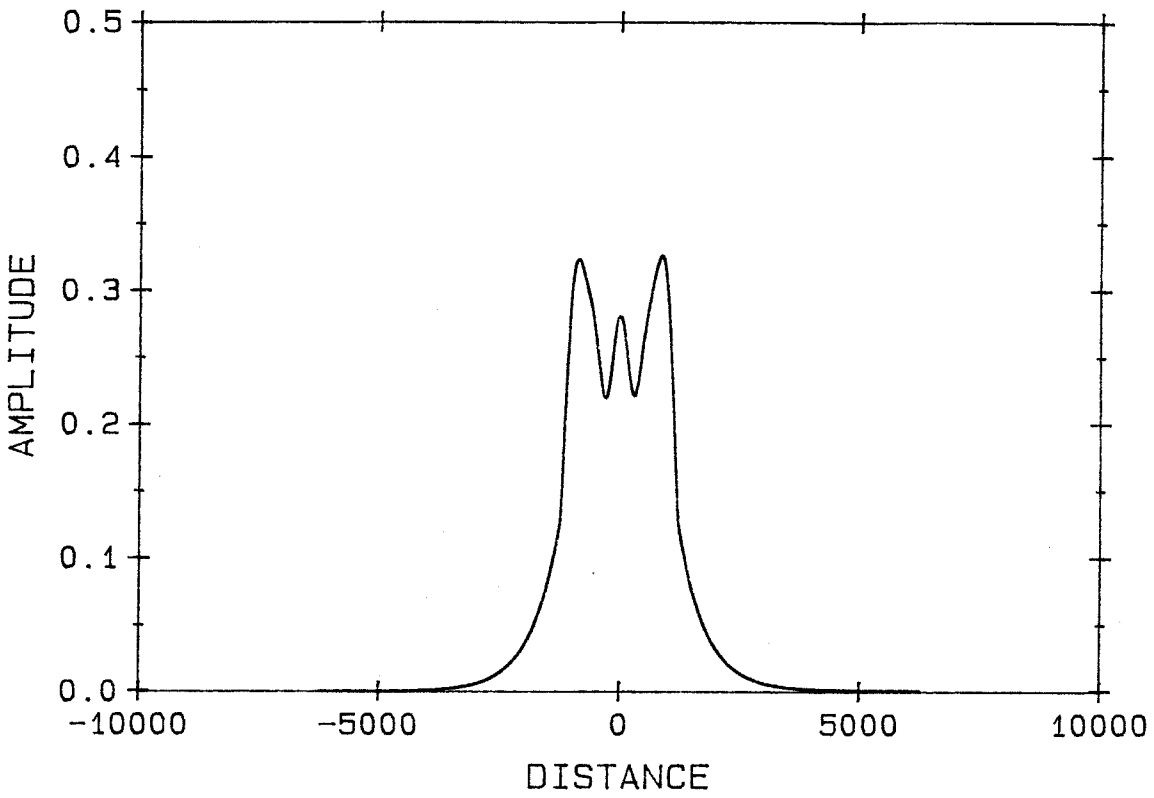

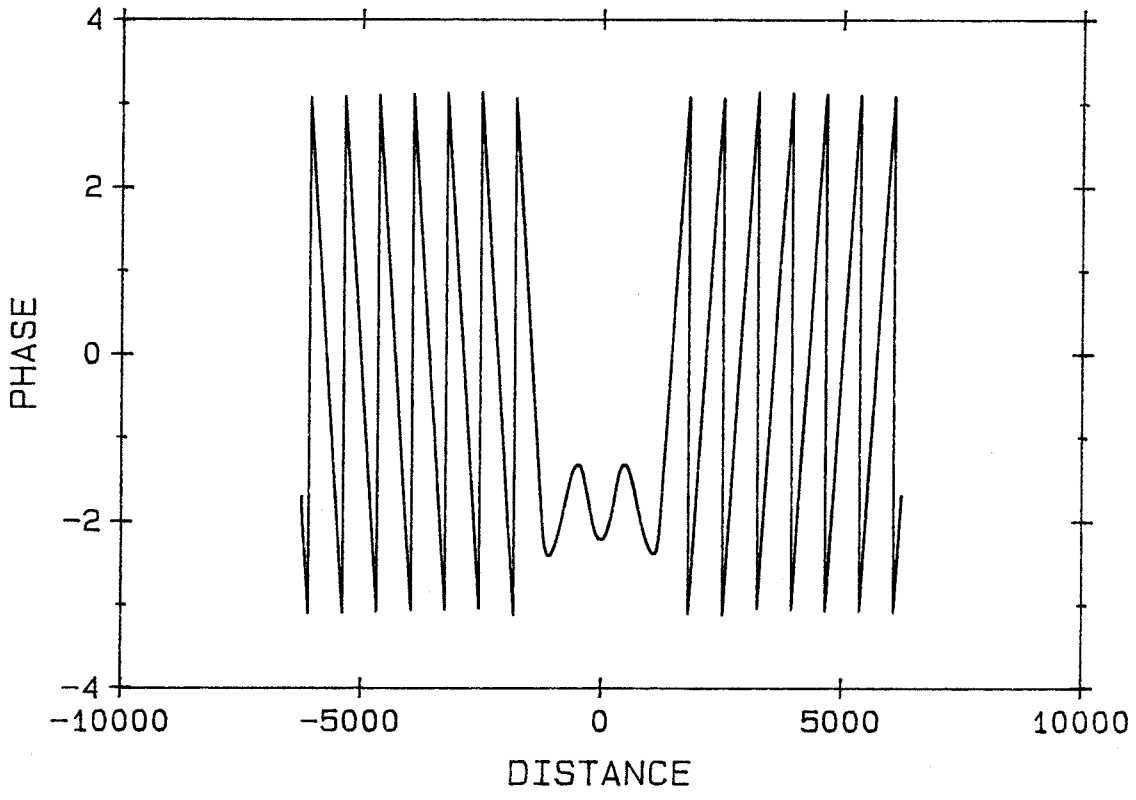

Figure 5.2.6. Amplitude and Phase versus Distance for Case 5.2.2(c)

damping value to obtain a total viscous damping, which was then applied internally. Therefore, only the terms in amplitude to the second power were added externally for the drag component. A similar approach was used for the inertia terms. It was observed in Chapters 2 and 3 that the inertia coefficient is a function of amplitude, frequency and roughness factor. For the ranges of motion considered in this dissertation, estimating the inertia coefficient as a constant of 2.0 was considered a reasonable approximation. This enabled the inertia effects due to the fluid to be added "internally" also, by increasing the effective mass of the cable per unit length. To compensate, this added mass term was removed from the force term in the active region.

The increase in the cable mass is reflected in the phase plots in the figures. The constant of proportionality for the linear phase variation tends to β at the ends of the inactive regions, where the fluid damping is purely viscous. For small damping, β is inversely proportional to the wave speed of the cable (see Equation 3.2.21). The wavespeed decreases with increasing mass, so one expects to see a more rapid phase variation, which is indeed observed.

It is also noticed that the amplitude is greater for this series of tests than for the preceding one, despite the fact that the internal damping, formed with the true internal damping and the asymptotic fluid viscous damping, is actually greater. This is due to the fact that the additional mass of the cable outside the active region effectively creates a more "fixed" boundary at the end of the active region, reflecting more of the supplied energy into the center region.

While the overall behavior with increasing active length is similar to the preceding examples, the algorithm becomes unstable for long active lengths, due to the presence

of the amplitude-dependent inertia term. The iteration scheme diverges and no solution is found. Section 5.5 discusses this aspect in more detail.

5.2.3 Effect of Convergence Damping

Before continuing here it is appropriate to comment on the convergence damping mentioned earlier, and in Appendix I. Clearly, the conversion of the external viscous damping, or fluid drag viscous asymptote, is an application of convergence damping. That is, the internal damping of the cable is assumed to be larger than the real value, and this is compensated by an adjustment of the external applied force. Conveniently, the above choice of convergence damping was found to give the best results for the reasons outlined above; i.e., the spanwise extent of the externally applied forces is minimized.

Many test cases were run with higher values of convergence damping to see if the convergence rate could be improved. It was found that increased convergence damping often led to poor convergence, due to the fact that the spanwise extent of the externally applied force was no longer minimized. Very high values of convergence damping will lead to convergence, but unless the discretization interval is decreased to an impractically small value, the high artificial internal damping totally dominates the solution, and convergence to an incorrect solution is obtained.

Rather than present a number of examples of these effects, it is considered sufficient to make the observation that the best convergence was obtained with the method outlined above, and to proceed with the results for vortex-induced forces.

5.3 Results for Vortex-Induced Forces

The following results were obtained by considering the application of a force representing that due to vortex shedding from a cable. The form of the applied force is given in Equations 3.5.5 - 3.5.7. These solutions assume that the cable is subjected to a spanwise uniform flow over the entire active region.

5.3.1 Vortex-Induced Force, Viscous Damping

To test the representation of vortex-induced forces in the form shown, a series of cases was run with linear viscous damping in the inactive region. These were used to eliminate any problems with the solution technique before proceeding with the more complex case of vortex-induced active forces and Morison-type fluid damping in the inactive region. The results for cases 5.3.1(a) - 5.3.1(c) are shown in Figures 5.3.1 - 5.3.3, respectively.

These results indicate some very interesting phenomena. While the most interesting cases are those in the following section, it is important to make a few observations here.

The peak amplitude of oscillation increases with increasing active length at a greater rate than for the constant spanwise force. This is a direct result of the force magnitude's being a quadratic function of amplitude. The actual value reached for a given active length is a function of the total damping in the system.

The amplitude variation with distance behaves in a curious way. For small active lengths, the behavior is qualitatively similar to that of the constant force case. However, as the active length increases, the amplitude at the center remains approximately constant, while the amplitude towards the ends of the active region

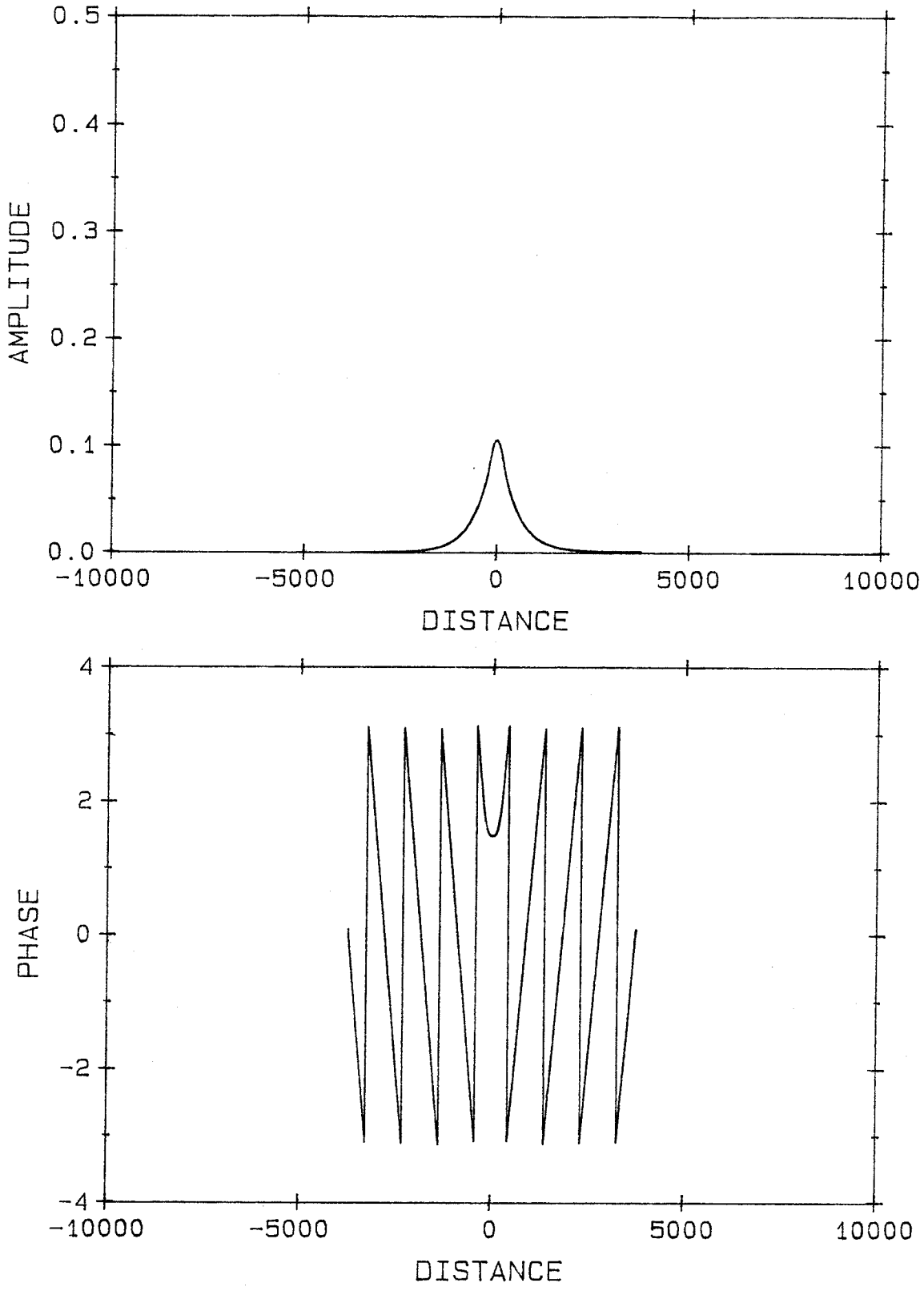

Figure 5.3.1. Amplitude and Phase versus Distance for Case 5.3.1(a)

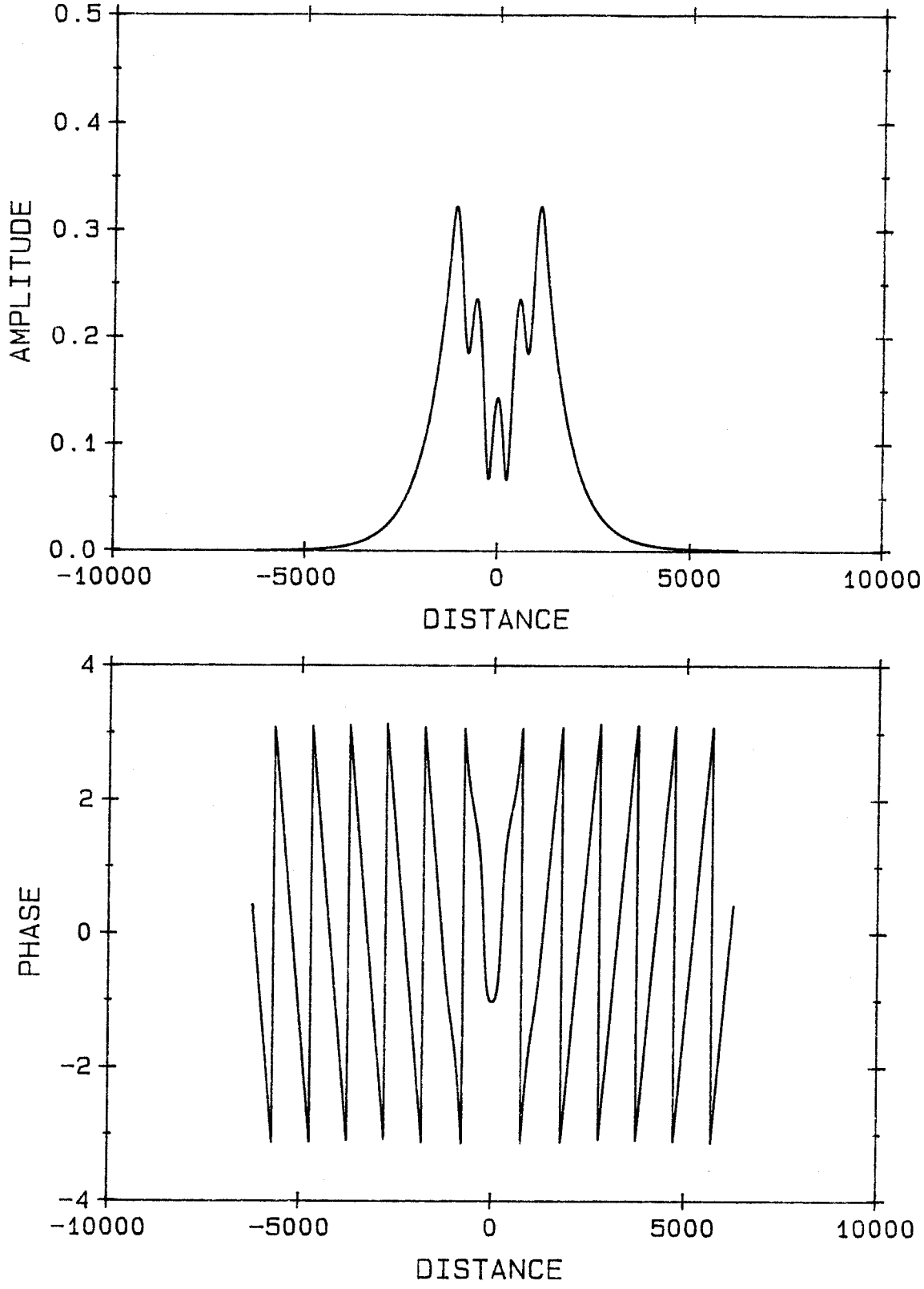

Figure 5.3.2. Amplitude and Phase versus Distance for Case 5.3.1(b)

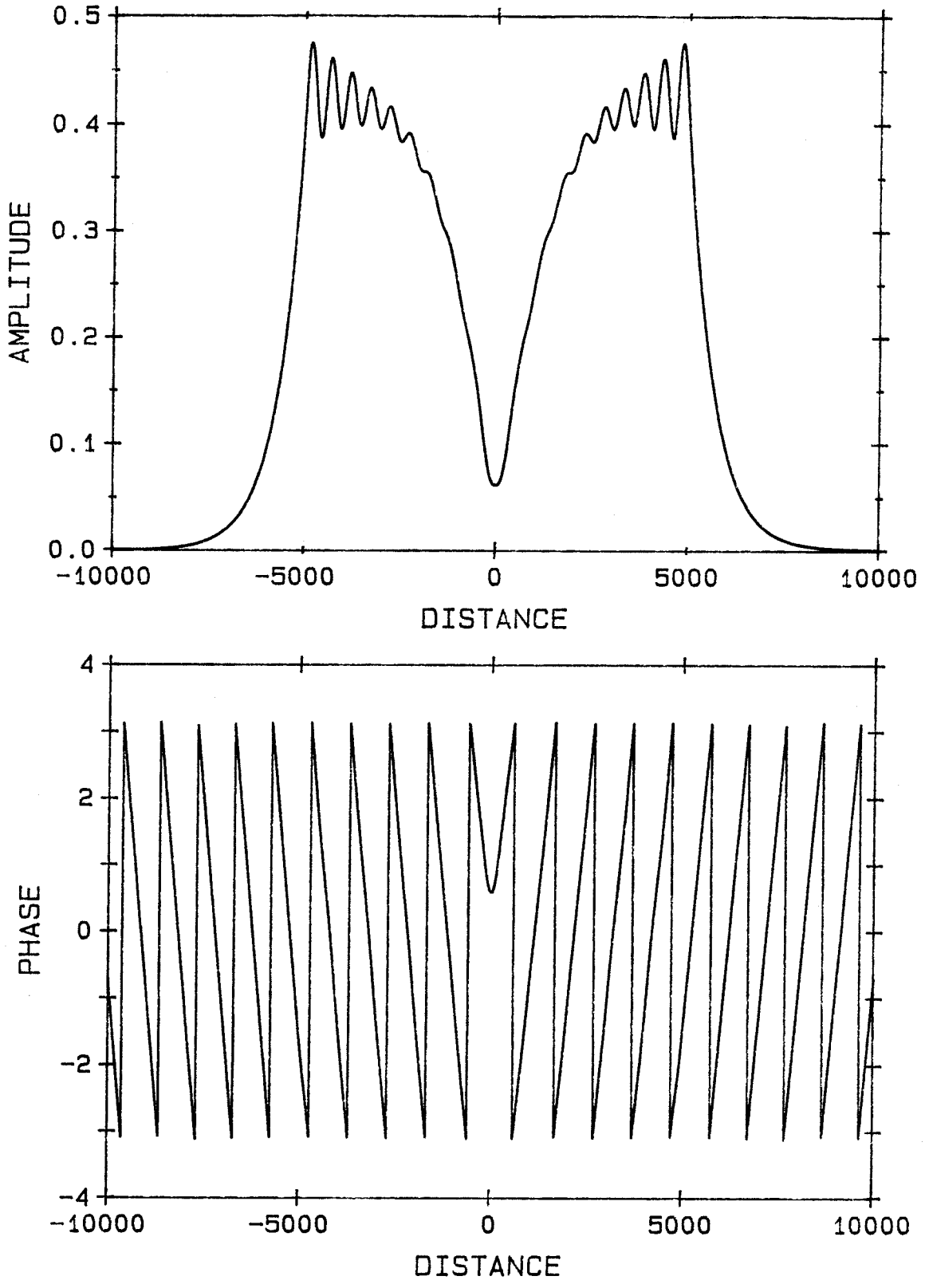

Figure 5.3.3. Amplitude and Phase versus Distance for Case 5.3.1(c)

increases. This behavior is also observed with Morison damping. As the active length increases, the solution tends to a low central region, of approximately constant width, growing symmetrically on either side to two regions of constant amplitude, then to an oscillating amplitude near the boundaries of the active region.

This behavior may be explained by the nature of the vortex-induced force. Unlike the constant force case, which has a given phase as a function of distance, the vortex force is proportional to the local cable velocity, an unknown during the iteration process. As iteration proceeds, the solution approaches an almost linear phase variation from near the center of the active region, representing a flow of energy toward the inactive regions. Away from the center, the shedding force "sees" a local cable velocity and exerts a force in phase with this motion. Thus, moving away from the center, each segment adds incrementally to a total wave that is effectively traveling away from the center of the active region.

While the extreme, long active length cases produce interesting amplitude behavior, it should be emphasized that this implies a uniform current velocity for a very large number of diameters. This is not usually found in practice, and is the motivation for the analysis of Chapter 4.

5.3.2 Vortex-Induced Force, Morison Damping

This section presents results which are of the most practical significance. Cases 5.3.2(a)-5.3.2(c) use similar parameters to those used in the preceding sections, and the results are presented in Figures 5.3.4 - 5.3.6. For cases 5.3.2(d) - 5.3.2(f), the parameters were varied to represent a taut steel cable, with a correspondingly higher value for the viscosity parameter, and a lower value of η. These are shown in Figures 5.3.7 - 5.3.9.

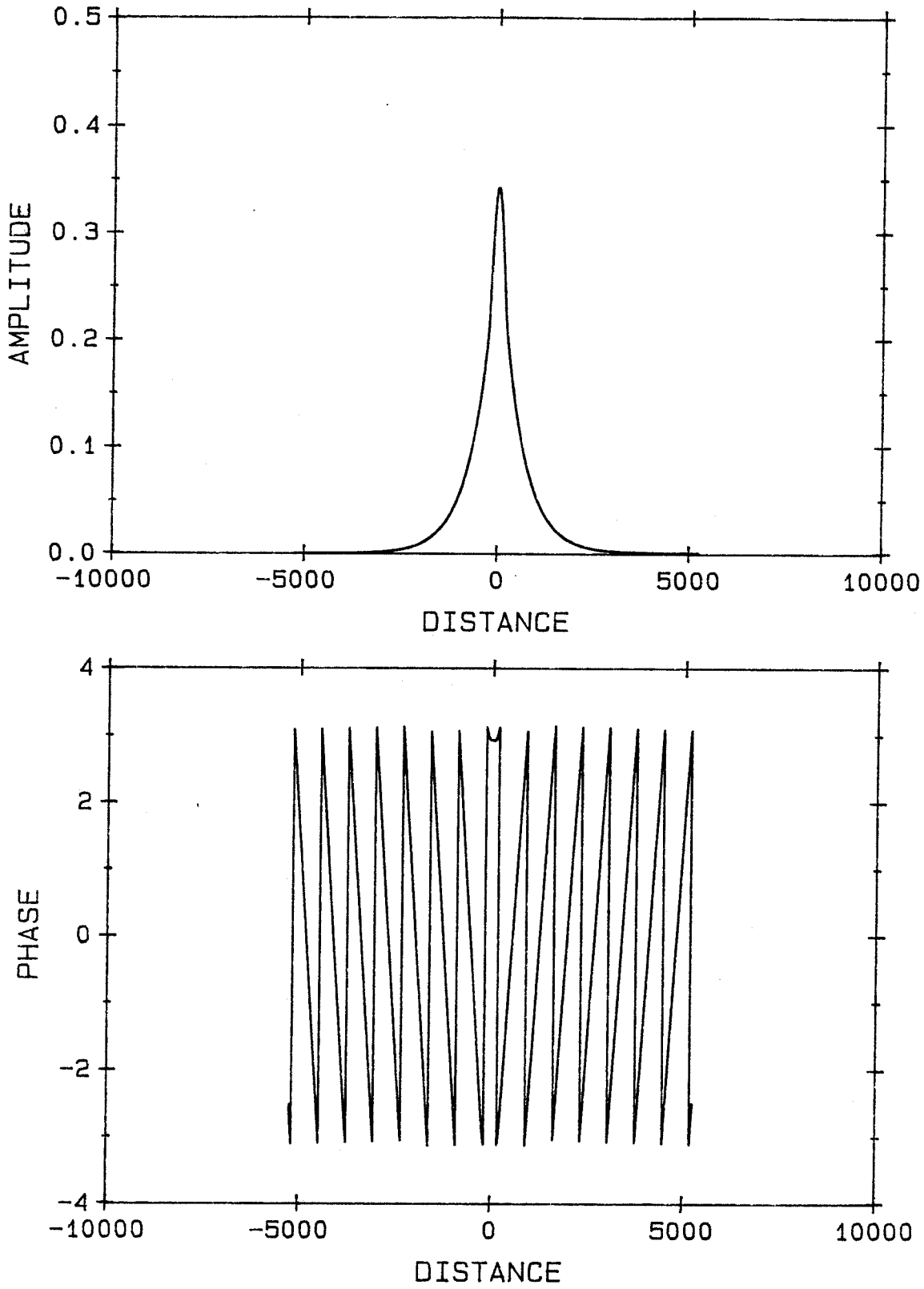

Figure 5.3.4. Amplitude and Phase versus Distance for Case 5.3.2(a)

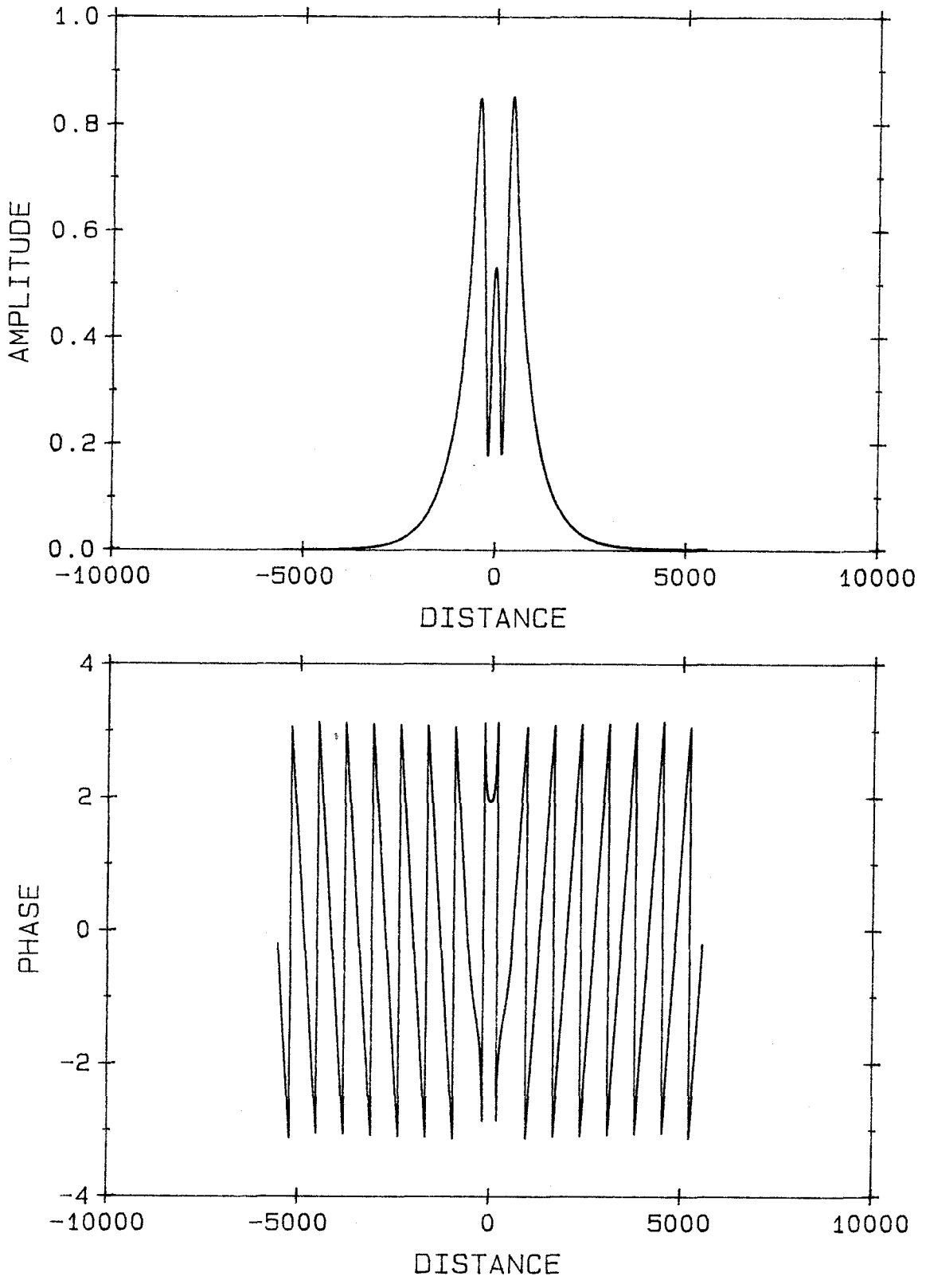

Figure 5.3.5. Amplitude and Phase versus Distance for Case 5.3.2(b)

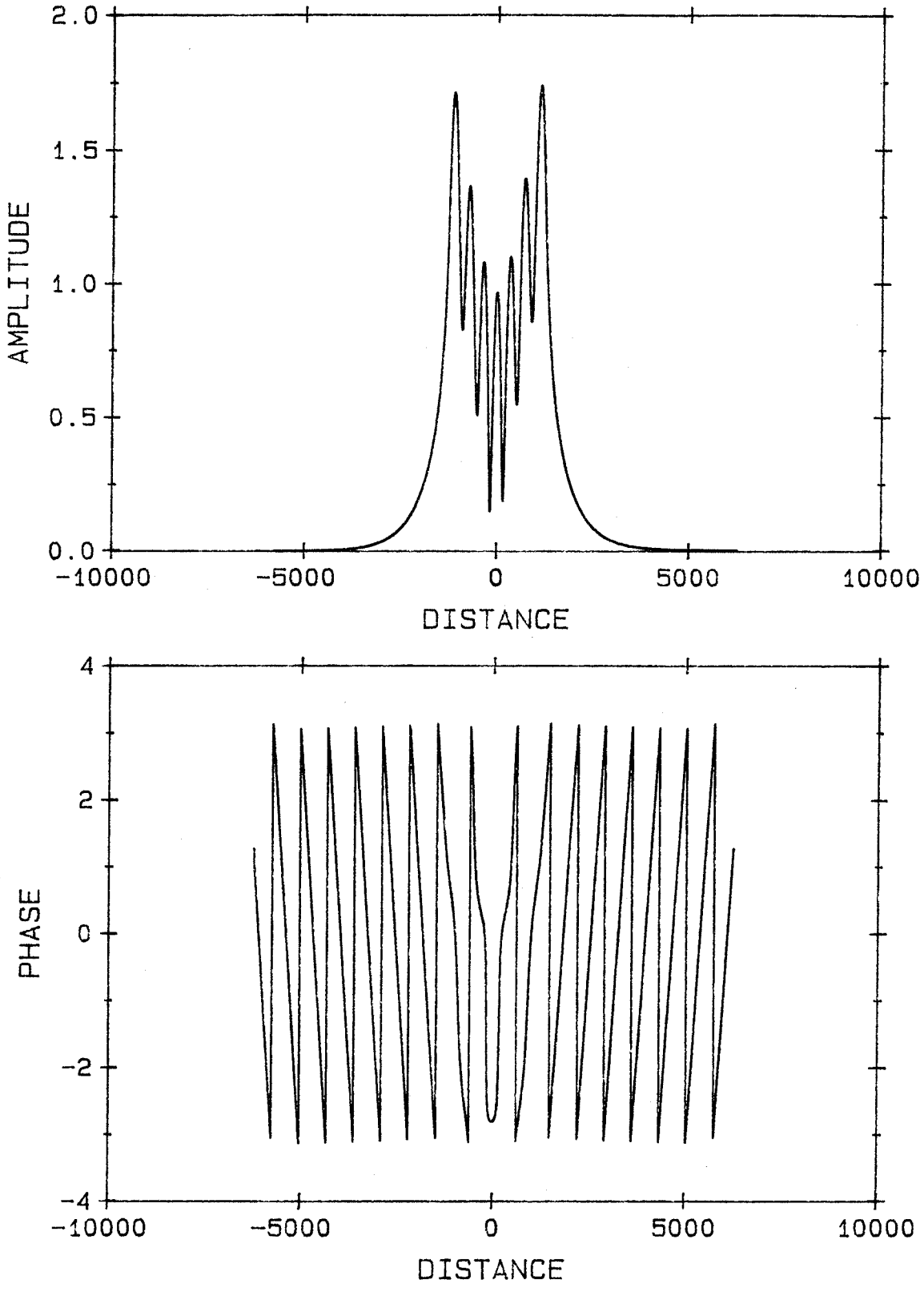

Figure 5.3.6. Amplitude and Phase versus Distance for Case 5.3.2(c)

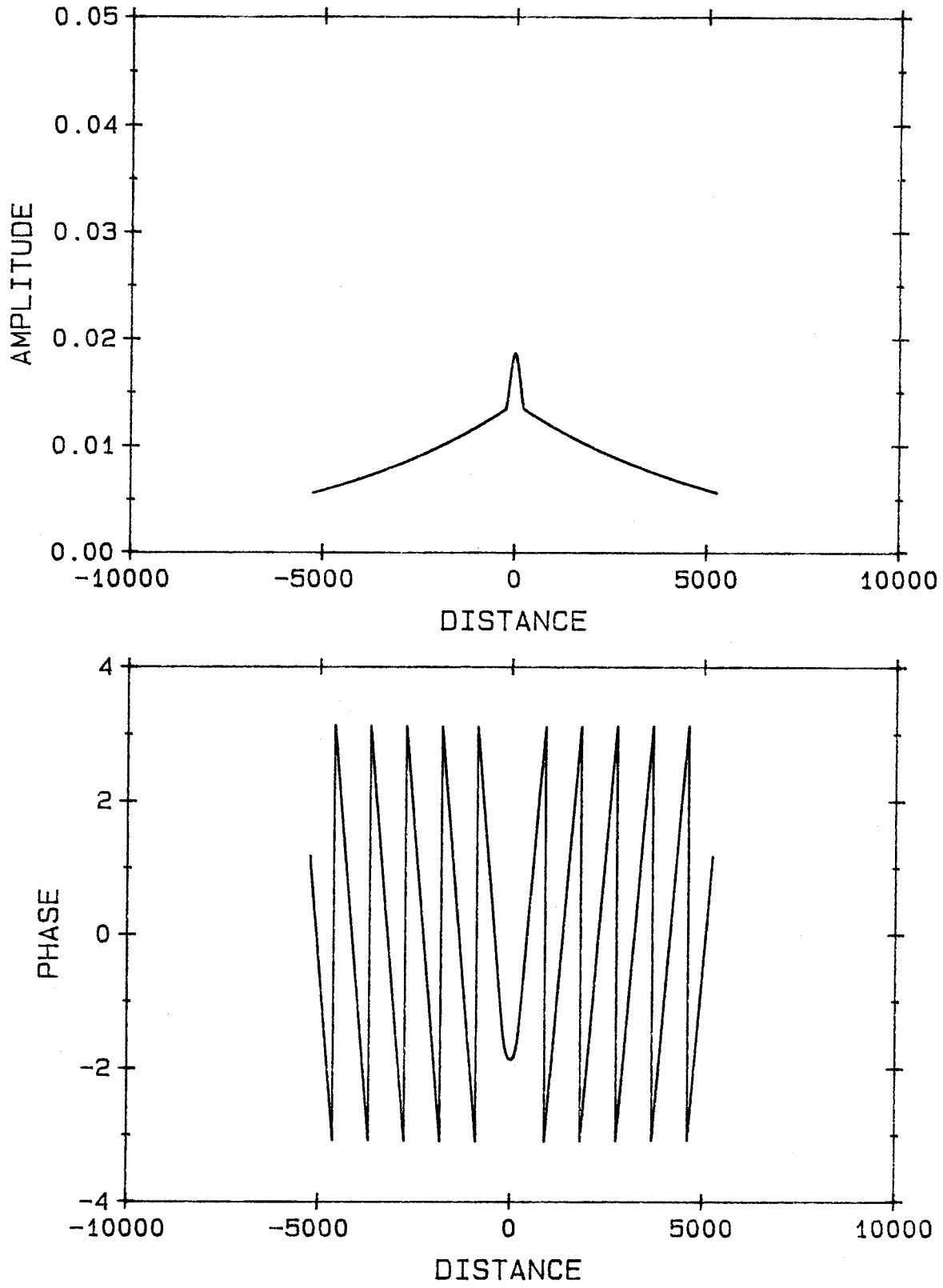

Figure 5.3.7. Amplitude and Phase versus Distance for Case 5.3.2(d)

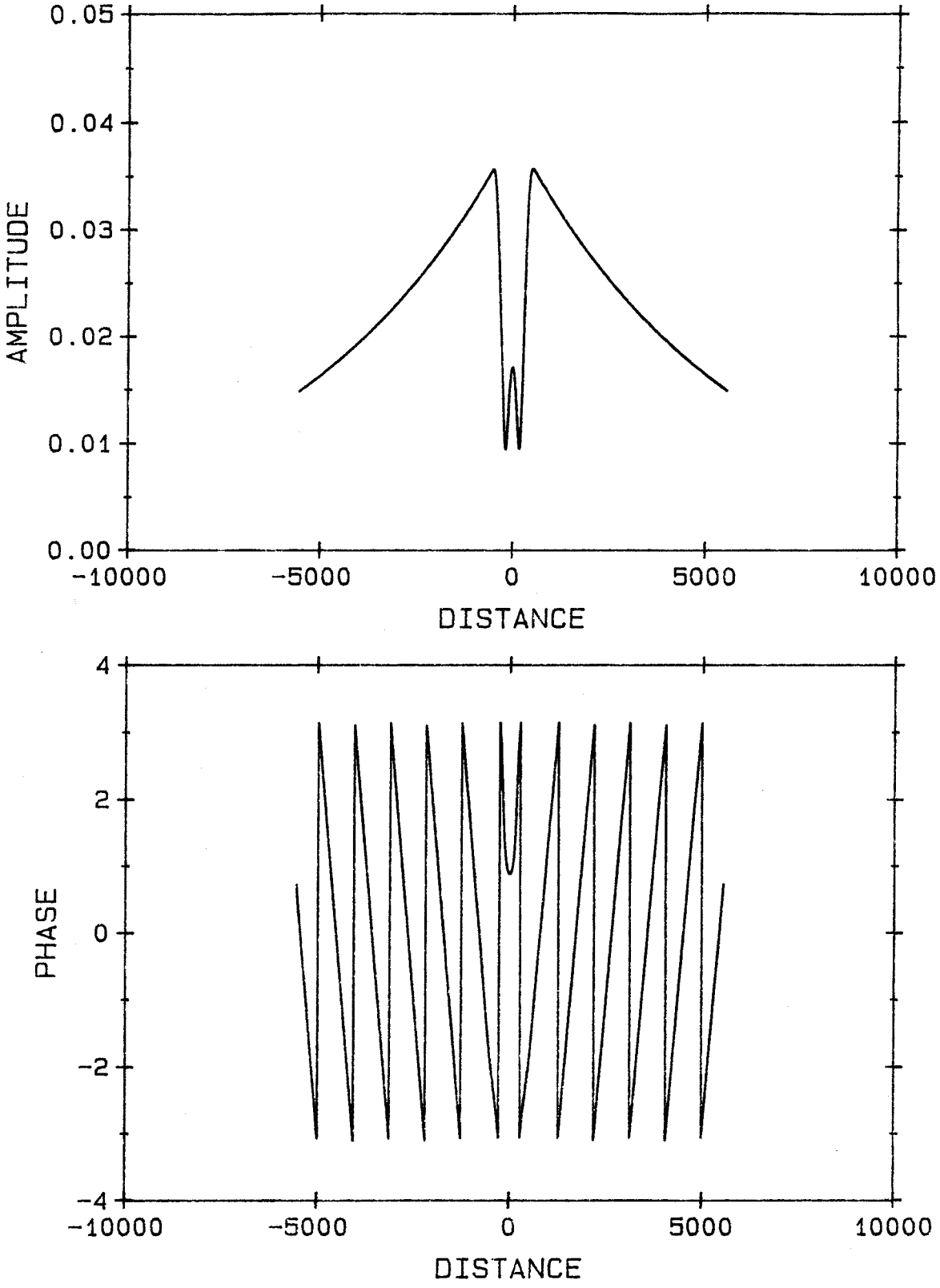

Figure 5.3.8. Amplitude and Phase versus Distance for Case 5.3.2(e)

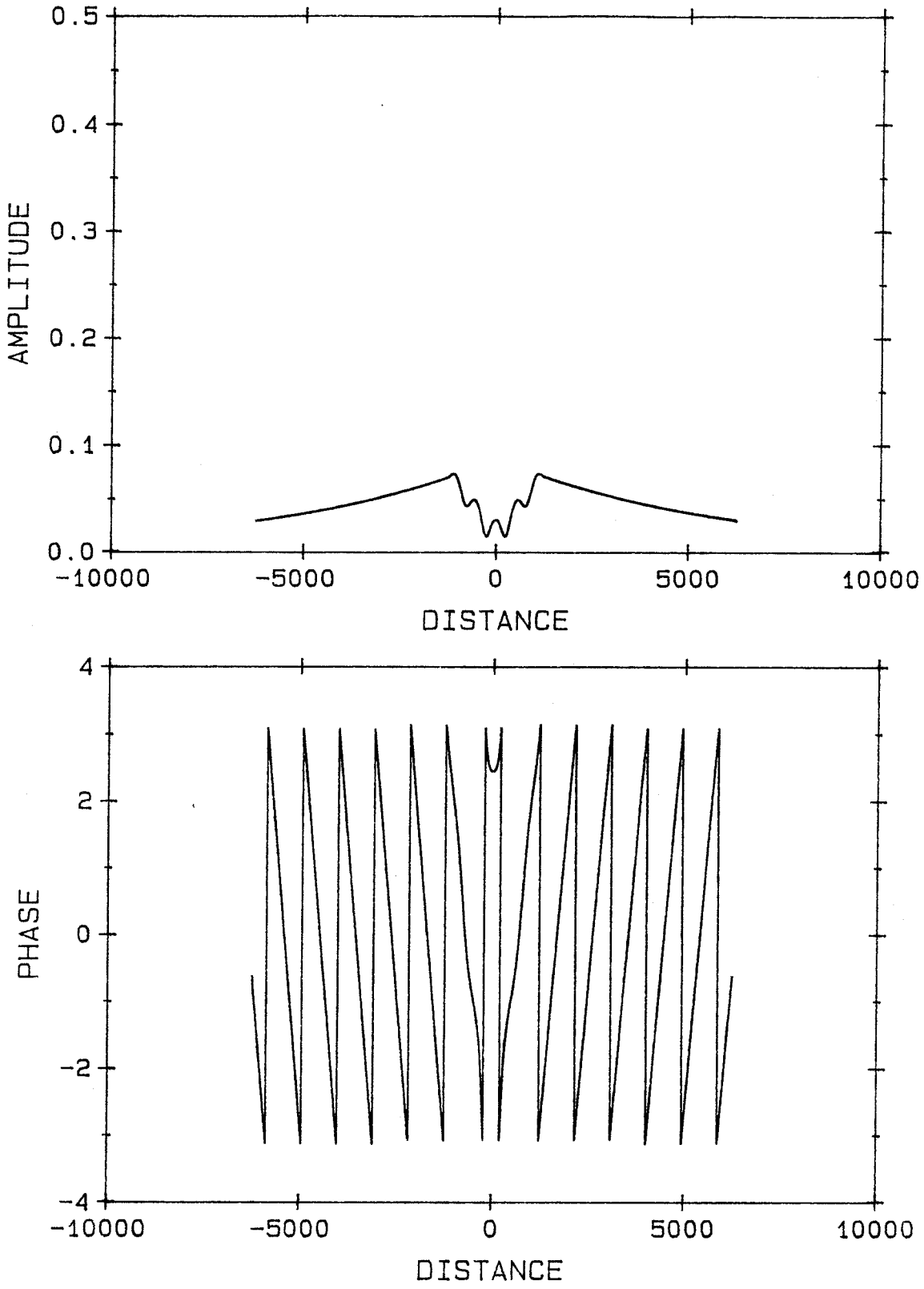

Figure 5.3.9. Amplitude and Phase versus Distance for Case 5.3.2(f)

The results obtained are qualitatively similar to those in Sections 5.2.2 and 5.3.1 where vortex-induced forcing and Morison damping were used. Notice that the magnitude of the oscillations in amplitude for longer active lengths is larger than for viscous damping. This is again believed due to the effective reflection of energy back into the active region from the now more "massive" inactive regions of the cable.

Notice also that the wavelength of the amplitude oscillations is shorter than for the viscous cases, even though the added fluid mass components have been made zero in the active region, consistent with Equation 3.5.5. Each of the inactive cable regions can actually be modeled as a spring-dashpot system, with appropriate choice of the stiffness and damping values. These parameters are easily shown to be linear functions of α and β/ω, respectively, where ω is the frequency of vibration. The system can then be represented as an active region, supported on a frequency and damping-dependent spring-dashpot system. The active region can then be thought of as having "modes," although the frequency-dependent boundary conditions make the calculation more complex than for constant stiffness/damping values. For example, as the damping in the inactive region is increased, the system sees a boundary condition that becomes more and more "fixed;" i.e., the system becomes stiffer, and the "natural frequencies" become higher. A similar effect occurs with increased mass in the inactive region - the stiffness parameter can be shown to increase, resulting in an overall stiffer system, with an associated higher "natural frequency." This is the effect that is observed in the figures.

Unfortunately, this question of modes raises some problems for the longer active length solutions. As the active length is increased, the solutions obtained become more and more unstable in nature, until finally, convergence is not obtained. This is

believed to be due to the fact that the true solution sought becomes more mode-like in nature, so a solution of linearly varying phase is not compatible. A pure mode would exhibit phase changes of π radians between adjacent peaks in amplitude. This is not possible for the type of solution generated from this algorithm. For long active regions, it is better to use existing modal techniques, assuming the ends of the active region to be fixed.

Note that this problem was not observed for the constant spanwise force examples. This is because the phase of the solution is controlled by the constant phase of the applied force. In the vortex-induced vibration case, the phase is free to vary, so the solution generated reflects the phase generated by the algorithm, which is not physically realizable.

The amplitudes of vibration in Figures 5.3.7 - 5.3.9 are much lower than in the preceding cases. This is a result of the increased cable mass. Much more energy is required to move the cable by the same amount. The higher value of Dc/nu also results in a lower damping for small amplitudes, so the decay of response outside the active region is slower. Note that for the last case, the algorithm was halted after 25 iterations. It is expected that a longer inactive region would enable a more rapid convergence.

A similar behavior of the amplitude with increasing active length is observed as in the viscously damped case. Again, these long active lengths are not of practical significance. The following section addresses the more commonly encountered design problem of nonuniform flow.

5.4 Results for Sheared Flows

In Chapter 4, an approximate method was presented for the analysis of nonuniform flows. This section uses that approach to analyze the cable deployed by Kim et al. [37] at the St. Croix location. The current profile as measured in this test is reproduced in Figure 5.4.1. Clearly, the spanwise velocity distribution is highly nonuniform. It was also noted that there was some uncertainty in the performance of the expendable current probe used to measure the profile. Based on this data, an approximate flow profile was estimated for analysis purposes. This is shown in Figure 5.4.2. The chosen curve attempts to capture some of the characteristics implied by both current measuring devices, by assuming a triangular distribution with a peak velocity of 1.5 ft/sec at the midpoint. At this stage, the low velocity regions were neglected.

For analysis, the wave velocity in the cable was calculated to be about 150 ft/sec. Using Equation 4.2.1, we estimated the shear parameter, β, for the assumed profile as 5.4 x 10^{-4}, and the corresponding correlation length, from Equation 4.2.4 as 370 diameters. The 100ft. active region was broken into 20 cells, each of 370 diameters, and the mid-cell velocity was calculated from Figure 5.4.2. The solution for each cell was then computed, yielding a series of curves all qualitatively similar to Figure 5.3.4. Note that the minimum wavelength of the shedding force, calculated from a flow velocity of 1.425 ft/sec, was 526 diameters. The active region was, therefore, at most 70% of the shedding frequency wavelength - well within the range of "well-behaved" solutions for these cable parameters.

The response amplitudes from the individual cells were combined as described in Chapter 4. The results are presented in Figure 5.4.3. Two sets of curves are given.

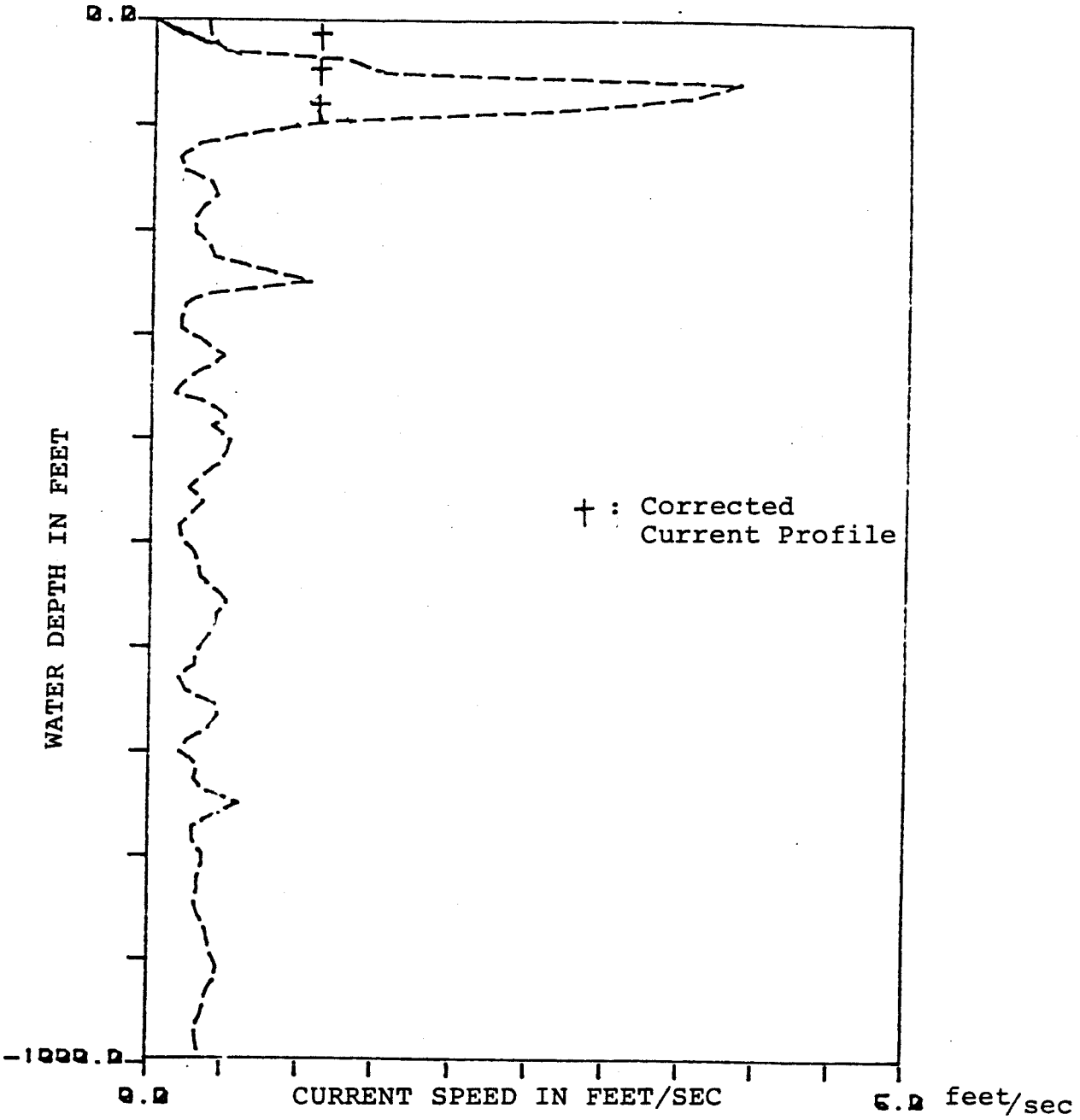

Figure 5.4.1. Measured Current Profile for St. Croix Cable (from [36])

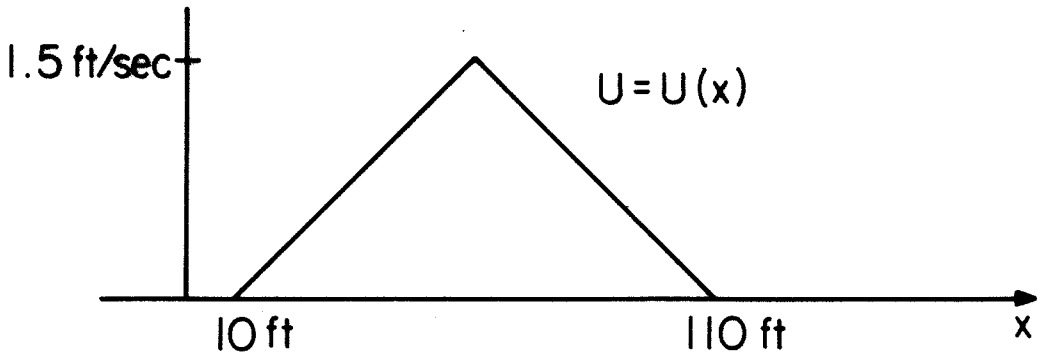

Figure 5.4.2. Idealized Current Profile - St. Croix Cable

The first, or "exact," approach is obtained by computing cell responses using frequencies corresponding to each mid-cell velocity. Thus, the responses of 20 cells (in fact, only 10 are needed, due to the symmetrical nature of the profile) need to be computed. The second, or "approximate" set is obtained by the approach outlined in Section 4.4, whereby the total amplitude is derived from the response computed for one cell at the mean velocity of the active region, 0.75 ft/sec. In fact, a velocity of 0.625 ft/sec was used, corresponding to one of the cells computed in the "exact" case.

In general, the predicted curves are consistent with the observations of Kim et al. Figure 5.4.4 shows recorded RMS amplitudes measured along the cable versus the local current velocity. Also plotted are points representing the peak amplitude computed in each cell. The two data sets are very consistent. For the central part of the active region, the predicted value of response is about 0.35 diameters. This, again, is consistent with the data in Figure 5.4.4. While overestimating the amplitude response at the ends of the cable, the approximate method predicts very well the amplitude in the central part of the active region.

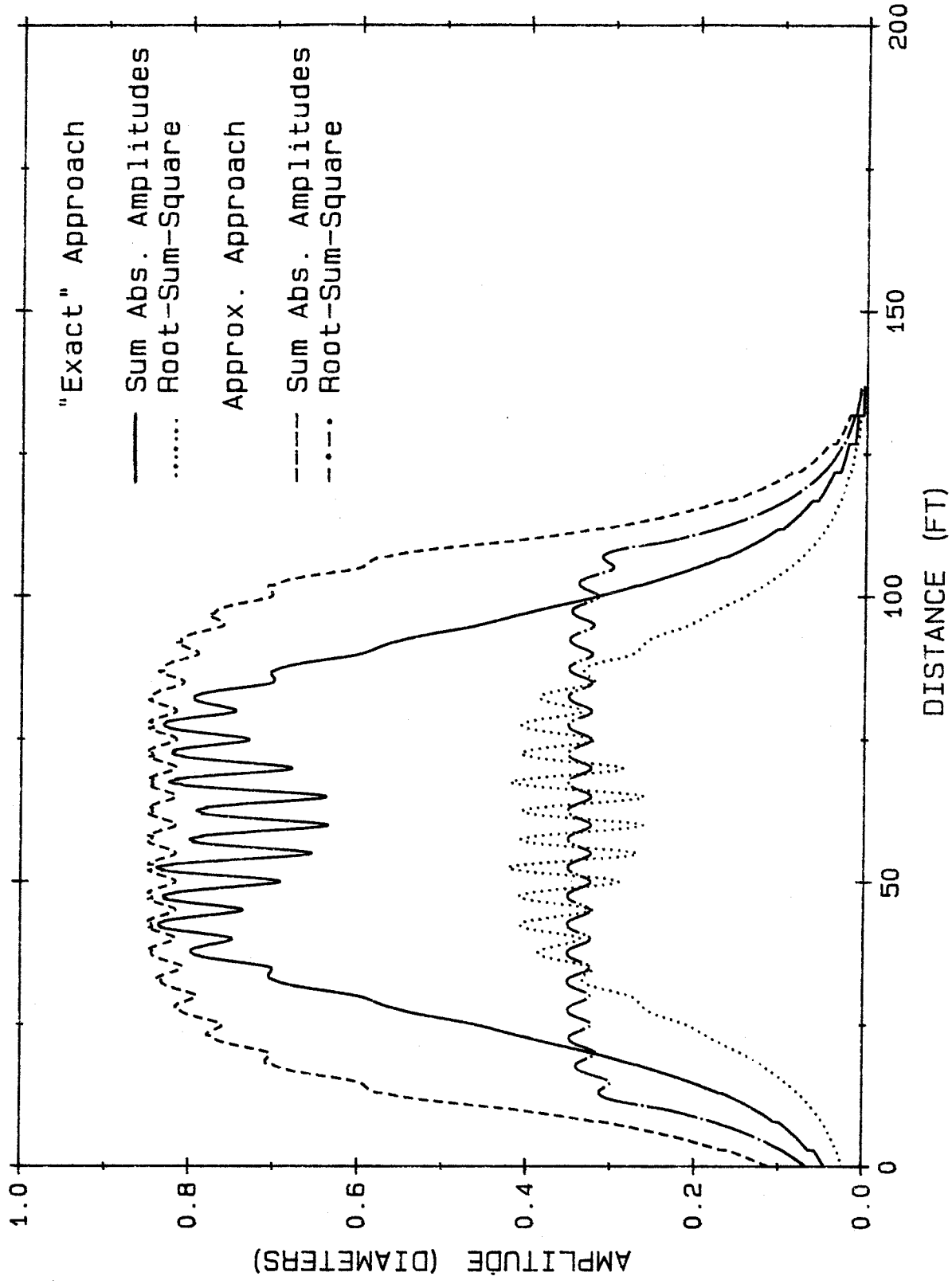

Figure 5.4.3. Computed Amplitude versus Distance for St. Croix Cable

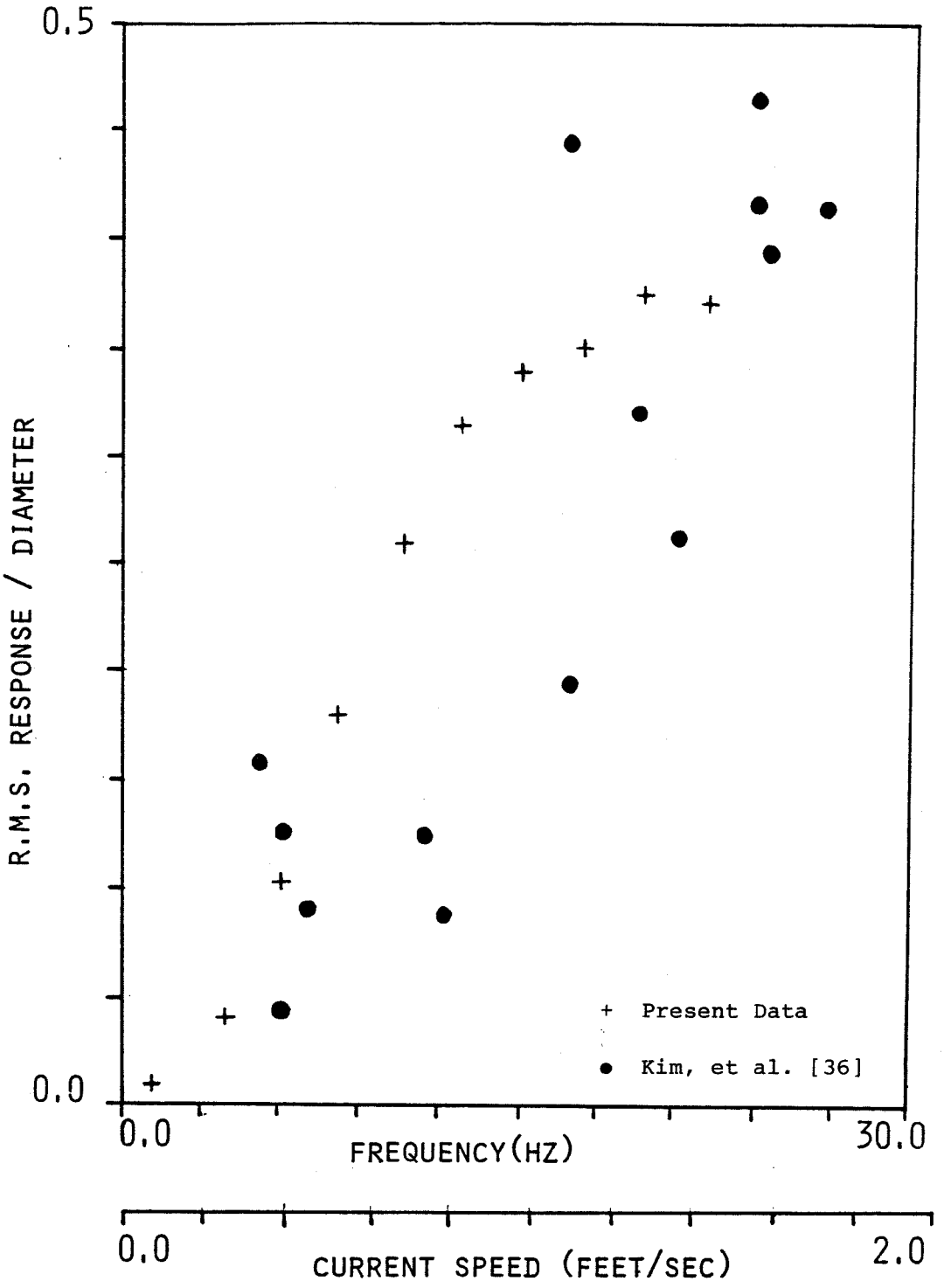

Figure 5.4.4. RMS Response Amplitude versus Current Velocity (from [36])

A few comments need to be made about the computed amplitude. First, the amplitude is nonzero at the right end of the cable. This, of course, means that some reflection will occur, so the solution as presented is not quite accurate. However, the magnitude of the amplitudes is small at that section of cable, so the errors introduced are considered small in light of the other assumptions made in the modeling. The effect of the reflections will be somewhat localized also, so the amplitudes at the center of the active region are unlikely to be affected. Second, the small "bumps" that occur in the amplitude curves are simply due to the truncation of the individual cell responses when the amplitude is a small, but finite value. This effect is not significant in the computation of the peak amplitudes, and the effect is clearly diminished when RMS values are considered.

The approximate technique clearly gives excellent results, considering that one tenth of the computing power was required to generate them. While overestimating the response at the ends of the cable, the overall response is well captured. The fact that the RMS amplitude, as calculated above, and the peak amplitude for an individual cell (by definition an RMS value) are similar tends to confirm the assumption of the localization of the individual cell responses; i.e., the effect of one cell on adjacent cells decreases rapidly with distance.

Note that the general performance, in comparison with a modal solution (for example [31]), is much improved. A modal solution, even assuming active shedding over only the 100 ft. span as done here, predicts an amplitude which is approximately constant along the cable, of 0.22 diameters. This is quite incorrect, as the observed data, and the prediction method used herein, confirm.

5.5 Some Observations on the Performance of the Solution Algorithm

At this stage it is considered appropriate to make some general observations on the performance of the solution algorithm. While the performance of the algorithm was satisfactory in most of the examples tested, there were a number obvious cases where the scheme diverged, and a solution was not found. In most instances, this occurred for long active lengths, generally at least twice as long as the wavelength corresponding to the shedding frequency. As stated earlier, these long active length solutions are not of much practical interest due to the unsteady nature of most flows in the marine or atmospheric environment. The causes of this instability and the general robustness of the algorithm are, however, of general interest, and should be investigated in some detail. A few ideas on this aspect are presented below, but the detailed analysis, and establishment of the boundaries of stability for the algorithm, are left as a topic for future work. Some of the points have been outlined already, but are reiterated here.

- The algorithm, as used to compute the results in the preceding sections, has been tested extensively during the course of this investigation. It is considered that the choices of initial conditions, convergence damping, and the details of the application of the loads to the system have been optimized to give a very efficient algorithm.

- The solution scheme either converges to an accurate solution, or diverges, and no solution is found. For a definition of "convergence" and "accuracy," refer to Appendix I. The source of the convergence difficulties lies with the force term in the kernel of the integral equation, Equation 3.3.11. In the constant force cases with viscous damping, no problems are observed. The same is true for vortex-

induced forces with viscous damping. In these cases, the force term is bounded in amplitude, the former in an unconditional sense, and the latter, if the amplitude remains less than about 1.2 diameters. However, when an inertia term is introduced, as in the modeling of Morison resistance, this force is linear in amplitude, and is therefore clearly unbounded. Depending on the size of the inertia force relative to the constant or vortex-induced force, instabilities in the algorithm may result. It is noted that these problems arise in two main cases. The first is long active lengths, where the amplitude is made large initially by the large amount of energy fed into the system, then driven unstable by the unbounded inertia term. The second case is for light cables. When the specific gravity of the cable is low, say around 1, the inertia due to the fluid is of the same magnitude as the inertia of the cable. This results in relatively large external inertia forces, which have a significant effect on the active cable segment. It is noted that convergence difficulties were not so common when higher density cables were modeled. Establishment of boundaries of stability for the scheme need to be established, as a function of the various forces and input parameters, but this is considered a topic for future work.

- As was outlined earlier, it appears that modal solutions may be more appropriate for long active length systems. Rather than using the whole system for a modal analysis, however, it is suggested that just the active region be considered, modeling the end points as either fixed, or with a spring boundary condition. This contrasts the conventional approach in which the whole cable is treated as the system, yielding inappropriate results for long systems.

CHAPTER 6

General Conclusions

6.1 Summary and Conclusions

In this thesis, a new treatment of the flow-induced vibration problem for long structures has been developed. In a departure from the standard modal analysis approach, a new method was attempted, based on a traveling wave or Green's function formulation. Many real structures, particularly in the ocean environment, are so long that the assumption of a modal response is quite unrealistic. The approach described herein models such systems as initial value problems, rather than the conventional boundary value problem, for which eigenfunction expansion, or modal analysis is generally used. The new method is applicable to nonuniform flow profiles in a more realistic way than previously possible.

Chapter 1 outlines some of the basic types of flow-induced vibration phenomena. The method developed in this dissertation is applicable to many types of flow-induced vibration problems, so some introduction to the various types of behaviors is useful. Vortex-induced vibration was used as the specific exciting mechanism in this work, so a brief introduction to some of the basic concepts of this phenomenon are described.

Various approaches have been used to model vortex-induced forces on structures. Chapter 2 outlines some of these models, both theoretical and empirical in nature, and also reviews a number of observations made on the response of long cable systems and of nonuniform flows. The empirical model of Iwan and Bothelo [32], based on the

experimental results of Sarpkaya [59,60] was chosen as the basis for this work. As the modeling approach used also enabled the application of nonlinear fluid resistance forces, the nature of these forces is also discussed in this chapter. In particular, the use of the Morison equation [43], and small oscillation asymptotic viscous fluid damping [2] are outlined. These latter representations are used to give an overall better representation of the fluid-structure behavior in regions of the cable where vortex shedding is not occurring.

In Chapter 3, the new model for predicting the vortex-induced response of long systems is developed. Beginning with a Green's function solution for a uniform cable, the exact solution for a spanwise constant force is derived by solving a linear integral equation. The cable system is discretized into a number of small segments, and the force over each segment is assumed to be approximately constant, but of unknown amplitude - the magnitude of the applied force is a function of the total amplitude of response of the system at a point. The total response of the whole system is obtained by summing the contributions of all the segments in an iterative manner. Iteration continues, using updated values of amplitude and phase, until convergence is attained.

Representation of various types of force are investigated. Linear viscous damping, constant spanwise force, vortex-induced forces, and Morison fluid resistance are all cast in a form that allows processing by the solution algorithm.

While the results obtained from the analysis in Chapter 4 are significant for uniform flow, in the field, most flow profiles are not uniform. As outlined in Chapter 2, linear sheared flow is a commonly assumption made for ocean current profiles. The results of Chapter 3 are used in Chapter 4, along with some simplifying assumptions, to tackle the problem of sheared velocity profiles on long cable systems.

Chapter 5 presents the results of the analysis in the preceding two chapters. Initially, an evaluation of accuracy and convergence through the modeling of a constant spanwise force is performed, making use of the exact solution already derived for this case. Next, various combinations of the active and inactive forces are made, and the results obtained by implementing the solution algorithm are discussed.

Some problems encountered with convergence are discussed, and techniques to avoid them, outlined. Care must be taken with the solution scheme presented. Poor choices of certain convergence parameters can lead to incorrect solutions or to complete lack of convergence.

Some very interesting results are obtained for the vortex-induced vibration case. The form of solution obtained indicated that shedding was progressive in nature, as evidenced by the linear variation of phase in the active and inactive regions. This prediction confirms the field observations of Alexander [1], who commented that exactly this type of behavior was recorded. The amplitude of oscillation was observed to increase for increasing active length, but it reached a maximum, as evidenced by the formation of a plateau of constant amplitude for very long active regions.

The combination of small active regions responding at different frequencies was made in the latter part of the chapter, implementing the solution technique outlined in Chapter 4. While there is a critical lack of experimental data in this area, the results obtained compared favorably to the data recorded by Kim et al. [37]. Clearly, more data are needed in this area to verify the modeling approach adopted.

6.2 Recommendations for Future Work

While the work presented herein successfully implements a new technique for the

solution of flow-induced vibration problems, there are many areas where it is thought that future work could be done. A number of these are listed below.

• A reasonable amount of work remains to be done on the solution algorithm utilized. While reasonable results were obtained in most cases, the amount of computation required for very long systems was significant, and convergence difficulties were sometimes experienced. A number of improvements to the code could be considered. A more efficient solution algorithm could be developed for integral equations of this type. Some initial work was done in this regard, but is not reported here. A finite element formulation of the system may yield better convergence, and more accurate results. Also, extension to semi-infinite systems (i.e., with one end of the active region of the cable system fixed) would be a useful enhancement. Again, some work towards this end was started, but is not reported here.

Once the efficiency of the solution algorithm is maximized, a useful and natural extension to the work would be the creation of a comprehensive package to handle nonuniform flow profiles, in general. This would be of most use to the design engineer, faced with a nonuniform current on a long cable system. The required breakdown of the system into independent active segments, analysis of each, and the combination for an overall solution could all be performed by one program.

Extension of the program to include other vortex-induced force models, such as the wake-oscillator and lift-oscillator models, would be of value, and would enable comparison of the different approaches. Comprehensive parameter studies of all models could be run, and compared with experimental data.

• It is considered an important extension to this work to apply one of the existing analytical models for vortex-induced vibration (for example, the lift-oscillator or

wake-oscillator model) to the traveling wave approach. This will serve to confirm the results reported herein, obtained using an empirical model, and will also enable extension of the method to incorporate a random vibration approach to the vortex-induced vibration of long systems.

• Due to the lack of recorded data, experimental verification (on both a large and a small scale) of the results are necessary. Although it would be difficult to model long systems in a laboratory in an efficient way, simple tests could be conducted to verify some of the results of the analysis. In the field, more comprehensive experimenting along the lines of Kim and Vandiver's work would be valuable.

• Clearly, the modeling of nonuniform ocean current and wind velocities as sheared flows is a very crude approximation at best. The construction of a new model, based on a random vibration approach, which could take into account the spanwise variation of the flow **and** the response, would be of definite value. Hand-in-hand with this development would be the need to conduct extensive experimental investigations into the random nature of these quantities, studying, for example, the correlation of shedding along the span under such a random flow field.

• The assumptions made in Chapter 4 about the superposition of the solutions for the various active regions, while physically argued in a reasonable way, have not been verified either analytically or experimentally. Most of Sarpkaya's work involved the monofrequency study of cylinder motion, and did not address the problem of a multifrequency response at all. Is the assumed independence, or lack of interaction between the two frequency components, observed in practice? How about three or more frequency contributions, or a random noise frequency content? These important questions need to be addressed before the modeling approach can be used with

confidence.

• The traveling wave solution adopted in this work could be adapted to slack cable systems. Once the Green's function for the slack system was derived, incorporation into the code would be a relatively simple matter. Obvious applications for such a system are the response of the mooring lines for guyed towers and vessels in deep water.

The accurate prediction of the response of long systems to flow-induced vibration is an important area for the engineer. While still at an early stage of development, it is believed that the approach used in this thesis will enable a much better understanding of the response of this type of system, and will open the door to more realistic modeling of the fluid-structure response through more sophisticated techniques.

REFERENCES

1. Alexander, C. M., "The Complex Vibrations and Implied Drag of a Long Oceanographic Wire in Cross-Flow," Ocean Engineering, Vol. 8, No. 4, 1981, pp. 379-406.

2. Batchelor, G. K., **An Introduction to Fluid Dynamics**, Cambridge University Press, Cambridge, 1967.

3. Bearman, P. W., "Vortex Shedding From Oscillating Bluff Bodies," Annual Review of Fluid Mechanics, Volume 16, 1984, pp. 195-222.

4. Bishop, R. E. D., and Hassan, A. Y., "The Lift and Drag Forces on a Circular Cylinder in a Flowing Fluid," Proceedings of the Royal Society (London), Series A, Vol. 277, 1964, pp. 32-50.

5. Bishop, R. E. D., and Hassan, A. Y., "The Lift and Drag Forces on a Circular Cylinder Oscillating in a Flowing Fluid," Proceedings of the Royal Society (London), Series A, Vol. 277, 1964, pp. 51-75.

6. Blevins, R. D., "Flow Induced Vibration of Bluff Structures," California Institute of Technology Dynamics Laboratory Report No. DYNL-74-01, Pasadena, California, February, 1974.

7. Blevins, R. D., and Burton, T. E., "Fluid Forces Induced by Vortex Shedding," Fluids Engineering Conference, Paper No. 75-FE-10, Minneapolis, Minnesota, May, 1975.

8. Blevins, Robert D., **Flow-Induced Vibration**, Van Nostrand Reinhold, New York, 1977.

9. Bothelo, D. L. R., "An Empirical Model for Vortex-Induced Vibrations," California Institute of Technology Earthquake Engineering Research Laboratory Report No. EERL 82-02, Pasadena, California, August, 1982.

10. Brooks, Alexander N., and Hughes, Thomas J. R., "Streamline Upwind/Petrov-Galerkin Formulations for Convection Dominated Flows with Particular Emphasis on the Incompressible Navier-Stokes Equations," Computer Methods in Applied Mechanics and Engineering, Volume 32, 1982, pp. 199-259.

11. Den Hartog, J. P., **Mechanical Vibrations**, 4th Edition, McGraw-Hill, New York, 1956.

12. Every, M. J., King, R., and Griffin, O. M., "Hydrodynamic Loads on Flexible Marine Structures due to Vortex Shedding," Journal of Energy Resources Technology, Vol. 104, No. 4, December, 1982, pp. 330-336.

13. Feng, C. C., "The Measurement of Vortex-Induced Effects in Flow Past Stationary and Oscillating Circular and D-Section Cylinders," M. A. Sc. Thesis, University of British Columbia, 1968.

14. Fung, Y. C., **The Theory of Aeroelasticity**, Wiley, New York, 1955 (reprint Dover, 1969).

15. Griffin, Owen M., "Flow Near Self-Excited and Forced Vibrating Circular Cylinders," Journal of Engineering for Industry, Vol. 94, May, 1972, pp. 539-547.

16. Griffin, O. M., and Ramberg, S. E., "The Effects of Synchronized Cylinder Vibrations on Vortex Formation and Strength, Velocity Fluctuations, and Mean Flow," Paper E-3, Presented at the Symposium on Flow-Induced Structural Vibrations, held in Karlsruhe, Germany, August 14-16, 1972.

17. Griffin, O M., Skop, R. A., and Koopmann, G. H., "The Vortex-Excited Resonant Vibrations of Circular Cylinders," Journal of Sound and Vibration, Vol. 31, No. 2, 1973, pp. 235-249.

18. Griffin, Owen M., and Ramberg, Steven E., "The Vortex-Street Wakes of Vibrating Cylinders," Journal of Fluid Mechanics, Vol. 66, Part 3, 1974, pp. 553-576.

19. Griffin, Owen M., "Vortex-Induced Lift and Drag on Stationary and Vibrating Bluff Bodies," Journal of Hydronautics, Vol. 9, No. 4, October, 1975, pp. 160-164.

20. Griffin, Owen M., Skop, Richard A., and Ramberg, Steven E., "The Resonant, Vortex-Excited Vibrations of Structures and Cable Systems," Offshore Technology Conference, Paper No. OTC 2319, 1975, pp. 731-744

21. Griffin, Owen M., "Vortex-Excited Unsteady Forces on Resonantly Vibrating, Bluff Structures," NRL Memorandum Report No. 3820, Naval Research Laboratory, Washington D.C., August, 1978.

22. Griffin, O. M., Ramberg, S. E., and Skop, R. A., "Flow-Induced Vibrations of Mooring Arrays," FY1979 Final Report, Ocean Technology Division, Naval Research Laboratory, Washington, D.C., September 30, 1979.

23. Griffin, Owen M., "Steady Hydrodynamic Loads Due to Vortex Shedding from the OTEC Cold Water Pipe," NRL Memorandum Report No. 4698, Naval Research Laboratory, Washington D.C., January 13, 1982.

24. Griffin, O. M., "Vortex Shedding from Structures and Cables in a Shear Flow: State-of-the-Art," Report No. CR 83.004, Naval Civil Engineering Laboratory, Port Hueneme, California, November, 1982.

25. Hall, S. A., "Vortex-Induced Vibrations of Structures," California Institute of Technology Earthquake Engineering Research Laboratory Report No. EERL 81-01, Pasadena, California, January, 1981.

26. Hall, S. A., and Iwan, W. D., "Oscillations of a Self-Excited, Nonlinear System," Journal of Applied Mechanics, Vol. 51, No. 4, December, 1984, pp. 892-898.

27. Hartlen, R. T., and Currie, I. G., "Lift-Oscillator Model of Vortex-Induced Vibration," Journal of the Engineering Mechanics Division, ASCE, Vol. 96, No. EM5, 1970, pp. 577-591.

28. Iwan, W. D., and Blevins, R. D., "A Model for Vortex Induced Oscillation of Structures," Journal of Applied Mechanics, Vol. 41, No. 3, September, 1974, pp. 581-586.

29. Iwan, W. D., "The Vortex-Induced Oscillation of Elastic Structural Elements," Journal of Engineering for Industry, Vol. 97, Series B, No. 4, November, 1975, pp. 1378-1382.

30. Iwan, W. D., "The Vortex-Induced Oscillation of Non-Uniform Structural Systems," Journal of Sound and Vibration, Vol. 79, No. 2, 1981, pp. 291-301.

31. Iwan, W. D., and Jones, N. P., "NATFREQ User's Manual - A FORTRAN IV Program for Computing Natural Frequencies, Mode Shapes, and Drag Coefficients for Taut Strumming Cables with Attached Masses and Spring-Mass Combinations," Report No. CR 84.026, Naval Civil Engineering Laboratory, Port Hueneme, California, June, 1984.

32. Iwan, Wilfred. D., and Bothelo, Dirceu L. R., "Vortex-Induced Oscillation of Structures in Water," Journal of Waterway, Port, Coastal and Ocean Division, ASCE, Vol. 111, No. WW2, March, 1985, pp. 289-303.

33. Jones, G. W., Jr., "Unsteady Lift Forces Generated by Vortex Shedding About a Large, Stationary and Oscillating Cylinder at High Reynolds Numbers," Symposium on Unsteady Flow at the Fluids Engineering Conference, ASME, Paper No. 68-FE-36, Philadelphia, PA, May, 1968.

34. Kennedy, M. B., "A Linear Random Vibrations Model for Cable Strumming," Ph.D. Thesis, Massachusetts Institute of Technology, 1979.

35. Keuligan, G. H., and Carpenter, L. H., "Forces on Cylinders and Plates in an Oscillating Fluid," Journal of Research of the National Bureau of Standards, Research Paper 2857, Vol. 60, No. 5, May, 1958, pp. 423-440.

36. Kim, Yang-Hann, "Vortex-Induced Response and Drag Coefficients of Long Cables in Ocean Currents," Ph.D Thesis, Department of Ocean Engineering, Massachussets Institute of Technology, October, 1984.

37. Kim, Y-H, Vandiver, J.K., and Holler, R., "Vortex-Induced Vibration and Drag Coefficients of Long Cables Subjected to Sheared Flows," Proceedings of the Fourth International Offshore Mechanics and Engineering Symposium, Vol. 1, ASME, Dallas, Texas, February, 1985.

38. Koopmann, G. H., "The Vortex Wakes of Vibrating Cylinders at Low Reynolds Numbers," Journal of Fluid Mechanics, Vol 28., Part 3, 1967, pp. 501-512.

39. Kretschmer, T. R., Edgerton, G. A., and Albertson, N. D., "Seafloor Construction Experiment, Seacon II - An Instrumented Tri-Moor for Evaluating Undersea Cable Structure Technology," Naval Facilities Engineering Command, Technical Report R848, December, 1976.

40. Marris, A. W., "A Review on Vortex Streets, Periodic Wakes, and Induced Vibration Phenomena," Journal of Basic Engineering, Vol. 86, June 1964, pp. 185-196.

41. Mazel, C. H., "Vortex-Excited Vibrations of Marine Cables," M.S. Thesis, Massachusetts Institute of Technology, 1976.

42. McGlothin, James C., "Drag Coefficients of Long Flexible Cylinders Subject to Vortex-Induced Oscillations," Master of Science Thesis, Department of Ocean Engineering, Massachussets Institute of Technology, January, 1982.

43. Morison, J. R., O'Brien, M. P., Johnson, J. W., and Schaaf, S. A., "The Force Exerted by Surface Waves on Piles," Petroleum Transactions, AIME, Vol. 189, 1950, pp. 149-154.

44. Parkinson, G. V., Feng, C. C., and Ferguson, N., "Mechanisms of Vortex-Excited Oscillation of Bluff Cylinders," Proceedings of the Symposium of Wind Effects on Buildings and Structures, Loughborough University of Technology, Vol.2, Paper 27, April, 1968.

45. Peltzer, R. D., and Rooney, D. M., "Wake Characteristics of High Aspect Ratio Cylinders in Subcritical Spanwise Sheared Flows," Winter Meeting, ASME, Paper 81-WA/FE-10, Washington, D. C., 1981.

46. Peltzer, R. D., "Vortex Shedding from a Vibrating Cable with Attached Spherical Bodies in a Linear Shear Flow," Ph.D. Thesis, Virginia Polytechnic Institute and State University, Blacksburg, Virginia, August, 1982.

47. Ramberg, S. E., and Griffin, O. M., "Vortex Formation in the Wake of a Vibrating Flexible Cable," Journal of Fluids Engineering, Vol. 96, December, 1974, pp. 317-322.

48. Ramberg, S. E., and Griffin, O. M., "Velocity Correlation and Vortex Spacing in the Wake of a Vibrating Cable," Fluids Engineering Conference, ASME, Paper No. 75-FE-7, Minneapolis, MN, May, 1975.

49. Ramberg, S. E., and Griffin, O. M., "The Effects of Vortex Coherence, Spacing, and Circulation on the Flow-Induced Forces on Vibrating Cables and Bluff Structures," Naval Research Laboratory, Report No. 7945, January, 1976.

50. Rayleigh, J. W. S., **The Theory of Sound**, Macmillan, 1894, Reprinted by Dover, New York, 1945.

51. Raposo, P. A., "Transverse Oscillations of a Cylinder in Uniform Flow," M. S. Thesis, Naval Postgraduate School, Monterey, California, June, 1976.

52. Rosenhead, L., "Formation of Vortices from a Surface of Discontinuity," Proceedings of the Royal Society of London, Series A, Vol. 134, 1931, pp. 170-192.

53. Roshko, A., "On the Drag and Shedding Frequency of Two-Dimensional Bluff Bodies," National Advisory Committee for Aeronautics, TN3169, July, 1954.

54. Russel, J. J., "A Finite Element Analysis of Vortex-Induced Cable Oscillations," Student Research Report 2080-79, Air Command and Staff College, Air University, Maxwell Air Force Base, AL, 1979.

55. Sarpkaya, T., "Forces on Cylinders and Spheres in a Sinusoidally Oscillating Fluid," Journal of Applied Mechanics, ASME, Vol. 42, March, 1975, pp. 32-37.

56. Sarpkaya, T., "An Analytical and Experimental Study of the In-Plane and Transverse Oscillations of a Circular Cylinder in Uniform Flow," Report No. NPS-59SL75051, Naval Postgraduate School, Monterey, California, May 30, 1975.

57. Sarpkaya, T., "In-Line and Transverse Forces on Smooth and Sand-Roughened Cylinders in Oscillatory Flow at High Reynolds Numbers," Report No. NPS-69SL76062, Naval Postgraduate School, Monterey, California, June 4, 1976.

58. Sarpkaya, T., "In-Line and Transverse Forces on Cylinders in Oscillatory Flow at High Reynolds Numbers," Offshore Technology Conference, Paper No. OTC 2533, May, 1976, pp. 95-108.

59. Sarpkaya, T., "Transverse Oscillations of a Circular Cylinder in Uniform Flow, Part I," Report No. NPS-69SL77071, Naval Postgraduate School, Monterey, California, July 20, 1977.

60. Sarpkaya, T., "Fluid Forces on Oscillating Cylinders," Journal of the Waterway, Port, Coastal and Ocean Division, ASCE, Vol. 104, No. WW4, August, 1978, pp. 275-290.

61. Sarpkaya, T., "Vortex-Induced Oscillations: A Selective Review," Journal of Applied Mechanics, Vol. 46, June, 1979, pp. 241-258.

62. Sarpkaya, T., and Schoaff, R. L., "A Discrete Vortex Analysis of Flow About Stationary and Transversely Oscillating Circular Cylinders," Report No. NPS-69SL79011, Naval Postgraduate School, Monterey, California, January, 1979.

63. Sarpkaya, Turgut, and Isaacson, Michael, **Mechanics of Wave Forces on Offshore Structures**, Van Nostrand Reinhold, New York, 1981.

64. Scanlan, Robert H., and Rosenbaum, Robert, **Introduction to the Study of Aircraft Vibration and Flutter**, Macmillan, New York, 1960.

65. Shiraishi, T., "The Vortex-Induced Oscillation of Elastic Structural Elements," M.E. Thesis, California Institute of Technology, Pasadena, California, 1977.

66. Simiu, Emil, and Scanlan, Robert H., **Wind Effects on Structures: An Introduction to Wind Engineering**, Wiley, New York, 1978.

67. Skop, R. A., and Griffin, O. M., "A Model for the Vortex-Excited Resonant Response of Bluff Cylinders," Journal of Sound and Vibration, Vol. 27, No. 2, 1973, pp. 225-233.

68. Skop, R. A., and Griffin, O. M., "On a Theory for the Vortex-Excited Oscillations of Flexible Cylindrical Structures," Journal of Sound and Vibration, Vol. 41, No. 3, 1975, pp. 263-274.

69. Skop, R. A., Ramberg, S. E., and Griffin, O. M., "Seacon II Strumming Predictions," Naval Research Laboratory, Memorandum Report 3383, October, 1976.

70. Staubli, T., "Calculation of the Vibration of an Elastically Mounted Cylinder using Experimental Data From Forced Oscillation," Journal of Fluids Engineering, June, 1983, pp. 225-229.

71. Strouhal, V., "Uber eine besondere Art de Tonerregung, Ann. Phys. und Chemie, New Series, Vol. 5, 1878, pp. 216-251.

72. Toebes, G. H., "The Unsteady Flow and Wake Near an Oscillating Cylinder," Journal of Basic Engineering, Vol. 91, September, 1969, pp. 493-505.

73. Von Karman, T., "On the Mechanism of the Resistance Experienced by a Moving Body in a Liquid," Nachrichten der K. Gessellschaft der Wissenschaften zu Gottinger Mathematisch- Physikalische Klasse, 1912, translated by the National Translation Center, No. 76-51072, pp. 547-556.

74. Vickery, B. J., "Fluctuating Lift and Drag on a Long Cylinder of Square Cross-Section in a Smooth and Turbulent Stream," Journal of Fluid Mechanics, Vol. 25, Part 3, 1966, pp. 481-494.

75. Woo, H. G. C., Peterka, J. E., and Cermak, J. E., "Experiments on the Vortex Shedding from Stationary and Oscillating Cables in a Linear Shear Flow," Fluid Mechanics and Wind Engineering Program, Colorado State University, Final Report on Contract N68305-78-C-0055 for the Naval Civil Engineering Laboratory, July, 1981.

APPENDIX I

Programming Considerations

To implement the traveling wave solution, a FORTRAN-77 program was developed. The structure and details of the program are discussed below. The basic approach used in the program was introduced in Section 3.4.2.

I.1 Program Structure

After input of the required dimensionless parameters for the program, initial values of the amplitude and phase of the total displacement are chosen. While initial values of zero for both $\bar{A}_i$ and $\bar{\phi}_i$ throughout will produce a solution, it was found better to choose values which approximate more realistically the final solution. The rate of convergence was generally improved by this choice of initial values, and some difficulties in convergence were overcome.

The forces corresponding to the initial amplitudes and phases are calculated and the waves generated summed over the required region. The new set of amplitudes and phases are calculated using Equations (3.4.16) and (3.4.17).

A test of convergence is performed and iteration continues until a predetermined condition is satisfied. The relative changes from one iteration to the next can be weighted to minimize the effect of changes in the low response amplitude regions of the cable.

The program computes amplitudes and phases of the total response along the

cable. Also written, although mainly useful for debugging purposes, are the force amplitude and relative phase corresponding to the motion described above.

I.2 Boundary Conditions

For many applications, the assumption of a symmetric doubly infinite string for modeling a structure with a large length-to-diameter ratio can be made. However, there are many cases when it is useful to include a fixed boundary in the traveling wave formulation. For example, an instrument suspended vertically in the ocean is essentially fixed at the suspension point, and has a free end with an attached mass at the other (Figure 4.1.1).

For most environments, the current profile decreases toward the bottom of a long cable. The relatively large fluid damping in this region, combined with the low energy input means that the lower boundary condition does not affect the modeling of the system as a semi-infinite string.

However, the fixity at the top of the cable can have a significant effect on the response. Upward traveling waves produced in the upper section of the cable are reflected from the fixed boundary and produce partial standing waves in that region.

A fixed boundary may be included in the formulation by simply generating an asymmetric solution, and considering only one-half of the system. The effect of the fixed boundary is to:

- Change the direction of travel of the wave
- Change the phase by 180° (or invert the incoming wave).

Equivalently, this effect can be produced by generating a wave at $x=-a$ that is 180° out of phase with the wave being produced at $x=a$. Summation of these pairs of

waves will produce the required fixed boundary condition at x=0.

I.3 Convergence and Accuracy

As with all numerical schemes, the areas of convergence and accuracy require some consideration. To clarify the difference between the two, it should be realized that it is possible for a solution scheme to converge to the wrong solution. Thus the two topics should be treated separately. While there are obvious sources of error from the modeling of the various forces involved in the systems considered, this section concentrates on the numerical errors produced by the solution technique.

The most significant source of error is the discretization of the system into finite length segments. The solutions presented are piecewise constant (discontinuous). Future work may concentrate on a smoother solution, continuous in the zeroth or first derivatives. This could be implemented, using a finite element formulation.

To minimize the discretization errors, the size of the finite length elements must be viewed in relation to both the wavelength corresponding to the forcing frequency and the diameter of the cable. The first requirement is that the length of a segment is much smaller than the wavelength of the forcing frequency (Equation 3.4.1). This condition ensures that the change in amplitude from one segment to the next is small. In practice, it was found that less than 10 diameters per segment produces reasonable results; i.e., the solution converges to the correct solution.

Discretization also affects the exponential amplitude modulation term in the basic traveling wave expression (Equation 3.4.8). If the α term in the exponent is too large, then little information is transmitted from one segment to the next, and the assumption of a constant force and displacement across the segment becomes a poor

approximation. Care should be taken not to use too high a value of convergence damping.

Another source of error is the use of insufficient length of cable beyond the active length to allow the amplitude of response to decay to zero. While this error is usually reflected in convergence difficulties, it is actually an accuracy problem, and care should be taken in using results in which the amplitudes at the end of the cable are non-zero.

Convergence difficulties with the approach also arise from a number of sources. Several methods were used to improve the convergence, and are discussed below.

As already mentioned, insufficient inactive cable length causes problems with convergence. If the amplitude is finite at the ends of the system, then clearly, insufficient damping forces have been applied, and the inactive length should be increased. Without sufficient length, the amplitudes begin to grow at the ends, and the solution scheme becomes unstable.

Another somewhat related difficulty is due to the fact that very low values of internal damping produce very small values of the parameter α in Equation 3.4.8. In the solution process, this results in a change being generated by an applied force at one segment affecting many other segments. In the worst case, if zero internal damping is assumed, a change at one location affects all the other segments by the same amount, depending on the phase at each location. This change then affects the applied forces at all the other segments, and very soon, the terms involved become unmanageable. The solution sought generally becomes the sum of a large number of large terms, and accuracy becomes a problem.

Physically, however, it is known that the fluid applies quite a large external damping to the structure. To overcome the above problem, it is necessary to assume that some of these external damping forces are applied internally, increasing the parameter α to a value that produces more reasonable convergence characteristics.

Application of this scheme essentially applies a damping force to both sides of Equation (3.2.2). On the left-hand side, the increased damping produces an increase in the value of α, while on the right-hand side, the applied force is increased by a corresponding amount. Note that on the left-hand side, the damping is being added in a continuous manner, while on the right it is approximated as a constant force over a segment. Care should be exercised in applying values of "convergence damping" which are too large, therefore, as the discretization errors will begin to have large effects.

The convergence *rate* is not necessarily increased by higher values of convergence damping. Addition of the compensating force to the right-hand side of Equation (3.2.2) increases the amplitude of the local peaks. These may require a moderate number of iterations to smooth out. The advantage of using the convergence damping comes from the fact that without it, there are many lightly internally damped systems which would not be able to be solved by this method.